NUMERICAL SIMULATIONS OF REINFORCED CONCRETE FRAMES TESTED USING PSEUDO-DYNAMIC METHOD

A THESIS SUBMITTED TO
THE GRADUATE SCHOOL OF NATURAL AND APPLIED SCIENCES
OF
MIDDLE EAST TECHNICAL UNIVERSITY

BY

MEHMET BAŞAR MUTLU

IN PARTIAL FULFILLMENT OF THE REQUIREMENTS
FOR
THE DEGREE OF MASTER OF SCIENCE
IN
CIVIL ENGINEERING

JULY 2012

Approval of the thesis:

NUMERICAL SIMULATIONS OF REINFORCED CONCRETE FRAMES TESTED USING PSEUDO-DYNAMIC METHOD

submitted by **MEHMET BAŞAR MUTLU** in partial fulfillment of the requirements for the degree of **Master of Science in Civil Engineering Department, Middle East Technical University** by,

Prof. Dr. Canan Özgen
Dean, Graduate School of **Natural and Applied Sciences** _____

Prof. Dr. Güney Özcebe
Head of Department, **Civil Engineering** _____

Prof. Dr. Barış Binici
Supervisor, **Civil Engineering Dept., METU** _____

Examining Committee Members:

Prof. Dr. Haluk Sucuoğlu
Civil Engineering Dept., METU _____

Prof. Dr. Barış Binici
Civil Engineering Dept., METU _____

Prof. Dr. Güney Özcebe
Civil Engineering Dept., METU _____

Assoc. Prof. Dr. Erdem Canbay
Civil Engineering Dept., METU _____

Dr. Nazan Kılıç
Disaster and Emergency Management Presidency _____

Date: 05.07.2012

I hereby declare that all information in this document has been obtained and presented in accordance with academic rules and ethical conduct. I also declare that, as required by these rules and conduct, I have fully cited and referenced all material and results that are not original to this work.

Name, Last name : Mehmet Başar MUTLU

Signature : _____

ABSTRACT

NUMERICAL SIMULATIONS OF REINFORCED CONCRETE FRAMES TESTED USING PSEUDO-DYNAMIC METHOD

Mutlu, Mehmet Başar
M.Sc., Department of Civil Engineering
Supervisor: Prof. Dr. Barış Binici

July 2012, 100 pages

Considering the deficiencies frequently observed in the existing reinforced concrete buildings, detailed assessment and rehabilitation must be conducted to avoid significant life and value loss in seismic zones. In this sense, performance based evaluation methods suggested in the regulations and codes must be examined and revised through experimental and analytical research to provide safe and economical rehabilitation solutions.

In this study, seismic behavior of three reinforced concrete frames built and tested in Middle East Technical University Structural Mechanics Laboratory is examined. The specimens are extracted from a typical interior frame of 3-story 3-bay reinforced concrete structure. One of the specimens has compliant design according to Turkish Earthquake Code (2007) and each of the other two specimens represents different types of deficiencies in terms of material strength and detailing. The test specimens were modeled using different modeling approaches and nonlinear dynamic analyses were conducted on the numerical models. Results of continuous pseudo-dynamic testing of three ground motions are presented and compared with the numerical simulations on models. Calibrated finite element models were used for evaluation of performance assessment procedure of Turkish Earthquake Code (2007) and further investigation on local deformation components in light of experimental findings and observations. Deformation sources of columns and joints were studied in terms of

their interaction and contributions to the total drift. Estimated plastic hinge lengths of columns were compared with the experimental observations and the proposed expressions in the literature.

Keywords: Pseudo-Dynamic Testing, Numerical Simulations, Finite Element Models, Performance Evaluation, Plastic Hinge Length.

ÖZ

DİNAMİK-BENZERİ YÖNTEMLERLE TEST EDİLMİŞ BETONARME YAPILARIN SAYISAL SİMÜLASYONLARI

Mutlu, Mehmet Başar
Yüksek Lisans, İnşaat Mühendisliği Bölümü
Tez Yöneticisi: Prof. Dr. Barış Binici

Temmuz 2012, 100 sayfa

Mevcut betonarme binalardaki yetersizlikler dikkate alındığında, deprem bölgelerinde oluşabilecek kayıpların önlenebilmesi amacıyla detaylı değerlendirme ve güçlendirme çalışmalarının yürütülmesi zorunludur. Bu anlamda, yönetmeliklerde önerilen performans esaslı hesap yöntemlerinin, deneysel ve analitik araştırmalar ışığında incelenmesi ve geliştirilmesi gerekmektedir.

Bu çalışmada, Orta Doğu Teknik Üniversitesi Yapı Mekaniği Laboratuvarı'nda inşa edilmiş ve dinamik-benzeri yöntemlerle test edilmiş üç farklı betonarme yapının deprem davranışları incelenmiştir. Deney numuneleri 3 katlı 3 açıklıklı betonarme bir yapının tipik orta açıklığını temsil etmektedir. Numunelerden biri Türk Deprem Yönetmeliği (2007) kurallarına uygun tasarımı, diğer ikisi ise malzeme dayanımı ve kesit detaylarında görülebilecek farklı yetersizlikleri temsil etmektedir. Deney numunelerinin farklı modelleme yaklaşımları kullanılarak oluşturulmuş sayısal modelleri üzerinde doğrusal olmayan dinamik analizler gerçekleştirilmiştir. Üç farklı yer hareketinin art arda uygulanmasıyla gerçekleştirilen dimanik-benzeri deneylerin sonuçları sayısal modeller üzerindeki simülasyon sonuçlarıyla karşılaştırmalı olarak sunulmuştur. Deney sonuçlarıyla eşleştirilmiş sonlu eleman modelleri, numunelerin Türk Deprem Yönetmeliği (2007) performans esaslı hesap yöntemi ile değerlendirilmesinde ve bölgesel şekil değiştirme istemlerinin incelenmesinde kullanılmıştır. Kolon açıklıklarında ve birleşim bölgelerindeki deformasyon bileşenlerinden herbirinin kat ötelemesine katkısı ve birbirleriyle etkileşimleri

irdelenmiştir. Ayrıca, sayısal modellerle tahmin edilen kolon plastik mafsal boyları literatürde önerilmiş yöntemlerle hesaplanan plastik mafsal boylarıyla karşılaştırmalı olarak sunulmuştur.

Anahtar Kelimeler: Dinamik-Benzeri Deney, Sayısal Simülasyonlar, Sonlu Eleman Modelleri, Performans Değerlendirmesi, Plastik Mafsal Boyu.

To My Family

ACKNOWLEDGEMENTS

This study was conducted under the supervision of Prof. Dr. Barış Binici. I would like acknowledge gratefully the expert guidance and support that he has provided me throughout my study.

The guidance provided by Prof. Dr. Haluk Sucuoğlu is also gratefully appreciated.

I would like to thank my colleagues F.Soner Alıcı, Kaan Kaatsız, Alper Özge Gür, Sadun Tanışer, Mustafa Can Yücel and Ahmet Kuşyılmaz for their help, friendship and three years of unforgettable memories in our office K7-Z01.

I am grateful to my colleagues Sadun Tanışer, M. Engin Ayatar and Pourang Ezzatfar for their technical support and cooperation in the research project that formed the basis of this study.

I wish to express my special thanks to my colleague F.Soner Alıcı for being a great friend and office mate. His endless support and patience will be remembered with gratitude.

I owe special thanks to my best friend and my colleague Emrah Erşan Erdoğan for the great friendship of more than 10 years. It is a pleasure to know that I will always have his friendship and support through my future life.

I would like to thank sincerely my beloved parents and my brother for their endless love and support that they have provided me throughout my life.

The financial support by the Scientific and Technological Research Council of Turkey (TÜBİTAK – 108G034) is gratefully acknowledged.

TABLE OF CONTENTS

LIST OF FIGURES

FIGURES

LIST OF TABLES

TABLES

CHAPTER 1

INTRODUCTION

1.1. General

Most of the reinforced concrete buildings in building stock of Turkey are vulnerable to seismic hazard according to modern seismic codes and regulations. Performance evaluation of these buildings emerged as a major concern especially after the recent earthquakes in our country, which caused significant loss in terms of human life and economy. Preliminary seismic performance assessments, conducted within the scope of urban regeneration projects, revealed that significant amount of buildings located in high seismic hazard areas have certain deficiencies. Most frequently observed deficiencies in the building stock are; plan irregularities, presence of heavy overhangs, poor detailing in structural members and joint regions, low material strengths, inadequate member sizes and use of plain reinforcements. Each of these deficiencies has different effects of the seismic performance of buildings that should be considered separately. In order to avoid possible life and value loss in seismic hazard, detailed assessment and rehabilitation of these deficient buildings must be conducted urgently.

Considering the life safety and economic aspects of the rehabilitation process, adequate performance evaluation methods must be developed for necessary detailed assessments on the deficient buildings. Research and revisions on the seismic guidelines or codes is necessary for development of adequate performance

based evaluation methods that provide safe and economical solutions for rehabilitation of existing buildings.

The release of FEMA 356 (2000) was one of the leading comprehensive documents on technical requirements for seismic rehabilitations of existing buildings. Performance based evaluation methods proposed in the document served as a basis for research and development of other seismic codes and regulations. Throughout the experimental and analytical studies on the acceptance criteria and performance limits, FEMA 356 was superseded by the document ASCE/SEI 41-06 (2006). In 2007, provisions related to rehabilitation of existing reinforced concrete buildings has been updated in the document ASCE/SEI-41 Supplement-1 based on experimental and analytical studies of researchers on the proposed effective stiffness models, modeling parameters and acceptance criteria.

Turkish Earthquake Code (2007) provides evaluation methods and performance limits which are currently used by engineers in Turkey for the rehabilitation purposes. Considering the current needs of Turkey in terms of seismic rehabilitation, research on the reliability of proposed evaluation and strengthening methods in the document is essential for development of revisions and updates on the document.

1.2. Problems in Models of Seismic Assessment

In reinforced concrete frame type of structures, lateral loads imposed by the seismic excitations are mainly carried by columns which are the members carrying the gravity loads of these structures. Therefore the columns should have adequate strength and ductility to meet the imposed lateral force and displacement demands. As a result, one of the main factors governing the seismic performance and failure mechanisms of reinforced concrete frames is the deformability of the columns. Accurate estimation of ductility of the columns is of great importance for the goal of adequate seismic assessment and economical retrofit solutions for the existing buildings.

In performance based evaluation methods, structural members are classified according to their failure modes based on their nonlinear deformation capacities. These classifications are used for determination of modeling parameters and deformation limits for each of pre-defined performance levels.

In FEMA 356, modeling parameters for reinforced concrete columns are classified according to whether the behavior is controlled by flexure or inadequate lap splicing while plastic deformation is not allowed for the modeling of columns which are controlled by shear. In the document ASCE/SEI 41-06, which superseded FEMA 356, concrete provisions were mainly the same in terms of failure mode classifications of columns and acceptance criteria. However it was pointed in EERI/PEER (2006) that the proposed acceptance criteria yielded conservative results and deformation limits should be revised for more accurate evaluation of the buildings and more economical rehabilitation solutions. Moreover, set of experimental studies by Sezen and Moehle (2006) revealed the limited plastic deformation capacities of columns due to flexural yielding prior to shear failure which is called flexure-shear failure. In this respect, classification of columns for determination of modeling parameters was revised in the document ASCE/SEI-41 Supplement-1, including the flexure-shear failure mode for columns which is controlled by both shear and flexure. In the proposed revisions, three conditions are defined and classification of columns is done based on shear capacity/shear demand ratio and the transverse reinforcement detailing of critical sections. In this way, modeling parameters and acceptance criteria are identified for each of flexure, flexure-shear and shear failure modes of columns.

In Chapter-7 of Turkish Earthquake Code (2007) for seismic assessment and retrofit design of existing buildings, there are two types of failure modes, similar to the case of FEMA 356. The members are classified as ductile or brittle which correspond to flexure failure and shear failure respectively. Considering the recent analytical and experimental studies which served as the basis of the revisions in the other seismic codes and regulations, it can be stated that the additional definition of flexure-shear mode in performance evaluation methods of Turkish Earthquake Code (2007) is necessary to avoid conservative assessments which may lead higher rehabilitation costs. In this sense, comparative experimental studies on different column failure types are essential for development of revisions in the defined modeling parameters and acceptance criteria of the document.

Turkish Earthquake Code (2007) provides a strain-based procedure for nonlinear performance assessment of existing buildings. In this procedure, both of the nonlinear static and nonlinear time history analysis methods are based on lumped

plasticity modeling approach where the nonlinear moment-rotation behaviors of members are modeled using rotational springs defined at member ends. In this modeling approach, deformation demands obtained from the analyses are in terms of plastic rotations whereas the performance levels are defined in terms of strain limits for concrete and longitudinal reinforcement. Therefore the plastic rotation demands need to be converted to the strain demands through moment-curvature analysis for each member. The first step in the conversion of plastic rotation demands to total strains is to convert the plastic rotations to plastic curvatures using the proposed value of plastic hinge length (*Lp*). Then, the total curvature demand is obtained by adding the yield curvature value to the plastic curvature value where the yield curvature value is calculated from the cross-sectional analysis under the axial load demands. Compressive strain demand on concrete and tensile strain demand on longitudinal reinforcement corresponding to the calculated total curvature value are determined from the cross-section analysis. The strain values obtained through this conversion procedure are used in the determination of damage regions for member ends. Although the use of strain demands instead of rotation demands in member ends seem to yield more realistic results for performance evaluation, it should be noted that the conversion procedure explained above requires separate cross-sectional analysis of members which consists of assumptions that may cause sensitivity in results and decrease the accuracy of the method. Moreover, the lack of practicality of this conversion procedure can be stated as another weakness of the strain based evaluation method.

Earthquake deformations in reinforced concrete moment resisting frames cause moment reversals in columns and beams which are transferred through the joints. As a result high shear demands occur in the joints regions. This may result in reduction in frame stiffness or premature strength loss due to damage depending on the capacity of the joint. Therefore, proper representation of joint strength and flexibility is essential for accurate simulation of these structures for both linear and nonlinear modeling.

Elastic modeling of the beam-column joints is mostly based on the definition of rigid offsets in element ends with different lengths or basically representing the joint flexibility through the connecting beam and column elements. In this sense, different approaches were recommended in standards and in the previous studies of

researchers for linear modeling of joint regions. In FEMA 356, simply use of rigid joint offsets in column and beam ends for whole joint dimension is recommended. ASCE/SEI 41-06 recommends the determination of rigid offset lengths based on the flexural strength proportions of connected beams and columns. For the case of strong column weak beam condition ($\sum M_c/\sum M_b>1.2$), the rigid offsets are defined only for columns, whereas for the strong beam weak column connections ($\sum M_c/\sum M_b<0.8$), the full rigid offset definition is recommended only for beams. For the cases in between these two limits, half length of the joint dimension is modeled as rigid offset for both columns and beams. Similar to the definition in FEMA 356, Turkish Earthquake Code (2007) permitted the use of infinitely rigid end offsets that span the entire dimension of joint regions in modeling of both columns end beams.

In the analytical study of Birely et. al. (2012), recommendations of FEMA 356 and ASCE/SEI 41-06 were evaluated using linear models of 45 frame sub-assemblages tests. It was stated that the stiffness recommendations of FEMA 356 resulted in overly stiff models that simulate the initial yield displacements inaccurately. ASCE/SEI 41-06 recommendations resulted in more flexible models however the model was found to be too stiff for the joints that do not satisfy the requirements of ACI 318-08 (2008). Depending on the condition of compliance or non-compliance with ACI 318-08, an alternative definition of optimum offset length factors (β) were recommended in this study based on the result of the analytical study for minimizing the error in the simulated initial yield displacement.

Behavior of beam-column joints was researched extensively in the past through concrete subassembly experiments which demonstrated that the joints experience high shear deformations prior yielding of longitudinal reinforcements. Considering the significance of modeling the nonlinear behavior of beam column joints, different modeling approaches were developed in literature. Rotational hinge model proposed by Alath and Kunnath (1995) represents one of these approaches. This model requires definition of single moment rotation relation representing the behavior of the joint which depends on multiple parameters. Therefore the calibration of the model for nonlinear behavior is not easily applicable for various types of joint detailing. Another approach for joint modeling is proposed by Altoontash (2004) which is based on implementation of nonlinear constitutive rules associated with shear panel deformations and slip of longitudinal reinforcement. Continuum modeling of joints is

another approach which is used more recently for seismic performance assessment. (Lowes (1999), Mitra (2008)). In this approach, additional interface elements are required for transition if the beams and columns are modeled using line elements and planar continuum elements are used to represent the joint region. Also, use of continuum-type elements in modeling columns and beams is possible while, this approach further increases the computational effort but offers a good potential for accurate and objective modeling of joints. It should also be mentioned about the continuum approach that, calibration of the models through the material constitutive parameters is required which is a challenging issue and the effects of assumptions about the material parameters need to be verified through parametric study.

1.3 Objective and Scope

Experimental and analytical research on suggested methods of codes and regulations is inevitable for development of adequate modeling parameters and acceptance criteria for seismic assessment and proper rehabilitation of existing buildings. In this respect, a research project funded by Scientific and Technological Research Council of Turkey (TUBİTAK) was initiated at the Structural and Earthquake Laboratory of Middle East Technical University in February 2010. The aim of the project is to develop the basis of revisions for performance-based evaluation procedures and strengthening methods of the Turkish Earthquake Code (2007) through experimental and analytical study. A series of pseudo-dynamic tests were conducted on the representative test frames of 3-story 3-bay reinforced concrete building. Following objectives are set forth in this study:

- Pseudo-dynamic testing of three reinforced concrete frame specimens representing different types of deficiencies.
- Calibration of continuum and discrete models of test specimens through numerical simulations and comparison of accuracies obtained from different modeling techniques.
- Investigation of local deformations components, their interaction and contributions to total response of structures using calibrated continuum models.
- Providing insight and directions for a better performance based design and assessment code.

- Estimation of plastic hinge lengths through continuum modeling in comparison with the experimental observations and proposed expressions in the literature.
- Evaluation of strain based nonlinear performance assessment procedure of Turkish Earthquake Code (2007) in light of experimental observations.

The experimental part of this research was conducted by a team of researchers at METU and it does not solely belong to the author. While the main focus of this thesis is numerical simulations, Chapter 2 briefly presents the results of experiments. Test results of specimens 1 and 2 were previously presented in other publications (Mutlu et. al. (2011), Mutlu et. al. (2012)). The results of the Specimen-3 are presented in this study for the first time. Numerical simulations of these three specimens are presented in the Chapter 3, in comparison with the experimental results and observations. Accuracies of two different modeling approaches are compared for each specimen representing different deficiencies and damage behavior. Local deformations parameters were studied in detail using calibrated nonlinear continuum models of the test frames. Performance evaluations of the specimens were conducted using the strain based method and the results are compared with the damages observed in the experiments. Finally in Chapter 4, summary and the main conclusions of this study are presented with further study recommendations.

CHAPTER 2

PSEUDO-DYNAMIC TESTING

2.1. General

Three specimens were built and tested at METU Structural Mechanics Laboratory as a part of a comprehensive research program on performance based design and assessment of RC buildings. This chapter summarizes the experimental results from that study. A prototype 3-story 3-bay reinforced concrete frame building was designed according to the regulations of Turkish Earthquake Code (TEC) (2007) for a residential building located in the first seismic zone on Z3 soil type. Three bay three story RC frame test specimens were scaled by ½ with respect to the typical interior frame of the prototype building which is 9.0 m high and 13.5 m wide. Specimens were named from one to three in the order of testing. One of the specimens (Specimen 2) was designed according to provisions of TEC (2007). For Specimen 1, concrete compressive strength was reduced to a code minimum value (20 MPa) and reinforcement was detailed such that transverse reinforcement would not satisfy the provision of TEC (2007), while keeping the other properties of the specimen same as Specimen 2. In this way, shear-flexure critical column deficiency was enforced. For the last specimen (Specimen 3), both reinforcement details and concrete compressive strength were changed to represent different deficiencies commonly observed in the Turkish building stock. These deficiencies were the lack of confining steel reinforcement, use of low strength concrete and plain longitudinal steel reinforcement. Further details of the test specimens are presented in the following sections.

Continuous pseudo-dynamic testing was employed for all specimens using synthetic ground motions compatible with the site-specific earthquake spectra developed for the city center of Duzce. Reliability of scaling of the test specimen and ground motions was verified by preliminary pushover and time-history analyses. It can be shown that the original ground motion series when compressed in time domain with a factor of $\sqrt{1/2}$ according to the similitude law, produces the desired earthquake demands on a ½ scaled specimen.

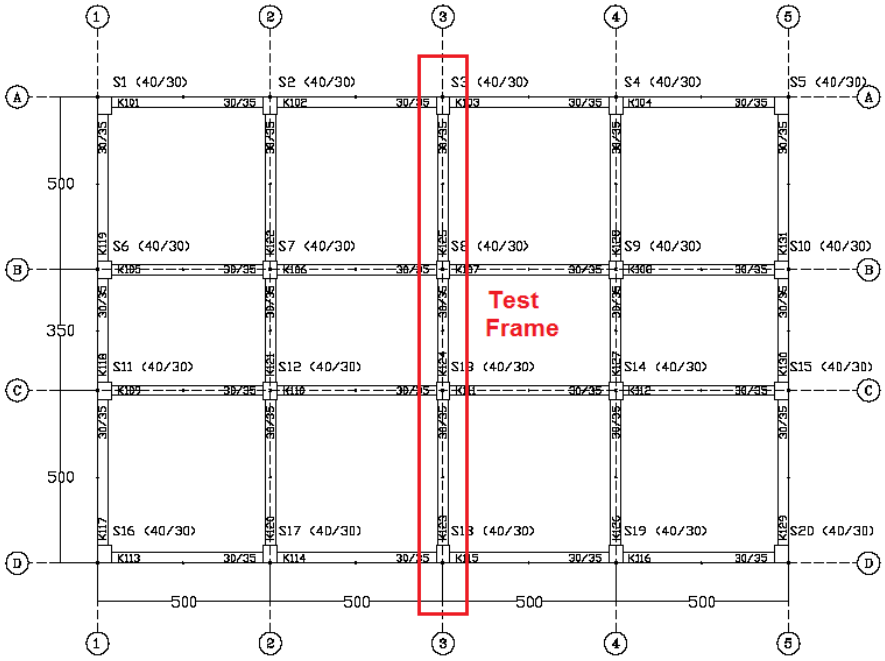

Figure 2. 1: Plan view of prototype building and test frame

2.2. Test Specimens

The dimensions of the test specimens were decided based on the dimensions of a prototype three story building with the floor plan shown in Figure 2. 1. First, the member sizes and longitudinal reinforcement details of this prototype building was designed according to the Turkish Earthquake Code (2007). The column dimensions were found as 400 mm x 300 mm for the building with about 2% longitudinal reinforcement ratio. The beam dimensions were 300 mm x 350 mm, being uniform in all spans. A typical interior bay frame (Figure 2. 1) was selected as the testing region. The dimensions of the members in the test specimen were taken as ½ of the prototype frame member sizes as shown in Figure 2. 2.

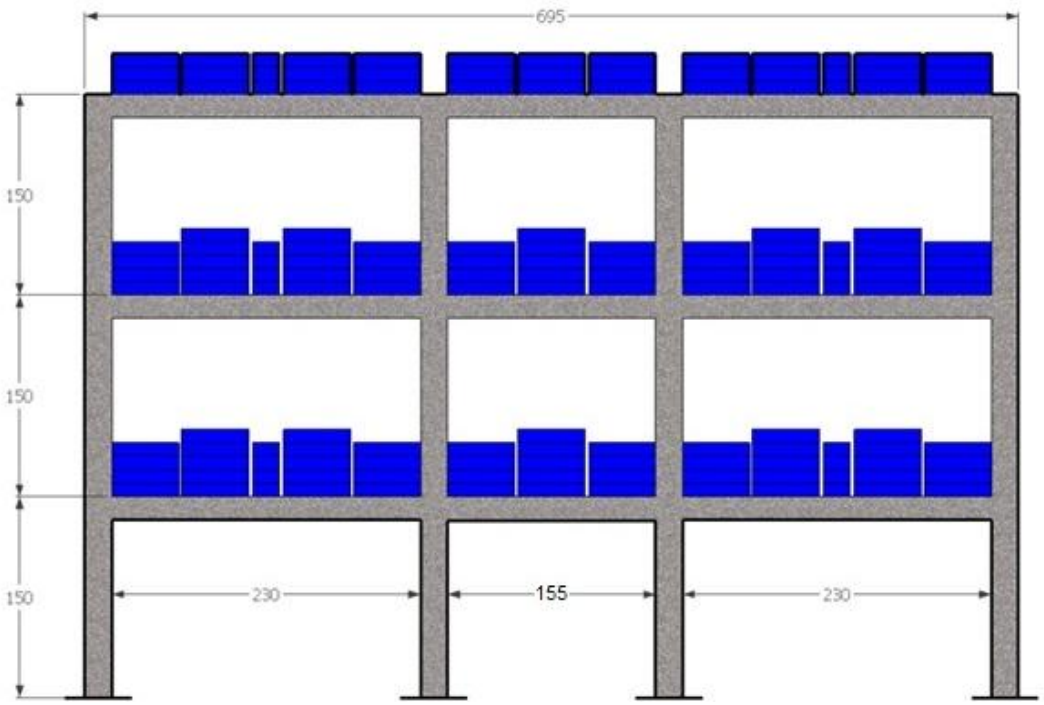

a) Elevation View

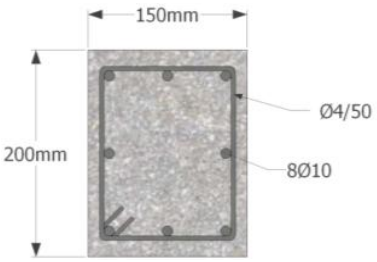

b) Column Cross Section

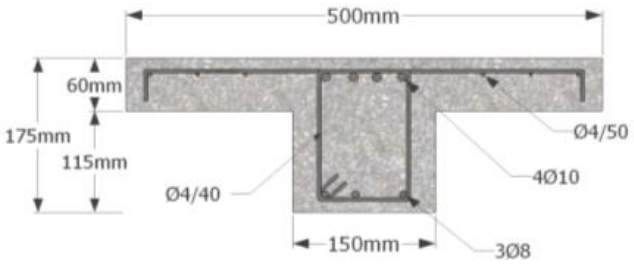

c) Beam Cross Section

Figure 2. 2: General view of test specimens

Three reinforced concrete frames were tested in the course of this study. The test frame with code compliant member sizes and reinforcement details was named as Specimen-2 and considered as the reference frame specimen for comparison with the other two deficient frames. Average uniaxial compressive strength of concrete used for Specimen-2 was 33.7 MPa. Deformed bars, used as longitudinal reinforcement, had yield strength of 480 MPa and plain bars, used as transverse reinforcement, had yield strength of 240 MPa determined from material tests. Detailed section drawings of Specimen-2, presented in Figure 2. 3, were the same for the elements in each story and each axis of the test frame.

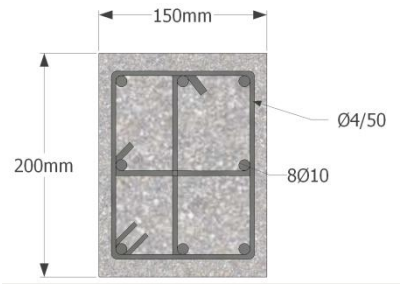

Column End-Regions

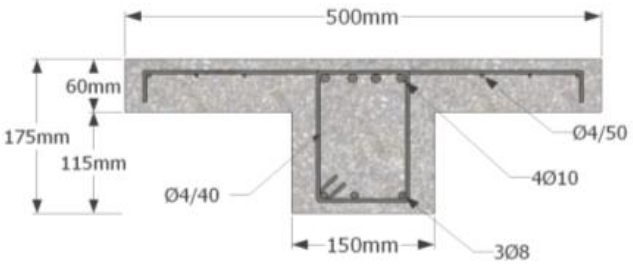

Beam Support Regions

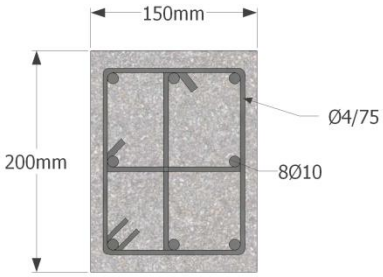

Column Mid-Regions

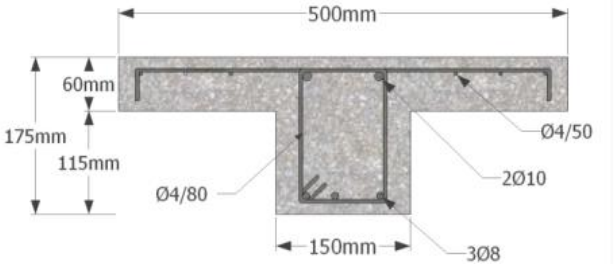

Beam Span Regions

Figure 2. 3: Specimen-2 column and beam section details

Specimen-1 had the same member dimensions as Specimen-2. For the columns of Specimen-1, the amount of column transverse reinforcement of Specimen-2 was reduced by removing the intermediate tie bars from the section and increasing the spacing between transverse reinforcements. Target uniaxial compressive strength of this specimen was set to a code minimum value of 20 MPa. In this way, the nominal shear capacity of columns were around 85% of the shear force demand calculated using the plastic moment capacities. In the calculation of shear force demand, the method proposed in Turkish Earthquake Code (2007) was employed. In this method, the shear force demand on a column ($V_e=(M_t+M_b)/l_n$) was determined by using the top and the bottom moments values (M_t *and* M_b). These moments were obtained by distributing the summation of plastic moment capacities of beams, connected to the joint, to the column ends in proportion to their stiffness. In the calculation of member end stiffness values, elastic lateral load analysis was used. For the bottom ends of the columns connected to the foundation, the plastic moment capacity (M_p) was directly taken as the bottom end moment (M_b).

The condition of inadequate shear capacity ($V_r < V_e$) corresponds to a shear-flexure combined failure mode according to ASCE/SEI-41. This failure mode is not included in Turkish Earthquake Code and it is considered as a perfectly brittle behavior. By employing such a modification in the column details of this specimen, it was aimed to observe deformation capacity of columns that are expected to fail in a flexure-shear mode. For Specimen 1, uniaxial compressive strength of concrete was determined as 20.2 MPa from cylinder tests. Deformed bars, used as longitudinal reinforcement, had yield strength of 480 MPa and plain bars, used as transverse reinforcement, had yield strength of 240 MPa determined from material tests. Section details of structural elements, which are the same for each story and each axis, are presented in Figure 2. 4.

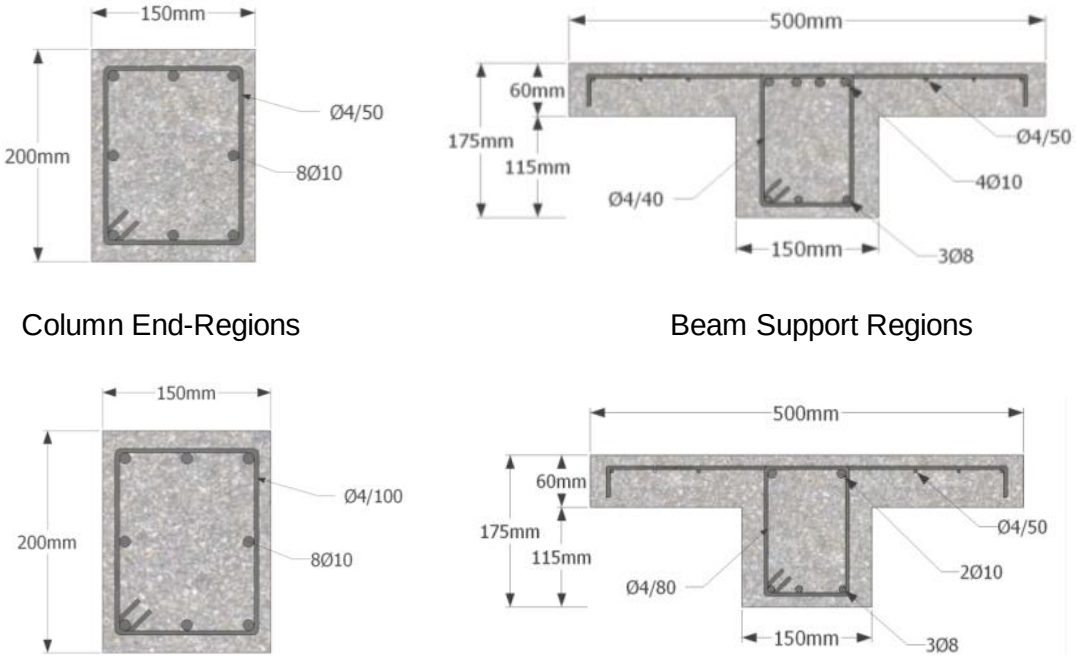

Figure 2. 4: Specimen-1 column and beam section details

Third and the last frame, Specimen-3, was obtained by keeping the member sizes same but changing the material strengths, reinforcement types, reinforcement details and joint details of the Specimen 1. Making such modifications in the design, it was aimed to reflect the commonly observed deficiencies of the Turkish Building stock. Specimen-3 contained different types of deficiencies obtained by changing materials and detailing of the reference frame Specimen-2. Column longitudinal

reinforcement was about 1.3%. Plain bars with 8 mm and 10 mm diameters were used for the columns and beams, respectively. The yield strength of 8 mm and 10 mm diameter bars were 320 MPa and 355 MPa, respectively. The ultimate strength of these bars were 460 and 555 MPa respectively. 4 mm plain bars used as transverse reinforcement were the same as the ones used in the other two specimens. Mean value of uniaxial compressive strength of concrete was determined as 11.9 MPa from cylinder tests for Specimen-3. Flexural and shear capacity of beams were set to be sufficient for gravity loads. Strong column-weak beam requirement was violated in this specimen. The transverse reinforcement spacing of the columns was kept constant through the column height which resulted in unconfined zones at element potential plastic hinge regions. Lateral reinforcements were absent at joints to reflect joint shear deficiencies. Detailed section and joint drawings of Specimen-3 are presented in Figure 2. 5. Detailing was the same for the elements in each story and each axis of the test frame.

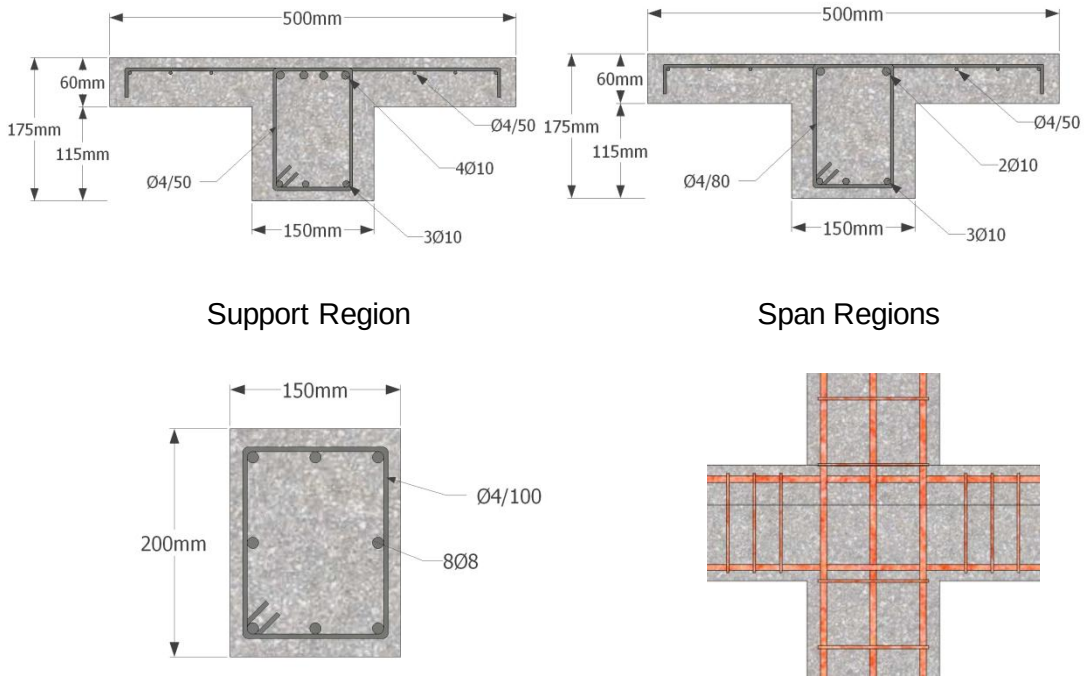

Figure 2. 5: Specimen-3 column, beam and joint details

Longitudinal and shear reinforcement details and moment capacities of columns and beams, calculated using the nominal strength values of all specimens, are presented in Table 2. 1 and

Table 2. 2 respectively. Table 2. 3 presents the shear capacities and capacity/demand ratios of the columns calculated using the nominal strength values (without using any safety factors) for the reference frame and for the two deficient frames according to TS-500 (2000), and ACI 318-11. It is important to remind that the longitudinal reinforcements used in columns and beams of Specimen-1 and Specimen-2 were deformed bars while the transverse reinforcements were plain bars for these specimens. However, plain bars were used as both longitudinal and transverse reinforcement in the Specimen-3.

Table 2. 1: Reinforcement details and moment capacities of columns

	COLUMNS				
	Reinforcement Details			Moment Capacities (kN.m)	
	Longitudinal	Lateral Reinforcement			
Specimen	Reinforcement	End Region	Mid Region	Mr	Mp
1	8Ø10 (def.)	2*Ø4/50	2*Ø4/100	24.6	28.3
2	8Ø10 (def.)	3*Ø4/50	3*Ø4/75	26.3	30.1
3	8Ø8 (pln.)	2*Ø4/200	2*Ø4/100	13.3	14.6

Table 2. 2: Reinforcement details and moment capacities of beams

	BEAMS							
	Reinforcement Details				Moment Capacities (kN.m)		Plastic Moment Capacities (kN.m)	
	Longitudinal		Transverse					
Specimen	Support	Span	Support	Span	Mr(i)	Mr(j)	Mp(i)	Mp(j)
1	4Ø10+3Ø8	2Ø10+3Ø8	Ø4/40	Ø4/80	22.3	10.5	23.6	13.2
2	4Ø10+3Ø8	2Ø10+3Ø8	Ø4/40	Ø4/80	23.0	10.7	25.1	13.3
3	4Ø10+3Ø10	2Ø10+3Ø10	Ø4/50	Ø4/80	17.0	11.5	19.2	16.6

Table 2. 3: Column shear capacities and capacity/demand ratios

	Shear Capacities		Shear Demands	Capacity/Demand Ratio Vr / Ve	
	TS-500	ACI 318-11			
	Vr (kN)	Vr (kN)	Ve (kN)	TS-500	ACI 318-11
SP1	32.0	30.6	36.6	0.87	0.84
SP2	48.8	47.0	38.7	1.26	1.22
SP3	27.0	25.9	25.9	1.04	1.00

2.3. Testing and Instrumentation

The dead and sustained live load on the prototype building and test frames were used to calculate the mass and gravity loads on the structure. In other words, the gravity loads and the floor mass were consistent in the test structures. Gravity loads were applied by using steel blocks for all test frames as shown in Figure 2.2.a. Steel blocks were arranged such that axial load ratios (i.e. ratio of axial load to the axial load carrying capacity of the column: $N_0=f_{ck}\ A_c$) of the columns in the prototype frame are similar to those of the test specimens. The axial load ratios of columns under gravity loads are presented in Table 2. 4.

Table 2. 4: Concrete strength and axial load ratios of columns

		N/No in Story 1	
Specimen	f_{ck} (mean) (MPa)	Inner Columns	Outer Columns
1	20.2	17.1	10.1
2	33.7	12.2	7.1
3	11.9	22.8	13.3

N: Axial Load due to steel blocks, N_o: Axial Load carrying capacity of columns $N_0=f_{ck}\ A_c$

Pseudo-dynamic testing is a hybrid simulation technique, in which, part of the structural properties are numerically modeled and rest of the structure is physically tested in parallel with computations (Takanashi et. al. (1975), Mahin and Shing (1985), Nakashima(1985)). This method emerged as an alternative to shake table testing by introducing the simplicity of quasi-static testing and made it possible to test large scale structures under seismic loads in a more economical way. Other advantages of the technique can be commented as the ability of observing the general behavior and damage formation of structures during the experiment and chance of holding the test at any time step for more detailed observations and evaluations in case of necessity. In each step of the experiment, restoring forces are measured by the load cells as in the case of quasi-static testing and this information is used together as a feedback with the pre-defined ground motion, mass, and damping properties for the step by step numerical integration of the equation of motion. The displacement excursions for the next step are calculated and applied to the degrees of freedom of the test structure by servo controlled hydraulic actuators. The methodology of the testing for the three degree of freedom test structure along with the view of the test specimen is presented in Figure 2. 6.

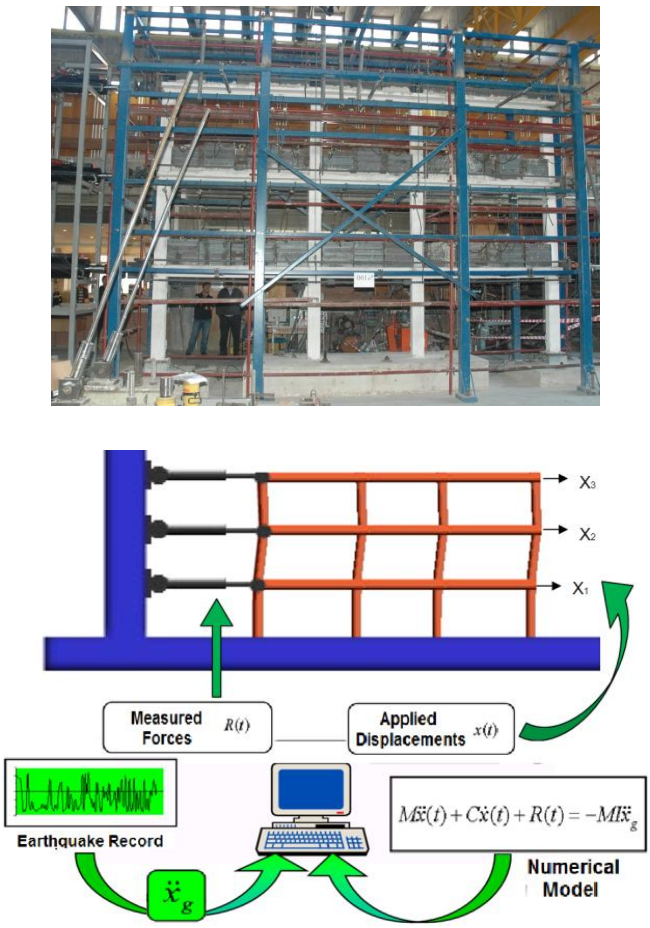

Figure 2. 6: Test Specimen and PsD Testing System Schema

Ground motions, employed for continuous Pseudo Dynamic Testing, were synthetic time-acceleration series for the center of Duzce which were generated within the scope of related work package of the research project. They were compatible with the site-specific earthquake design spectra for different probabilities of being exceeded on different soil classes as shown in Table 2. 5. Three of the generated acceleration series were used in the tests which were named as D1, D2 and D3. Acceleration time series with the sequence of application and corresponding spectra of the ground motions are shown in Figure 2. 7.

Table 2. 5: Ground motion properties

Earthquake	Probability of Being Exceeded in 50 years	Soil Class/Type	PGA (g)
D1	50 %	Z1 / Rock	0.254
D2	10 %	Z1 / Rock	0.545
D3	10 %	Z3 / Soft	0.604

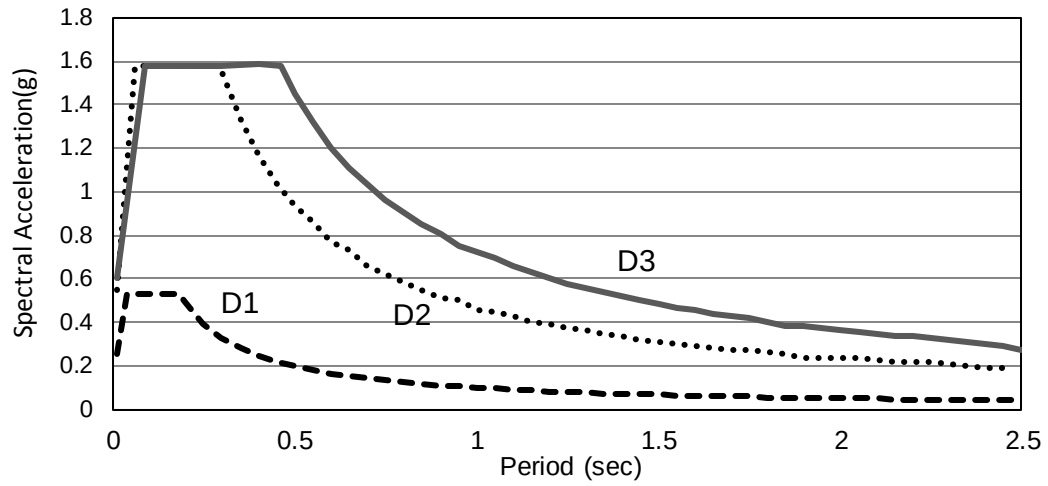

a) Design Spectra

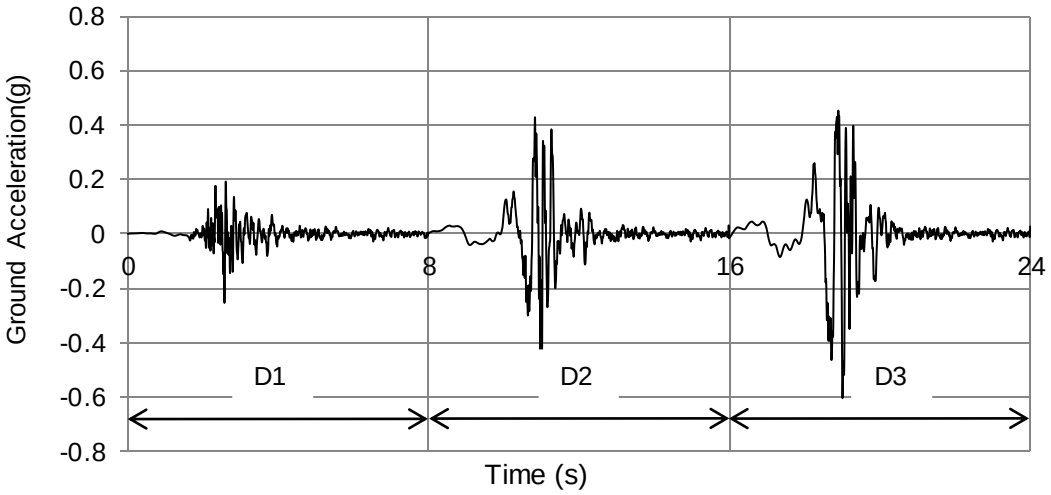

b) Acceleration-Time Series

Figure 2. 7: Ground motions and acceleration spectra

Reaction forces applied on the specimen were measured both by the PsD testing system and by a separate data acquisition system using load-cells connected to the actuators at each story level of the test frames. LVDT's placed at story levels were used to measure the lateral displacements of each story. In addition to the story displacements, curvatures and rotations at the bottom ends of 1st story columns and both ends of the beams of 1st and 2nd stories were measured using two LVDT's on opposite faces parallel to the direction of loading. Details of the instrumentation are shown in Figure 2. 8.

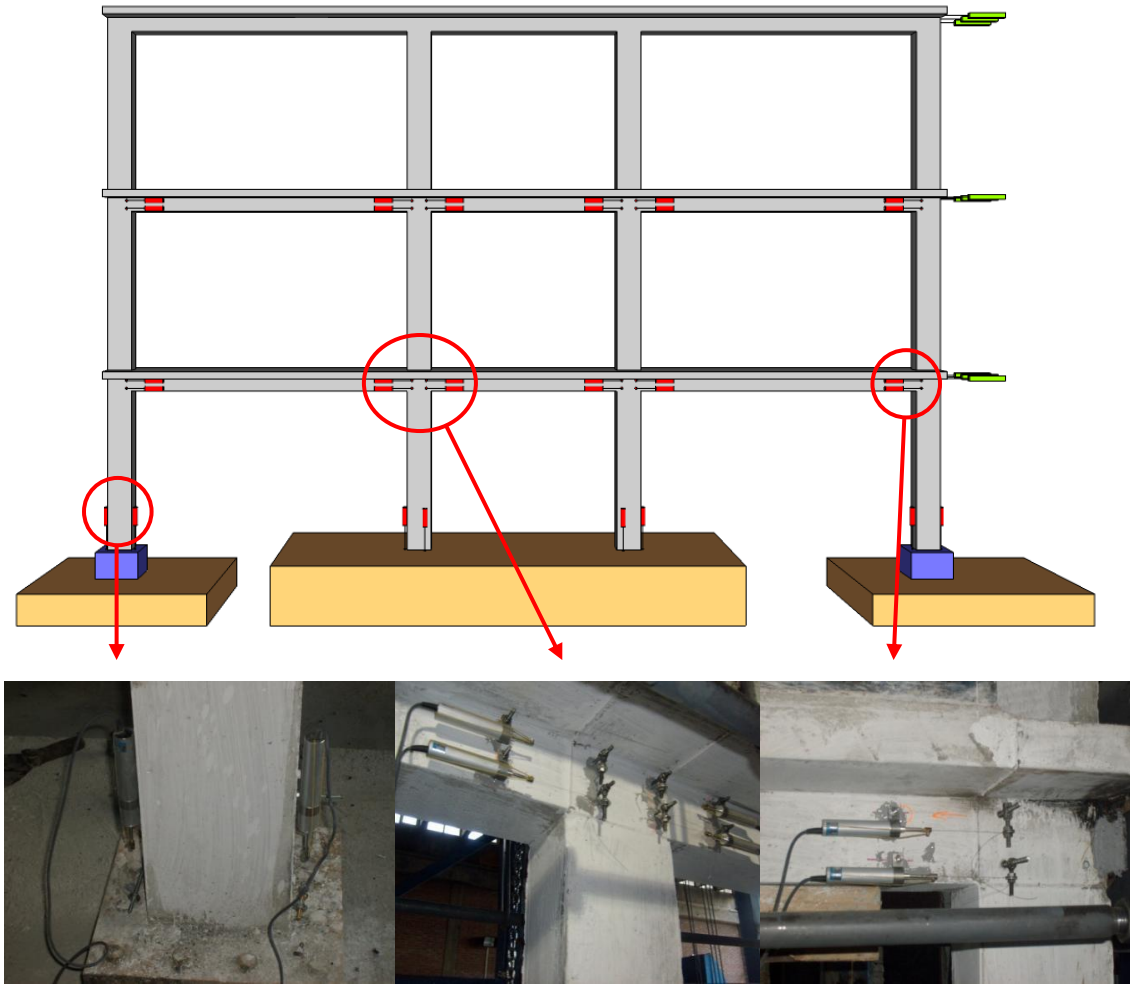

Figure 2. 8: Measuring instruments and their alignment

2.4. Test Results

Test results of the three specimens are presented in this section along with the damage picture of the specimens. Story displacements, inter-story drift ratios, story shear forces are the main global test results presented below. Local demands parameters such as member end rotations are discussed in the next chapter along with the numerical simulation results.

2.4.1. Specimen-1

Roof displacement response history obtained from tests is presented in Figure 2. 9 along with the damage patterns observed at some peak deformation instants. No damage, except some minor column base cracking, was observed during the D1 ground motion. Flexural cracking of columns, beams and inclined cracking at beam column joints were observed during D2 ground motion. In the final test (D3), wide flexural cracks indicating yielding of longitudinal reinforcement were observed. At the interior column bases, crushing and spalling of cover concrete was observed. When the roof displacement reached to 126 mm, inclined cracks on the interior columns, indicating flexural-shear critical nature of these columns, were observed.

Inter-story drift ratio responses of each story obtained from continuous pseudo-dynamic tests are presented in the Figure 2. 10. The ground motions D1, D2 and D3 demanded about 0.2%, 1.5% and 3.5% maximum inter-story drift ratios. The inter-story drift deformations were nearly uniform for D1 and D2 motions. In the D3 motion, large inter-story deformations concentrated at the first two floors due to the presence of physical damage observed in the first two stories. The time elapsed between two peaks (an indicator of the period as shown in Figure 2. 10) increased from D1 to D3 earthquake motions, exhibiting that the frame became more flexible with increasing ground motion intensities. Measured shear force versus inter-story drift ratio of each story and base shear versus roof displacement responses are presented in Figure 2. 11. It can be observed that none of the plots in this figure exhibit a sharp drop of lateral strength indicating that the structure was able to maintain its capacity without loss of strength up to about 3.5% inter-story drift, despite the formation of shear cracks. This actually contradicts the definition of “brittle failure mode” in the TEC (2007), since our test results show significant amount of deformability even the nominal shear capacity was below the estimated shear demands by about 15% and shear cracking was evident in the specimens.

Based on the subjective visual observations after each ground motion, the test can be in the minimum damage state, moderate damage state and severe damage state after ground motions D1, D2, and D3, respectively.

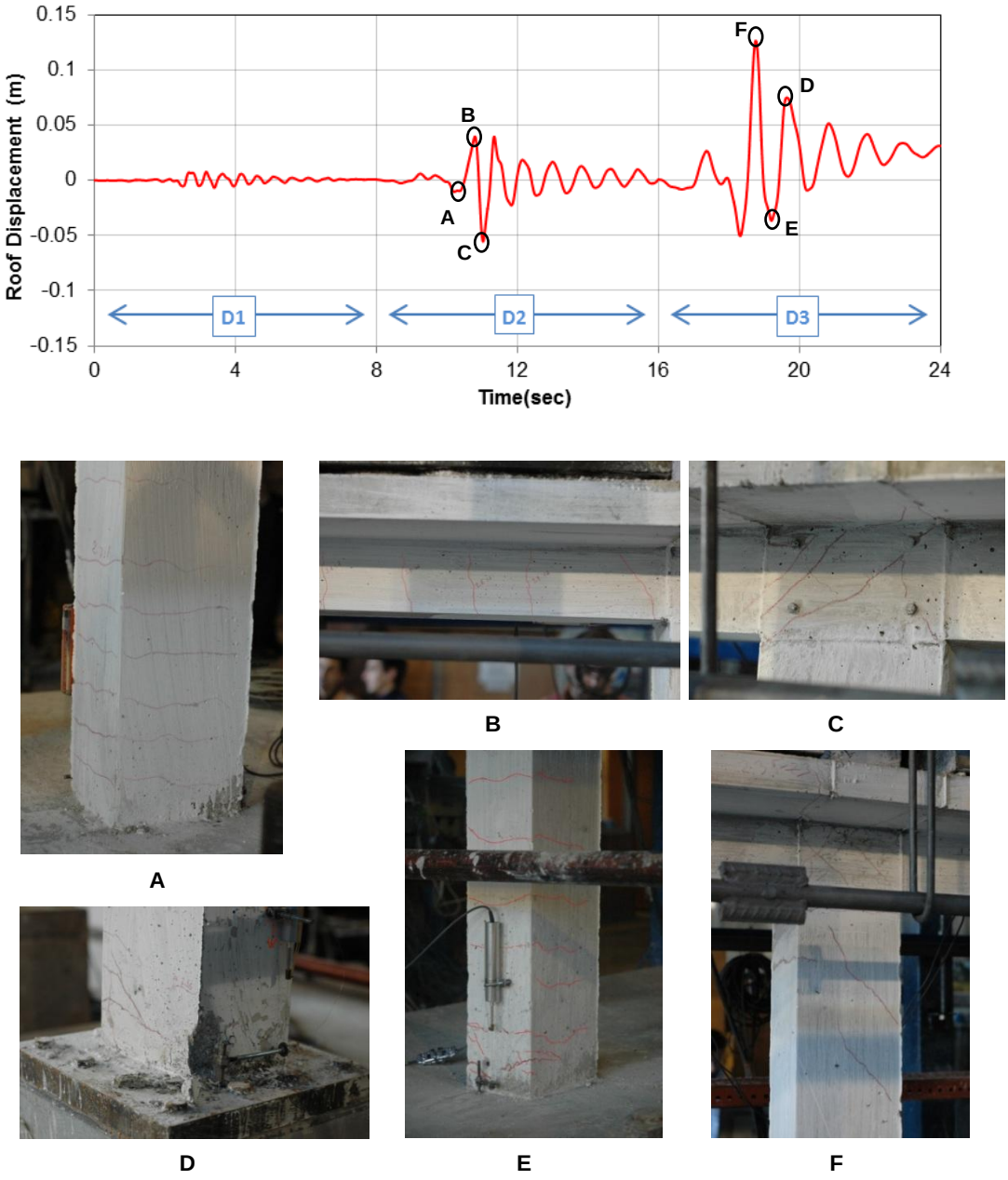

Figure 2. 9: Roof displacement history and observed damages for SP1

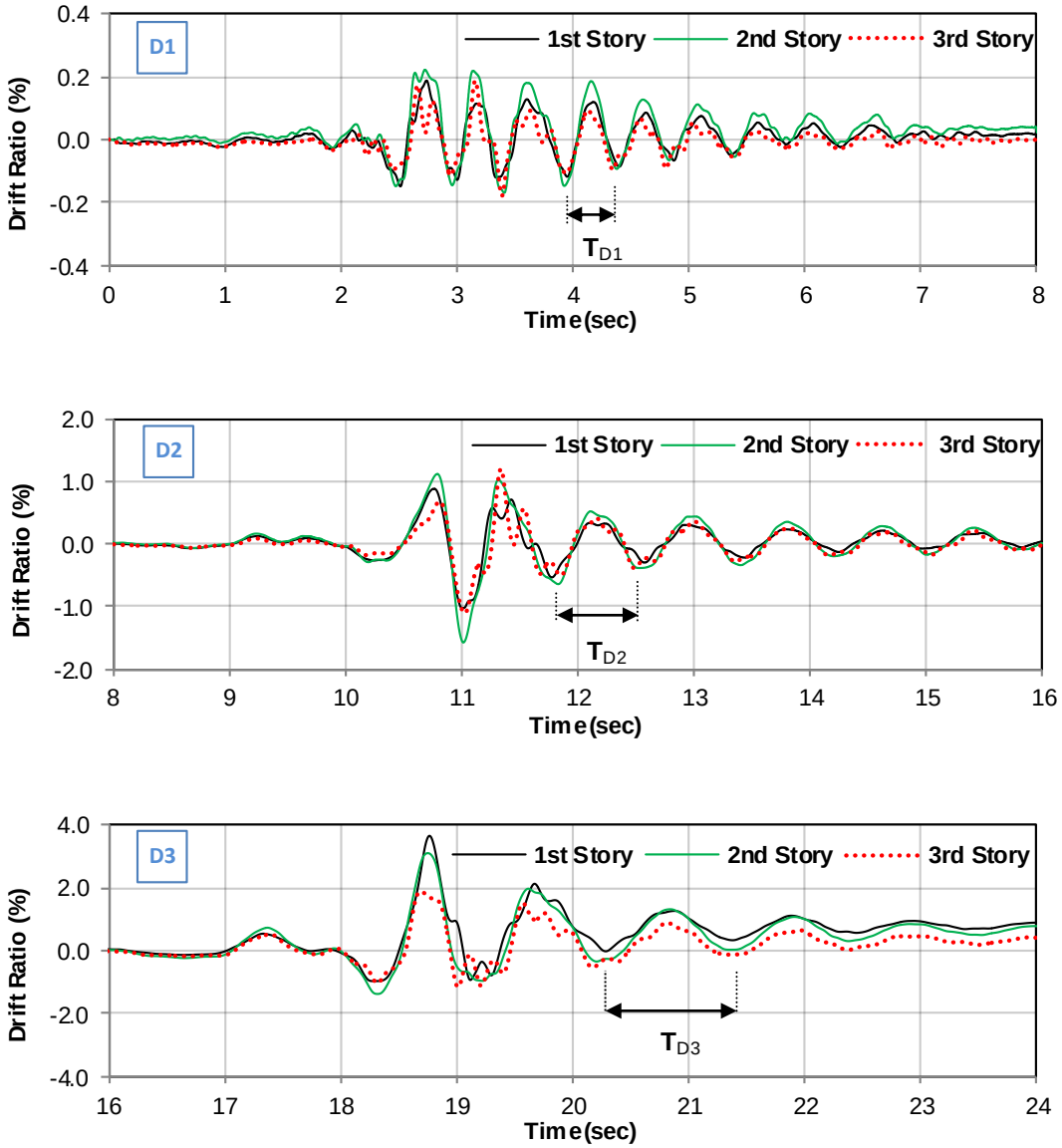

Figure 2. 10: Inter-story drift ratio response from each ground motion for SP1

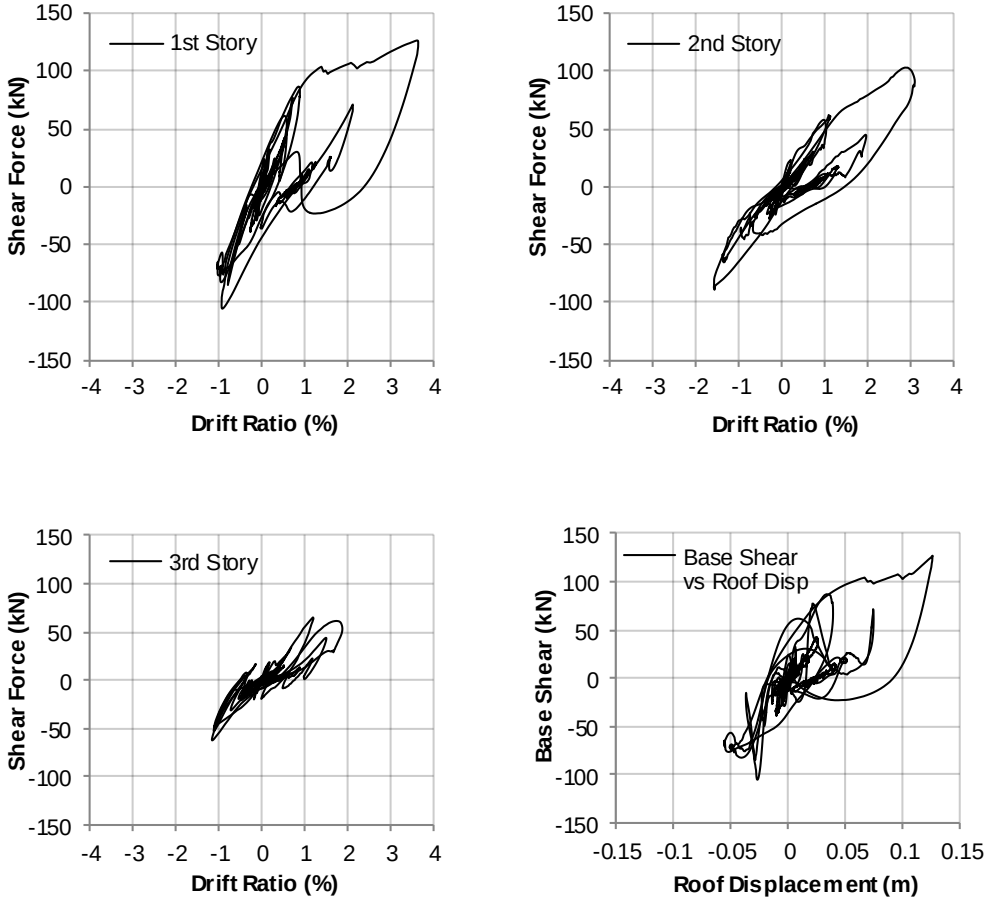

Figure 2. 11: Story shear force vs. drift response for SP1

2.4.2. Specimen-2

Roof displacement response history obtained from tests is presented in Figure 2. 12 along with the damage patterns observed at some peak deformation instants. No damage, except some minor column base cracking was observed during the testing of the specimen under D1 ground motion. Flexural cracking of columns, beams and inclined cracking at beam column joints were observed during D2 ground motion, similar to that observed in Specimen 1. In the final test (D3), wide flexural cracks indicating yielding of longitudinal reinforcement were observed. The inclined cracks at the beam column joints widened as shown in Figure 2. 12. Minor spalling was also observed at column bases during the D3 ground motion.

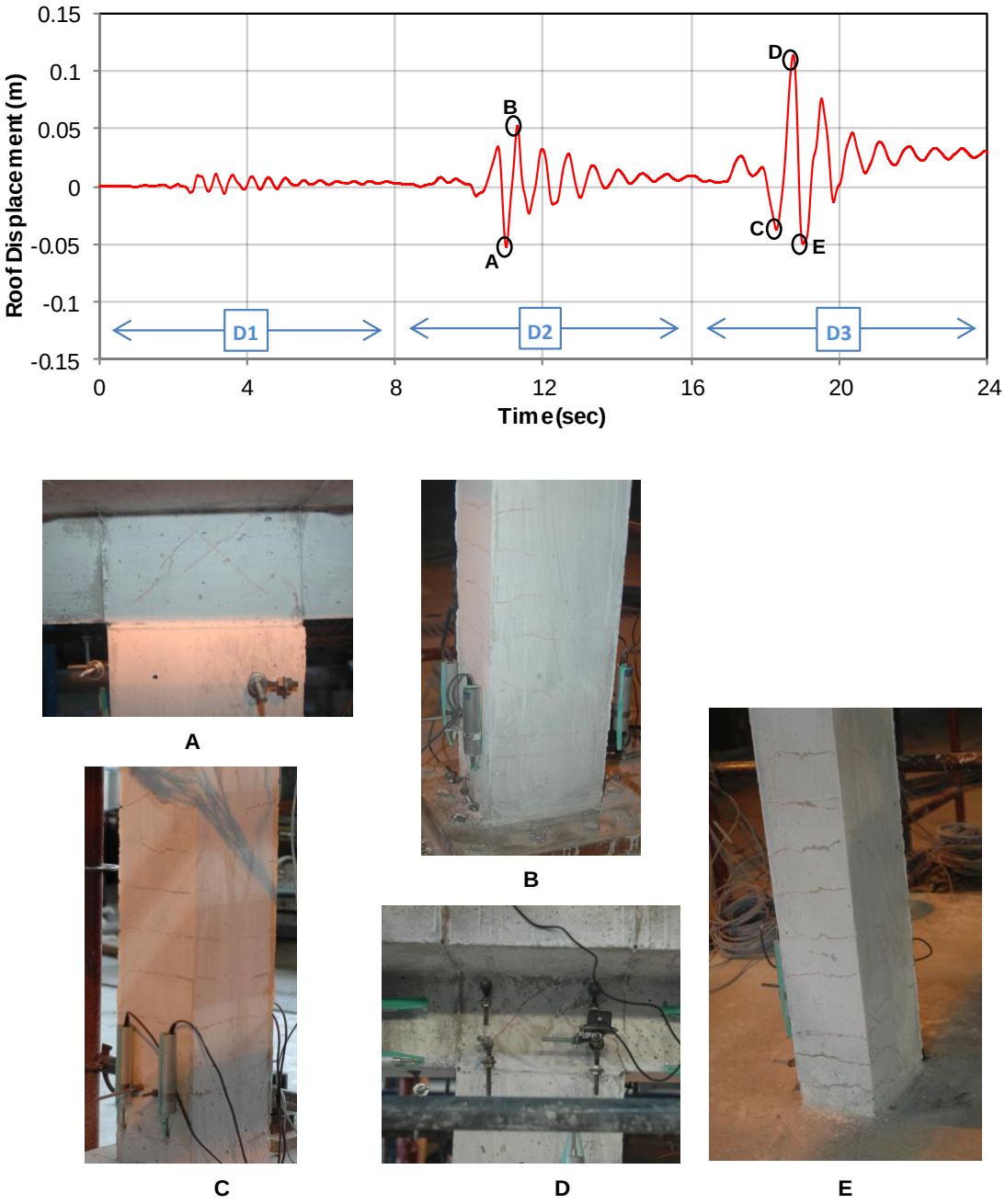

Figure 2. 12: Roof displacement history and observed damages for SP2

Inter-story drift ratio responses of each story obtained from continuous pseudo-dynamic tests are presented in the Figure 2. 13. The maximum inters-tory drift ratios during D1, D2 and D3 motions were 0.3%, 1.5% and about 3.5%, respectively. These maximum inters-tory deformation levels are similar to those obtained in Specimen 1 indicating the negligible influence of transverse reinforcement detail on the deformation demands for similar specimens. Measured shear force versus inter-

story drift ratio of each story and base shear versus roof displacement responses are presented in Figure 2. 14. The specimen exhibited a ductile response with good maintenance of the base shear capacity throughout the ground motions.

Based on the subjective visual observations after each ground motion, the test can be in the minimum damage state, moderate damage state and moderate damage state after ground motions D1, D2, and D3, respectively.

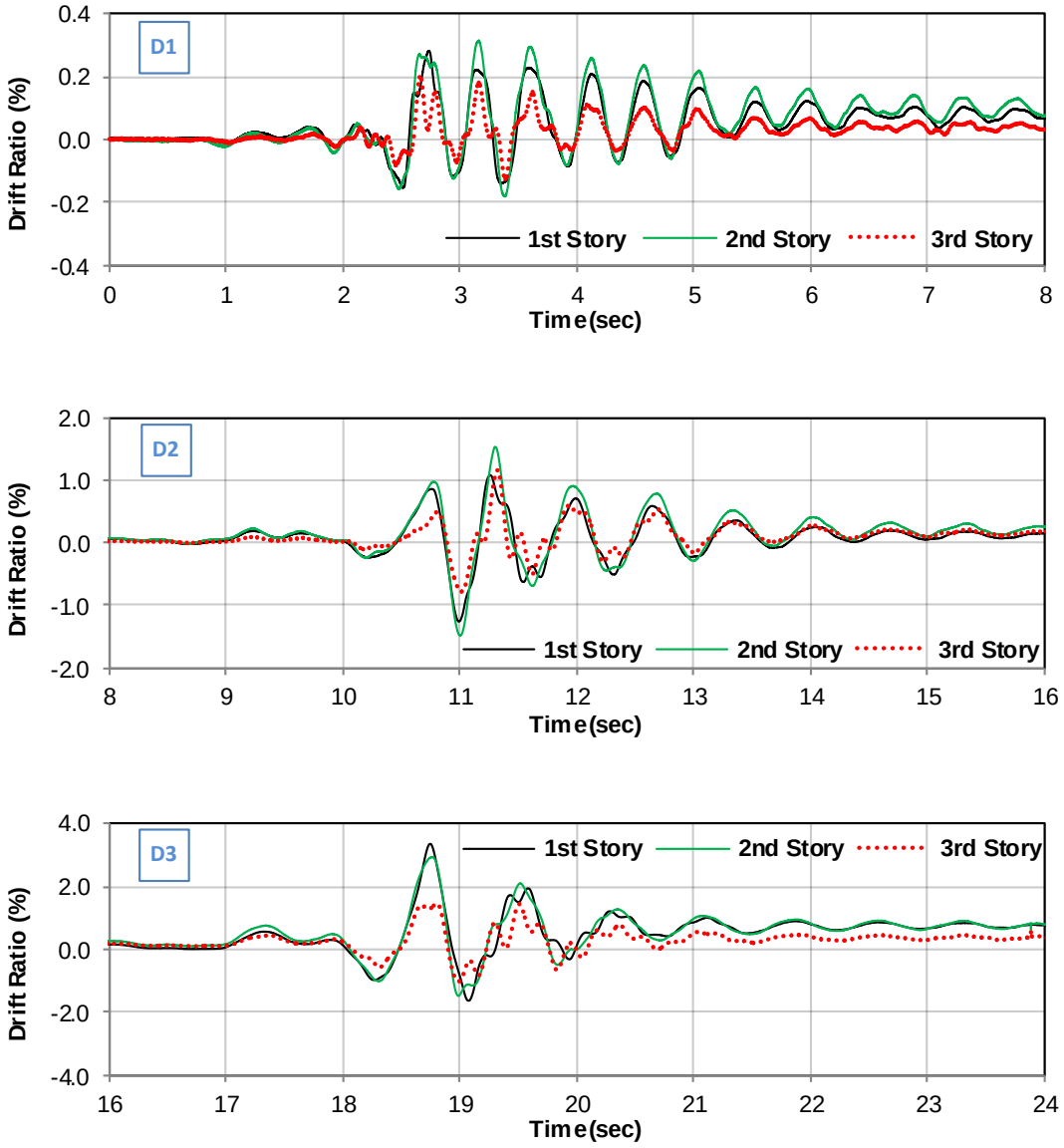

Figure 2. 13: Inter-story drift ratio response from each ground motion for SP2

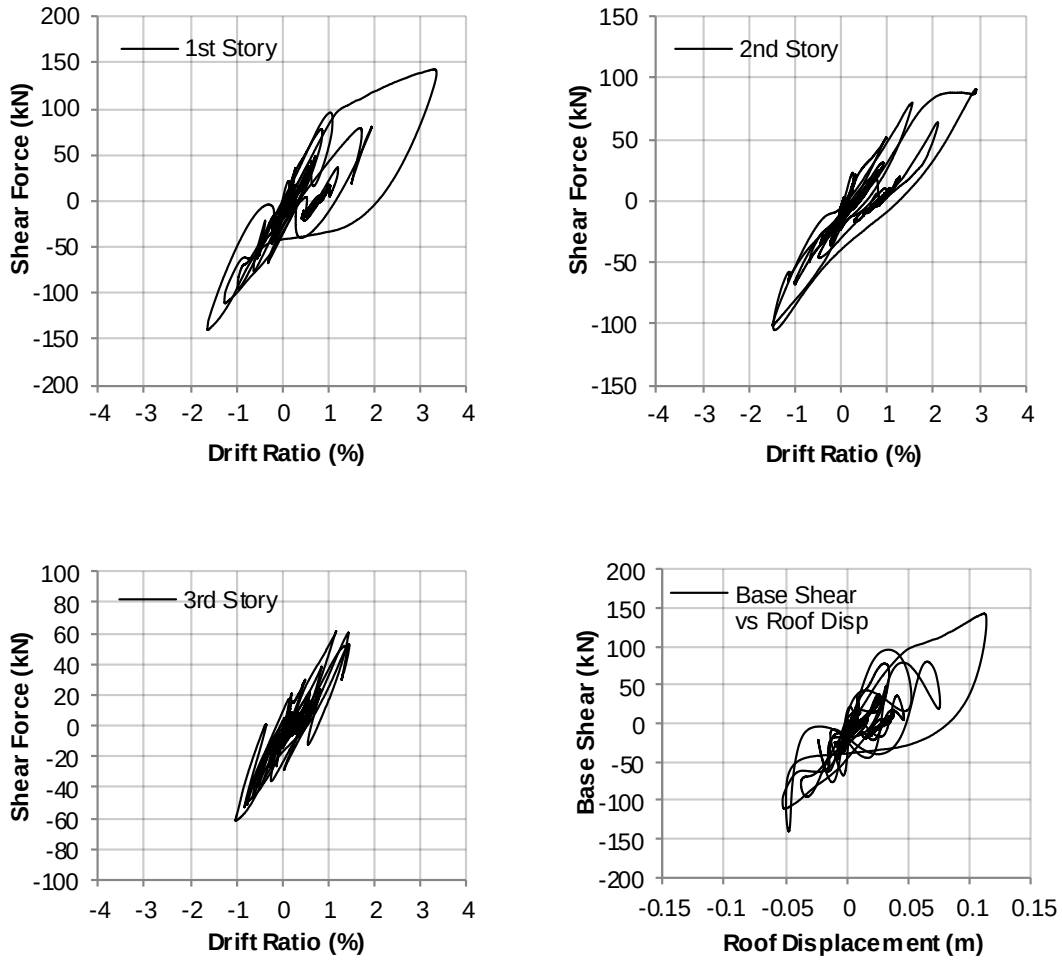

Figure 2. 14: Story shear force vs. drift response for SP2

Different from other two specimens, pseudo-dynamic test using 4th ground motion D4 was conducted on Specimen-2. Ground motion properties and test results including the ground motion D4 are presented in Appendix A, along with the numerical simulations.

2.4.3. Specimen-3

Roof displacement response history obtained from tests is presented in Figure 2. 15 along with the damage patterns observed at some peak deformation instants. Inter-story drift ratio responses of each story obtained from continuous pseudo-dynamic tests are presented in Figure 2. 17. Under the ground motion D1 with the smallest magnitude, no damage was observed on the test frame. Inter-story drift ratio was

measured to be under 0.3% for each story and the maximum roof displacement was recorded as 9.4 mm. The ground motion D2 resulted in a maximum inter-story drift ratio of 1.3% and maximum roof displacement of 49 mm on the specimen. Major damages observed under this ground motion were the flexural cracks in both interior and exterior columns of the 1st story and visible cracks in first story joint regions which initiated prior to the cracks in connecting beam and column ends. It was clearly observed that both of these damage formations were directly related to the deficiencies of lack of confinement in column ends and joint regions. These observations state that some inelastic deformations occurred in the first story and the specimen was in a moderate damage state. During the application of the third and the last ground motion D3, spread and widening of the cracks in bottom ends of columns were observed. Damage in the columns was followed by the spread of inclined cracks in the joint regions and flexural crack formations at the beam ends. Inter-story drift ratio of the first story reached a value of 4.1% in the peak acceleration part of the ground motion and the maximum roof displacement was measured as 206 mm. Meanwhile, spread of damage in the upper stories was observed in the form of shear cracks in the joints and flexural cracks in the upper ends of the 2nd and 3rd story columns. Inter-story drift ratio of upper stories reached the values of higher than 5% and which were even higher than the drift ratio value of the 1st story. These large deformations on the specimen mostly remained as residual displacements toward the end of the ground motion as can be seen clearly from both drift and roof displacement response plots. Large cracks observed at the top ends of 3rd story columns (Figure 2. 16) indicated the longitudinal reinforcement pull-out from unconfined joints. Considering the observations and measurements on the specimen, it was concluded that, the specimen experienced severe damage under the ground motion D3. Measured shear force versus inter-story drift ratio of each story and base shear versus roof displacement responses are presented in Figure 2. 18. It can be observed that severe strength degradation is present in the base shear-roof displacement plot. This shows that the specimen lost its lateral load carrying capacity exhibiting a softening response.

Based on the subjective visual observations after each ground motion, the test can be in the minimum damage state, moderate damage state and severe damage state (being at the verge of collapse) after ground motions D1, D2, and D3, respectively.

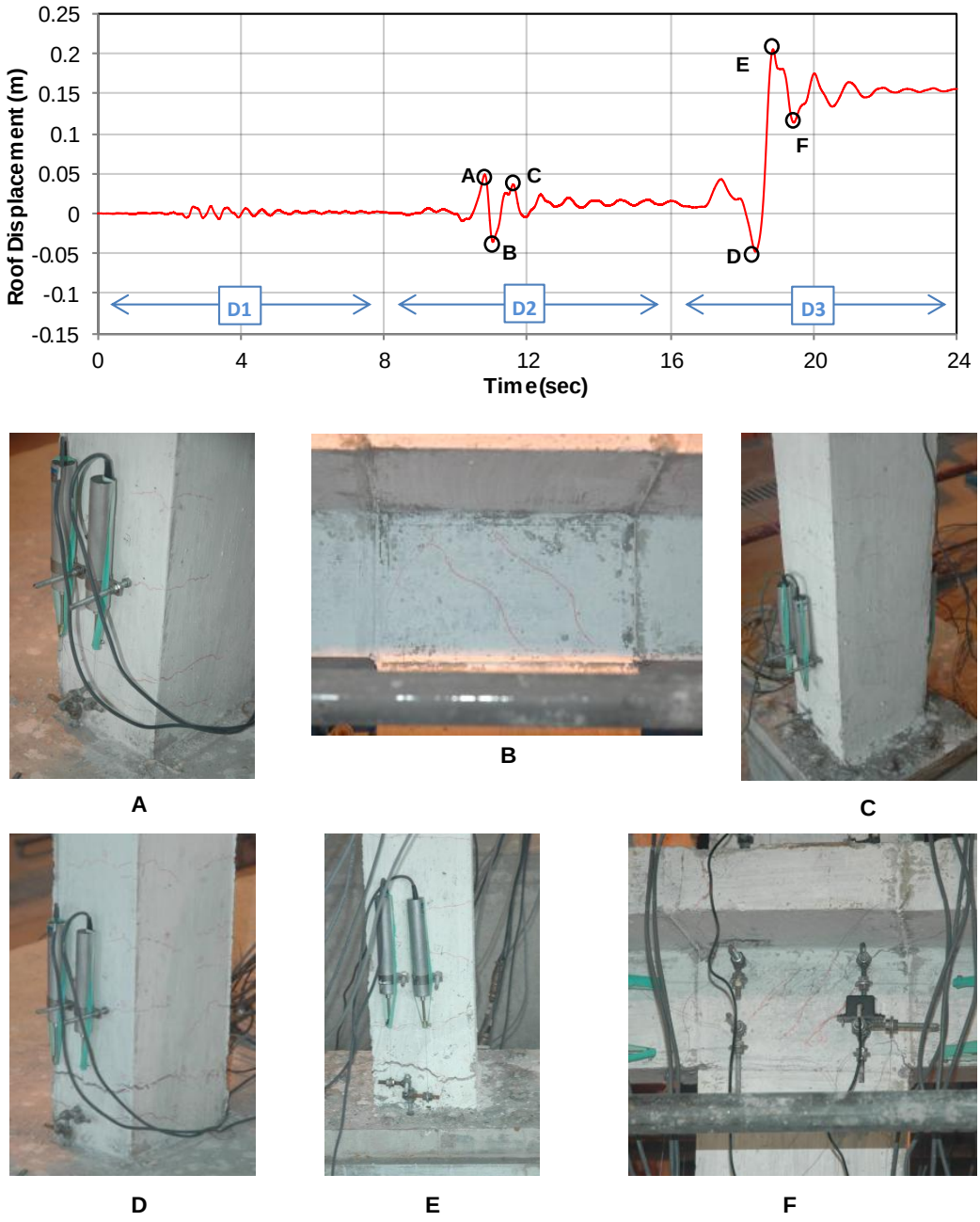

Figure 2. 15: Roof displacement history and observed damages for SP3

Figure 2. 16: Damage observations from 3rd Story Columns (SP3)

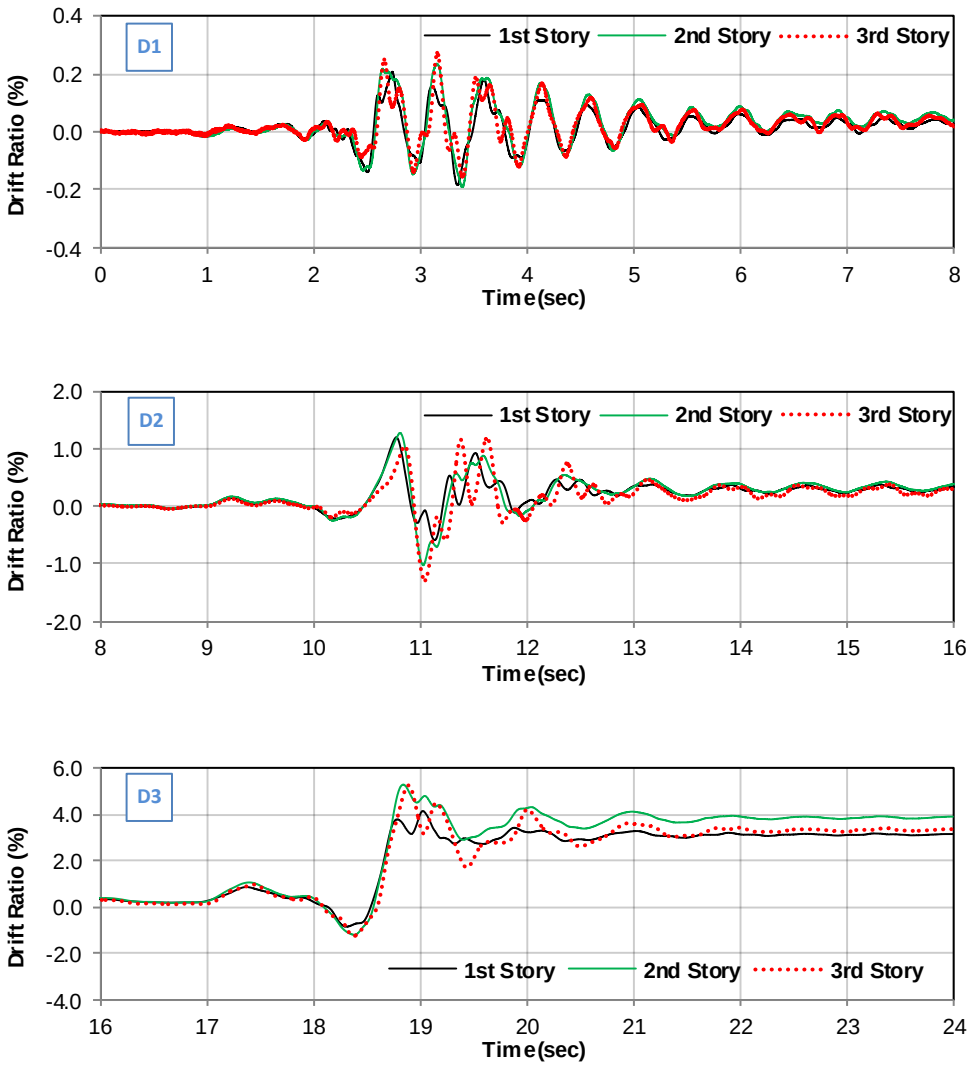

Figure 2. 17: Inter-story drift ratio response from each ground motion for SP3

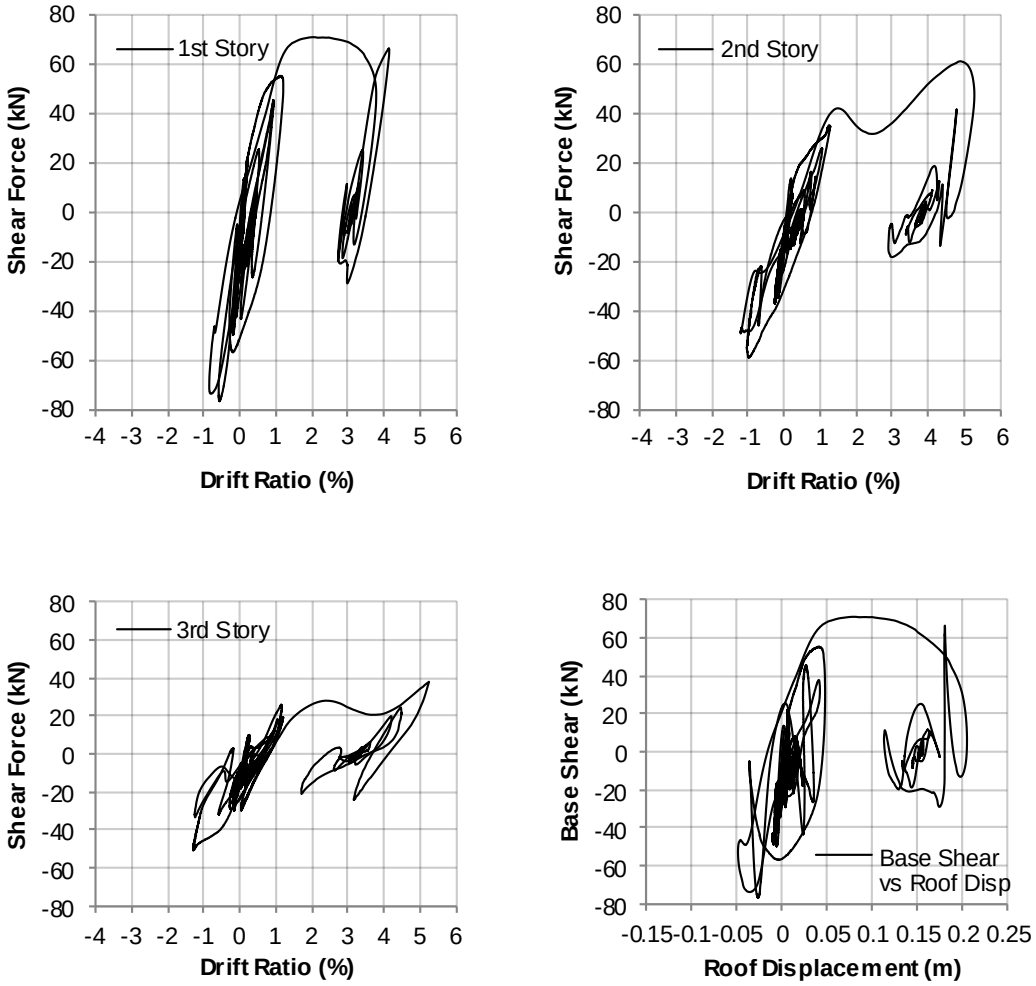

Figure 2. 18: Story shear force vs. drift response for SP3

2.5 Comparison of Test Results

Test performance of three test specimens was compared in terms of the 1st story drift ratio, base shear vs. roof displacement response and identified vibration periods of 1st mode to obtain the effects of deficiencies with reference to the code compliant design. The identification of time dependent periods of test frames was conducted according to the procedure of Molina et. al. (1999). In this procedure, experimental displacements **u**(n), velocities **v**(n) and restoring forces **r**(n), which are recorded

during the pseudo-dynamic testing, are related to each other using the following expression:

$$[\boldsymbol{u}^{\boldsymbol{T}}(\mathrm{n})\ \ \boldsymbol{v}^{\boldsymbol{T}}(\mathrm{n})\ \ \mathbf{1}]\,.\begin{bmatrix}\boldsymbol{K}^{\boldsymbol{T}}\\ \boldsymbol{C}^{\boldsymbol{T}}\\ \boldsymbol{o}^{\boldsymbol{T}}\end{bmatrix}=\boldsymbol{r}^{\boldsymbol{T}}(\mathrm{n}) \tag{2.1}$$

where ***K*** and ***C*** are secant stiffness and viscous equivalent damping matrices, ***o*** is a constant force offset term. The equation contains $2.ndof^2+ndof$ unknowns and the number of available equations is *N*.*ndof*, for *N* time intervals. Therefore, satisfying the condition of $N>2.ndof+1$ and estimating ***K*** and ***C*** by a least squares solution, the complex eigen-frequencies and mode shapes can be obtained by solving the generalized eigenvalue problem given by:

$$\boldsymbol{s}\begin{bmatrix}\boldsymbol{C} & \boldsymbol{M}\\ \boldsymbol{M} & \mathbf{0}\end{bmatrix}\boldsymbol{w}+\begin{bmatrix}\boldsymbol{K} & \mathbf{0}\\ \mathbf{0} & -\boldsymbol{M}\end{bmatrix}\boldsymbol{w}=\mathbf{0} \tag{2.2}$$

where, ***M*** is the theoretical mass matrix, ***w*** represents the eigenvectors, and ***s*** represents the conjugate couples of eigenvalues.

1st story drift histories of test frames are presented in Figure 2. 19 for each ground motion. Base shear vs. roof displacement responses are compared in Figure 2. 20 and maximum measured values of these response parameters are given in Table 2. 6. Figure 2. 21 presents the identified 1st mode period variations.

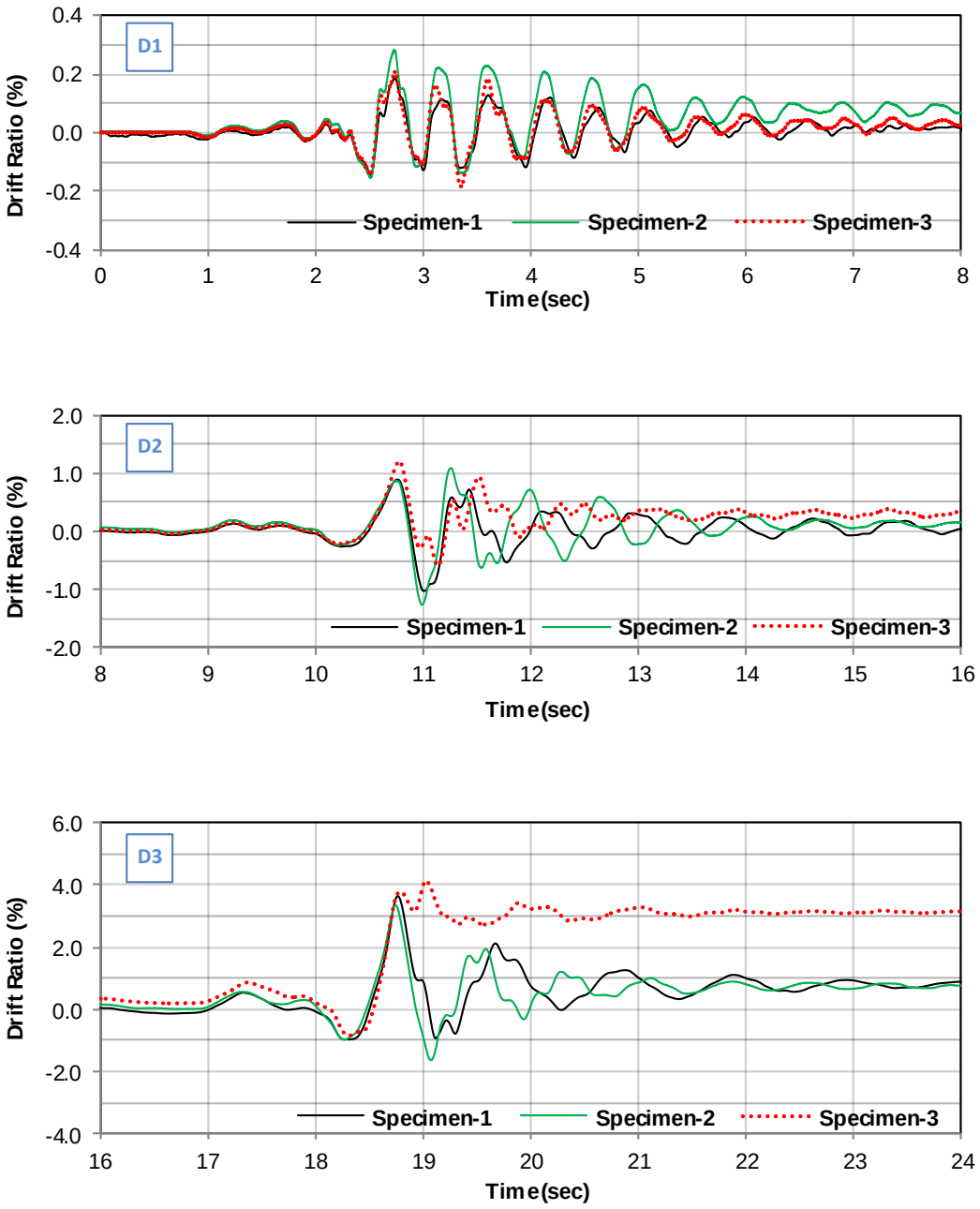

Figure 2. 19: 1st Story drift vs. time response comparison of specimens for each ground motion

It can be observed that response is similar for all specimens during D1 and D2 ground motions. However, during the D3 motion, the major difference is the residual deformations observed in Specimen-3. This can be attributed to the major structural deficiencies that result in significant strength degradation and less energy dissipation as shown in Figure 2. 20.

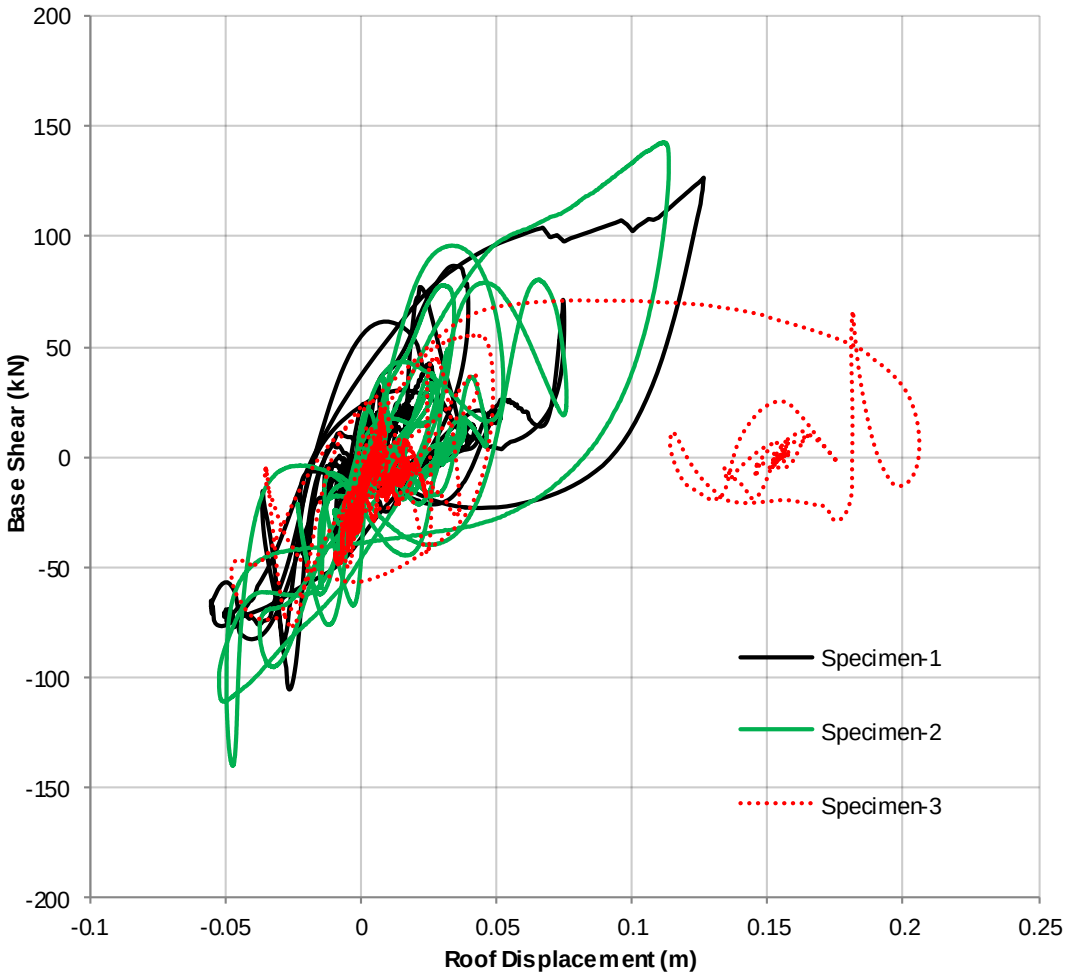

Figure 2. 20: Base shear vs. roof displacement comparison of specimens

Table 2. 6: Maximum Base Shear, Roof Displacement and 1st Story Drift Comparison

Ground	Max. Base Shear(kN)			Max. Roof Displacement(mm)			Max. 1st Story Drift (%)		
Motion	SP-1	SP-2	SP-3	SP-1	SP-2	SP-3	SP-1	SP-2	SP-3
D1	32.3	36.2	49.7	7.7	10.7	9.4	0.19	0.28	0.21
D2	86.8	111.0	76.8	55.4	52.5	48.7	1.02	1.26	1.21
D3	126.8	142.9	73.8	126.4	113.5	206.0	3.64	3.35	4.14

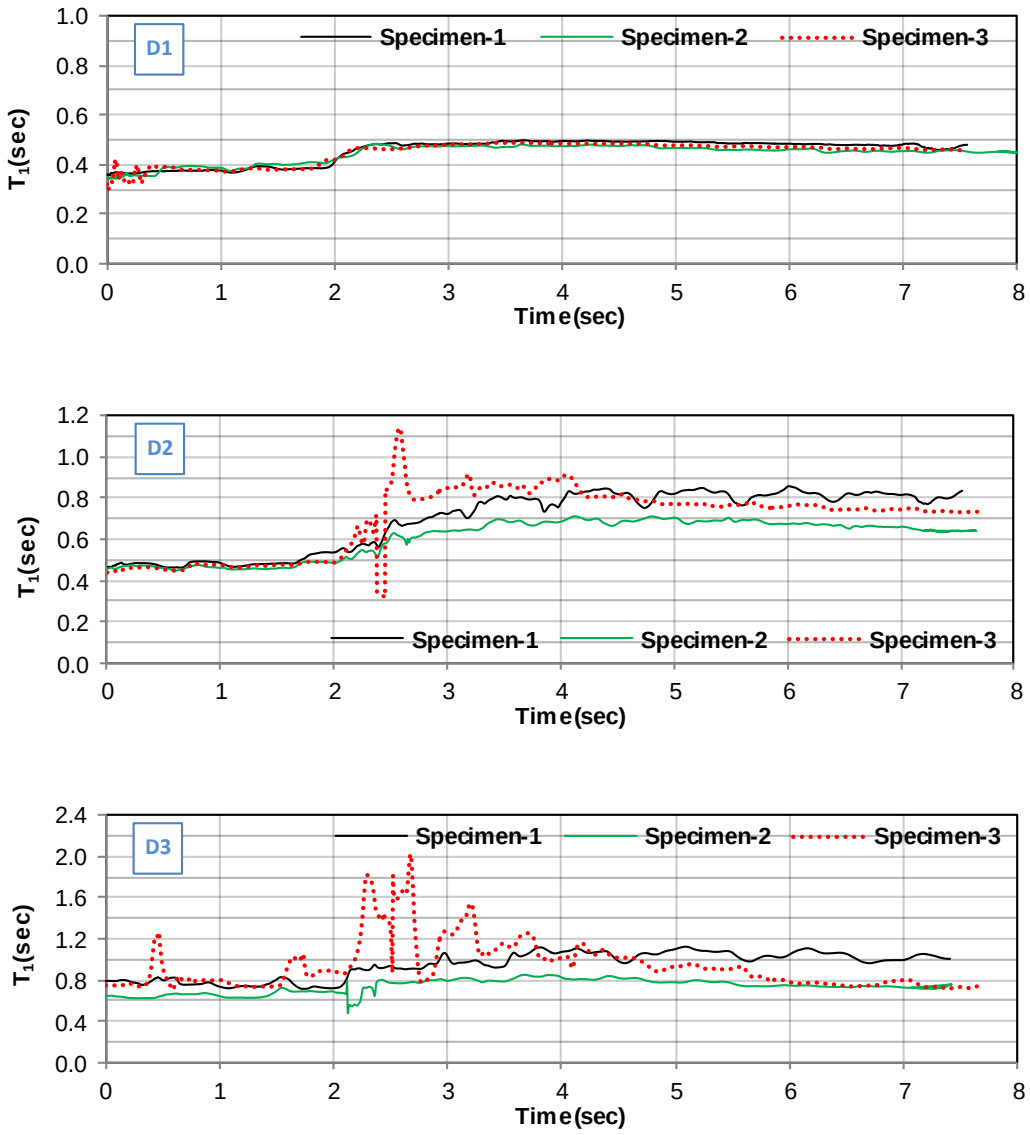

Figure 2. 21: Identified 1st mode period vs. time

The identified period of all of the test frames was about 0.35 sec. in the beginning of D1 test. Towards the end of D1 motion, the period elongated to 0.5 sec. due to cracking. The inelastic deformations, occured during D2 test, caused the period to elongate to 0.8 sec. It was observed that the period-time curve for Specimen-3 exhibited some oscillations and spikes that can be correlated with large inelastic actions between the seconds 2 and 4. During the D3 motion, period was identified as changing between 0.8 and 1.0 sec. throughout the ground motion. The identified period of Specimen-3 contained some major spikes between the seconds 2 and 4. The period elongated up to 2 sec. for Specimen-3 during the D3 motion.

These results show that, the larger the inelastic actions occur the longer was the identified periods. During the 2-4 seconds of D2 and D3 ground motions, there were some sudden jumps in period for Specimen-3, which can be related to the extensive damage. The decrease in the period of Specimen-3 through the end of D3 motion can be related to changes in stiffness due to reloading after large amounts of residual displacements that the specimen experienced.

CHAPTER 3

NUMERICAL SIMULATIONS OF THE TEST SPECIMENS

Numerical simulations of the pseudo dynamic tests for each specimen were carried out by employing two different modeling techniques. In Model-A, a continuum approach was taken to model the test frames, i.e. two-dimensional nonlinear plane stress elements with embedded reinforcements were employed. In Model-B, force-based frame elements defined with nonlinear fiber sections at integration points were used for the simulations. In this way, the ability of numerical simulations to estimate observed engineering demand parameters and damage states were evaluated by using models with different degrees of sophistication. The observed performance of the test frames were also compared with the performance estimations obtained using the numerical simulations along with TEC (2007) limit states.

3.1. Numerical Modeling

3.1.1. Model A

Nonlinear time history analyses of the 2-D models were performed to examine the ability of estimating the global dynamic response of the test frames obtained in Pseudo-Dynamic tests. TNO DIANA Release 9.3 (2008) Finite Element Analysis software was utilized for generating the Model A for the test frames. The specimen

was modeled using the CQ16M element, which is an eight-node quadrilateral isoparametric plane stress element based on quadratic interpolation and Gauss integration. The element has 8 nodes having 2 degrees of freedom and 3 x 3 Gauss integration scheme was employed for the solution. Concrete cracking behavior was modeled using Total Strain Crack Models that was originally proposed by Vecchio & Collins (1986) which is well suited for Serviceability and Ultimate Limit State analyses of reinforced concrete structures which are known to be predominantly governed by cracking or crushing of the material.

There are two concepts available for the total strain cracking approach, which are fixed crack concept and rotating crack concept. In the fixed crack concept, stress-strain relationships are evaluated in a fixed coordinate system upon cracking and it is necessary to model the degradation of shear behavior along the cracks. On the other hand, in the rotating crack model, which was used in this study, direction of the principal stress is assumed to coincide with the direction of principal strain (Figure 3. 1). As a result, no shear strain occurs perpendicular to cracking and only two normal stress components may be calculated using uniaxial stress-strain models.

In the total strain crack models, the strain vector ε_{xyz} in the element coordinate system "xyz" is updated in each step using the strain increment $\Delta\varepsilon_{xyz}$ according to:

$$^{t+\Delta t\ i+1}\boldsymbol{\varepsilon}_{xyz} = {}^{t}\boldsymbol{\varepsilon}_{xyz} + {}^{t+\Delta t\ i+1}\Delta\boldsymbol{\varepsilon}_{xyz} \tag{3.1}$$

The strain vector in element coordinates "xyz" is transformed to strain vector in the crack directions "nst" with the strain transformation matrix **T**,

$$^{t+\Delta t\ i+1}\boldsymbol{\varepsilon}_{nst} = \mathbf{T}\ {}^{t+\Delta t\ i+1}\boldsymbol{\varepsilon}_{xyz} \tag{3.2}$$

The strain transformation matrix **T** is fixed upon cracking in a fixed concept, whereas it depends on the current strain vector in the coaxial rotating crack concept:

$$\mathbf{T}=\mathbf{T}\left(\ {}^{t+\Delta t\ i+1}\boldsymbol{\varepsilon}_{xyz}\ \right) \tag{3.3}$$

In both concepts, compressive stress is evaluated in the rotated coordinate system. However, in a fixed concept case, the behavior in compression is evaluated in the fixed coordinate system which is decided on the direction of cracks. The constitutive model is formulated in the cracked coordinate system that is given by:

$$^{t+\Delta t\ i+1}\boldsymbol{\sigma}_{nst} = \sigma\ \left(\ {}^{t+\Delta t\ i+1}\boldsymbol{\varepsilon}_{nst}\ \right) \tag{3.4}$$

Updated stress vector in the element coordinate system is finally given by:

$$^{t+\Delta t}{}_{i+1}\boldsymbol{\sigma}_{xyz} = \mathbf{T}^{T}\ {}^{t+\Delta t}{}_{i+1}\boldsymbol{\sigma}_{nst} \tag{3.5}$$

Summary of the formulation of rotating crack concept in 2-D is summarized in the following part. The stiffness matrix [*k*] of an individual element is constructed by using the material stiffness matrix [*D*] which is required to relate stresses to strains (Equations 3.6, 3.7). In the rotating crack concept, the material stiffness matrix which is defined with respect to the global coordinate system X, Y is determined by using appropriate transformation after combining the contributions of concrete and reinforcement components. They are defined in element coordinate system x, y as shown in Figure 3. 1. Material stiffness matrices for concrete component $[D_c]'$ (Equation 3.6) and each of the reinforcement components $[D_s]_i'$ (Equation 3.7) are defined seperately to take into account the anisotropy of materials (Equation 3.8). Using the principal axes system 1, 2 of the cracked reinforced concrete, principal average tensile strain (ϵ_{c1}) and principal average compressive strain (ϵ_{c2}) are calculated. Afterwards, stiffness matrix in the global coordinate system is calculated by using transformations (Equations 3.9, 3.10).

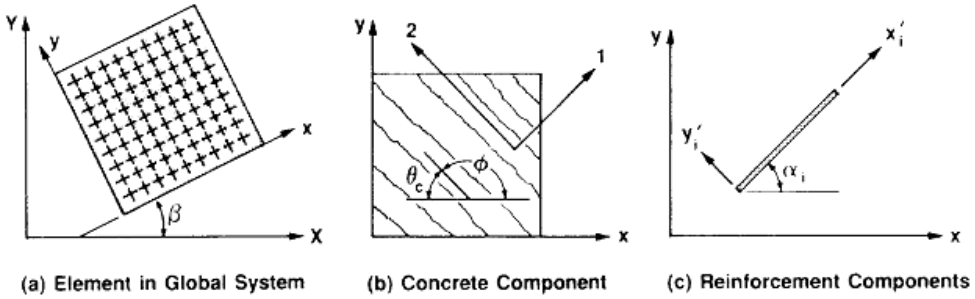

Figure 3. 1: Reference coordinate systems for elements

$$[D_c]' = \begin{bmatrix} \bar{E}_{c2} & 0 & 0 \\ 0 & \bar{E}_{c1} & 0 \\ 0 & 0 & \bar{G}_c \end{bmatrix} \tag{3.6}$$

$$[D_s]_i' = \begin{bmatrix} \rho_i \bar{E}_{si} & 0 & 0 \\ 0 & 0 & 0 \\ 0 & 0 & 0 \end{bmatrix} \tag{3.7}$$

$$[D] = [D_c] + \sum_{i=1}^{n} [D_s]_i \tag{3.8}$$

$$[D_c] = [T_c]^T [D_c]' [T_c] \tag{3.9}$$

$$[D_s]_i = [T_s]_i^T [D_s]_i' [T_s]_i \tag{3.10}$$

where the secant moduli for concrete and steel are;

$$\bar{E}_{c1} = \frac{f_{c1}}{\epsilon_{c1}} \qquad \bar{E}_{c2} = \frac{f_{c2}}{\epsilon_{c2}} \qquad \bar{G}_c = \frac{\bar{E}_{c1} \cdot \bar{E}_{c2}}{\bar{E}_{c1} + \bar{E}_{c2}} \qquad \bar{E}_{si} = \frac{f_{si}}{\epsilon_{si}}$$

Reinforcement steel was modeled as embedded reinforcements which do not have degrees of freedom on their own but add stiffness to the finite element model. In this modeling technique, reinforcing bars assumed not to occupy any space or mass in the finite element model and the mother elements do not provide any weight or stiffness resulting from the addition of embedded bars. Reinforcement strains are computed from the displacement field of the mother elements assuming perfect bond with surrounding material. Nonlinear compression behavior of the concrete material was defined as a parabolic function of stress and strain which is based on compressive fracture energy. The tensile behavior of concrete was defined by linear elastic brittle stress-strain function based on the tensile strength as shown in Figure 3. 2. Unloading and reloading behavior was modeled with the secant approach, determined by the maximum and minimum strain in each crack direction where the stiffness degradation in tension and compression are modeled separately.

Tensile and compressive stress-strain behavior of reinforcing steel was defined with isotropic plasticity using Von Mises yield criterion. Work hardening hypothesis was employed for modeling the post-yield behavior of the steel and the stress-strain relationship for the steel was modeled by a tri-linear model using the yield and ultimate strength values obtained from material tests.

Resulting from meshing of the geometry and placing the embedded reinforcements, the generated finite element model had 2568 plane-stress elements and 9153 nodes. Finite element mesh, alignment of embedded reinforcements, and related material models are presented in the Figure 3. 2 for summarizing the modeling strategy that was employed.

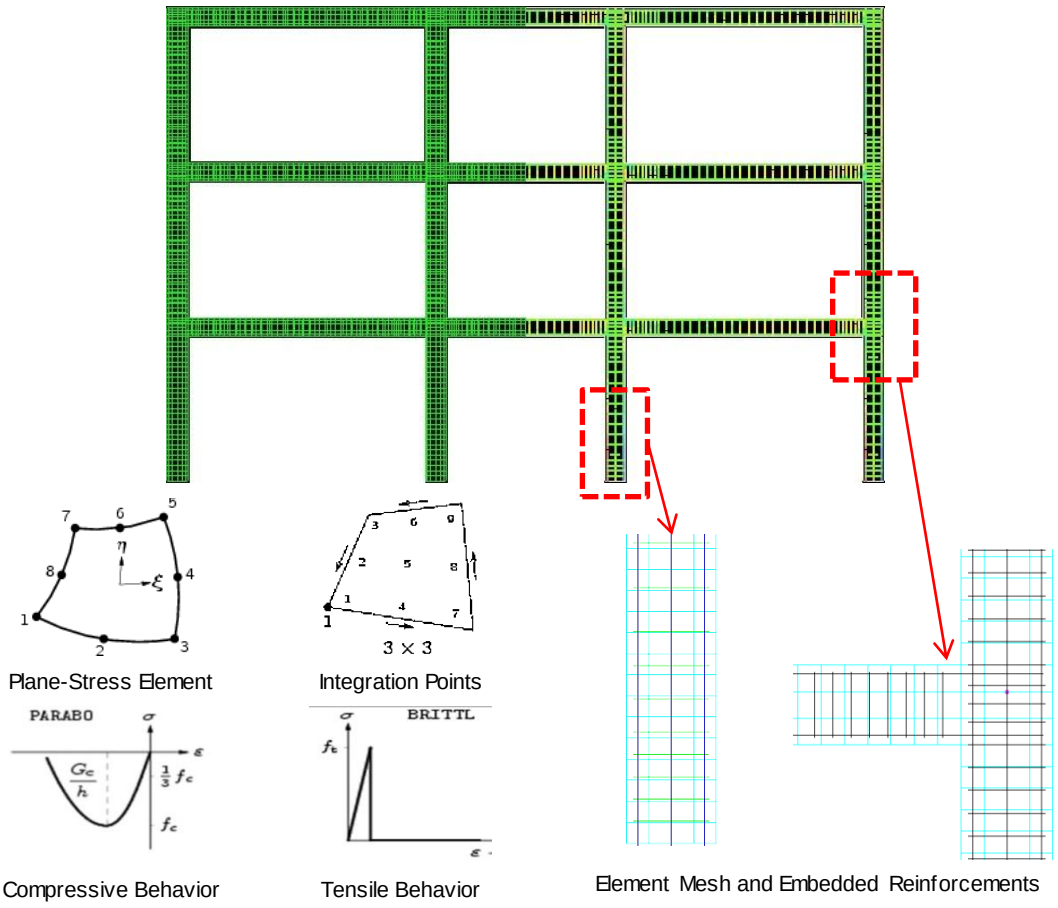

Figure 3. 2: Finite element model with embedded reinforcements

In addition to the mass contribution of plane stress elements defined with mass density, lumped masses were defined at the joints of each story using point mass elements to simulate the total mass of each story. For dynamic analyses, Rayleigh coefficients were set to obtain 5% damping between the 1st and the 3rd modes. Time history analyses were conducted and comparisons of obtained results with experimental results are presented in the related part.

The main aim of detailed finite element modeling of the structure in this study is to investigate the local responses of elements after calibrating the model with the global response parameters obtained from experiments. In this way, it is possible to obtain curvature profiles, plastic hinge lengths and plastic rotations at member ends, distortions in the joint regions, shear deformations in columns and contributions of each of these local deformation sources to the global response of the structure which were not measured in the experiments.

3.1.2. Model B

In the second modeling approach, a more practical frame model was employed. Beams and columns of the specimen were modeled using force based line elements defined by fiber sections at integration points where second order geometric nonlinearity effects were also considered in columns. Formulation of the *Nonlinear Beam Column Elements* follows the Euler-Bernoulli beam theory which does not include shear deformations. For modeling of the joint regions, rigid joint assumption was made by defining offset lengths at the element ends. OpenSees Simulation Platform (Mazzoni et.al. 2010) was utilized for generating the Model B for each specimen to examine the ability of estimating the seismic response of the test frame by performing nonlinear time history analyses on the model.

Material model used for concrete behavior is the one named as *Concrete01* which is the uniaxial Kent-Scott-Park (1971) concrete material model with no tensile strength and degraded linear unloading/reloading stiffness proposed by Karsan-Jirsa (1972). Using this material model, confinement effect of transverse reinforcement was taken into account by increasing the strength and strain capacity of the unconfined concrete to reflect the behavior of the concrete in the confined zones. Figure 3. 3 summarizes the modeling strategy.

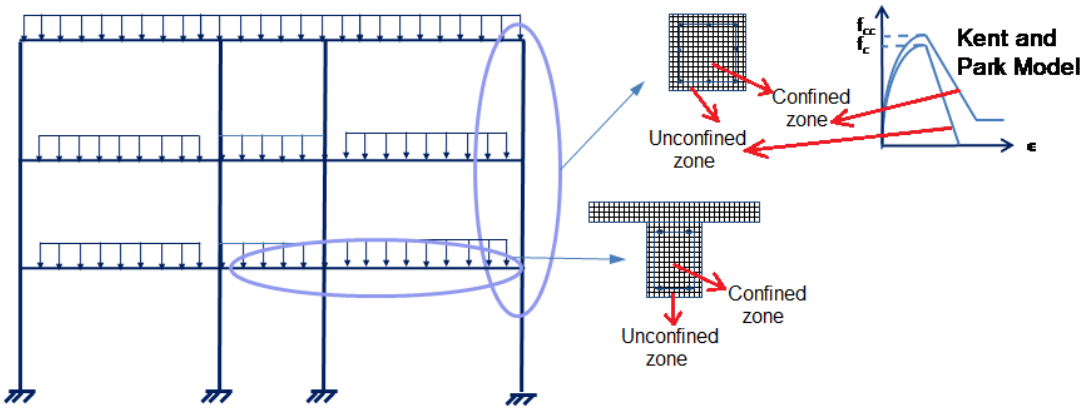

Figure 3. 3: Modeling with force based fiber elements

For modeling the behavior of steel reinforcement, tri-linear stress strain relationship was defined using *Uniaxial Hysteretic Material* command according to the yield and ultimate strength values obtained from material tests. Due to use of continuous longitudinal bars in columns of all specimens and welding of these reinforcements to

the foundation, bond-slip deformations at the base are thought to be minimal during experiments. Therefore, it was deemed suitable to use the assumption of perfect bond between steel reinforcement and concrete. Dynamic properties of the frame were modeled by defining lumped masses in the nodes distributed with certain proportions and 5% Rayleigh damping was utilized for time history analyses.

3.2. Comparison of Numerical Simulation and Test Results

3.2.1. Specimen-1

Consecutive time-history analyses results of earthquakes D1, D2 and D3 are presented in this section along with the comparisons of the pseudo dynamic test results. Roof displacement time history estimations of the two models are compared with the experimental results in Figure 3. 4. Inter-story drift ratio time histories are presented in Figure 3. 5 for each story. Shear force versus deformation estimations of the numerical simulations are compared to the test results in Figure 3. 6. Accuracy of the two numerical models in estimating the experimental results was evaluated first by means of global response parameters, which are the peak roof displacement and peak base shear forces obtained during each continuously applied ground motion. Error estimations are presented in Table 3. 1, Table 3. 2 and Table 3. 3.

Results presented in this part show that analyses results of Model A captures the global engineering demand parameters more successfully compared to the estimations of Model B. Main reasons of this fact can be listed as: 1) Joint deformations are modeled more accurately with a continuum approach, 2) Member shear deformations are automatically included in the model by using continuum elements, 3) Local demand parameters such as strains are computed under the action of two dimensional stresses in a more realistic way.

Despite these reasons, it should be stated that Model A takes about 12 hours to complete the analysis and post process the results with an i7 3.4 GHz processor. On the other hand, Model B runs in about 4 minutes and post processing is much easier due to the direct output of rotations and member end displacements. Taking the more refined approach of continuum modeling, it is reasonable to investigate

further the local deformations by means of comparison of the damage patterns, rotation demands, joint deformations, shear distortions of columns, which were not measured during some of the experiments.

Performance of Model-A in capturing damage patterns and locations, was examined in comparison with the experimental findings. Damage pictures given in Figure 3. 7 correspond to the instant of peak roof displacement during the experiments where the visible cracks in critical damage regions were marked. As explained in the modeling strategy of Model-A, the rotating crack concept results in crack strains along the direction of principal stresses, which provides a realistic cracking behavior for reinforced concrete plane elements under biaxial loadings. Plots, given in Figure 3. 7, include the lines corresponding to the direction of cracking at material points in the numerical model. Good agreement between the damage locations and crack patterns in the simulations and experiments further support the ability of the model in simulating the behavior of the test specimen.

Initial 1st mode periods obtained from Model-A and Model-B after gravity loading are 0.33 and 0.47 seconds respectively. Higher initial period of Model-B is mainly due to limitation of concrete material model with zero tensile strength.

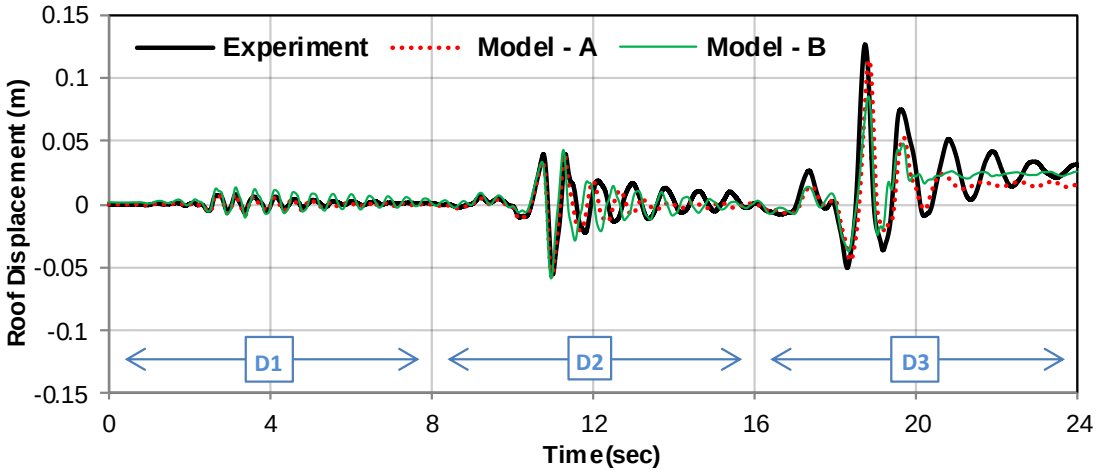

Figure 3. 4: Roof displacement history comparison for SP1

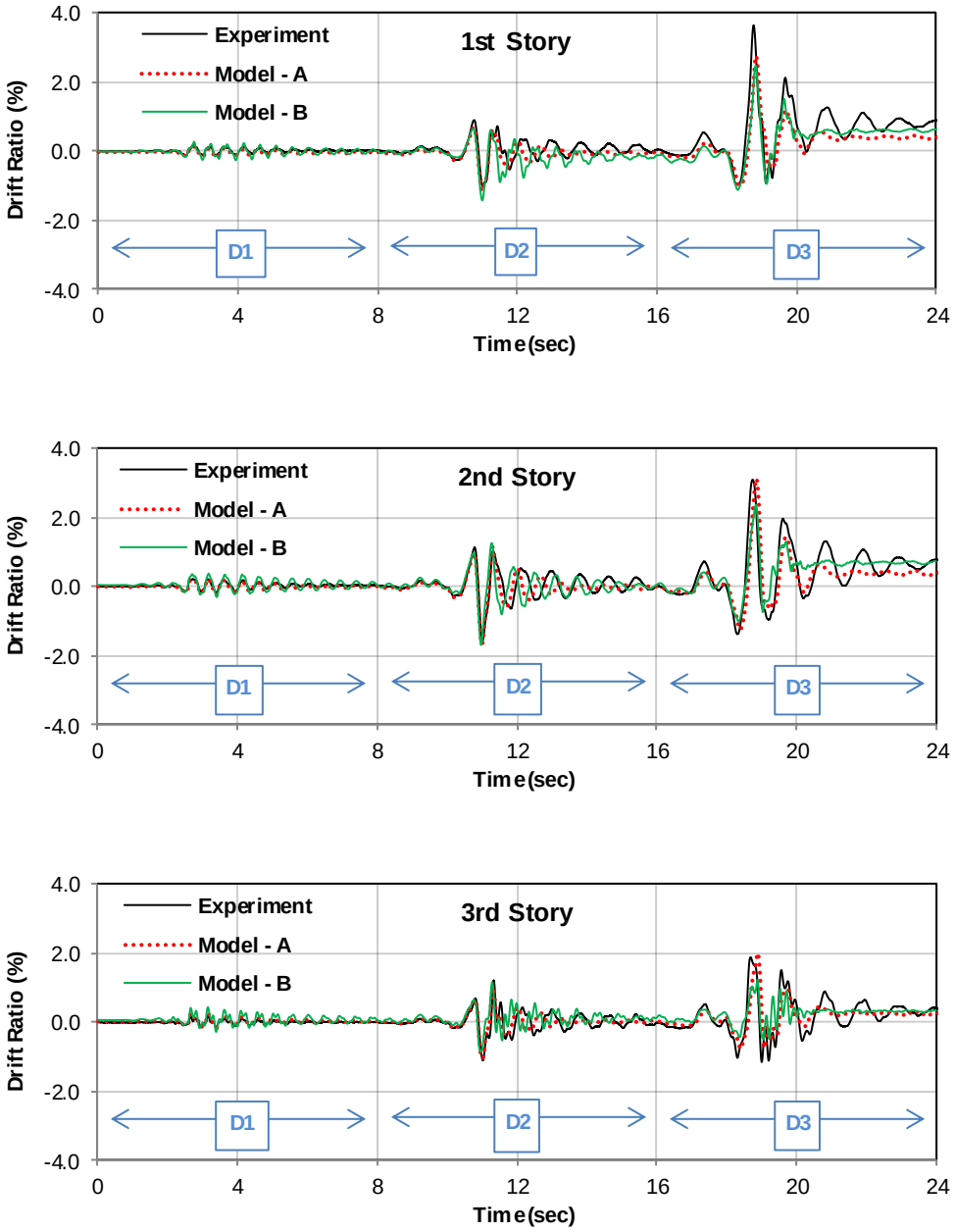

Figure 3. 5: Comparison of inter-story drift ratio histories for SP1

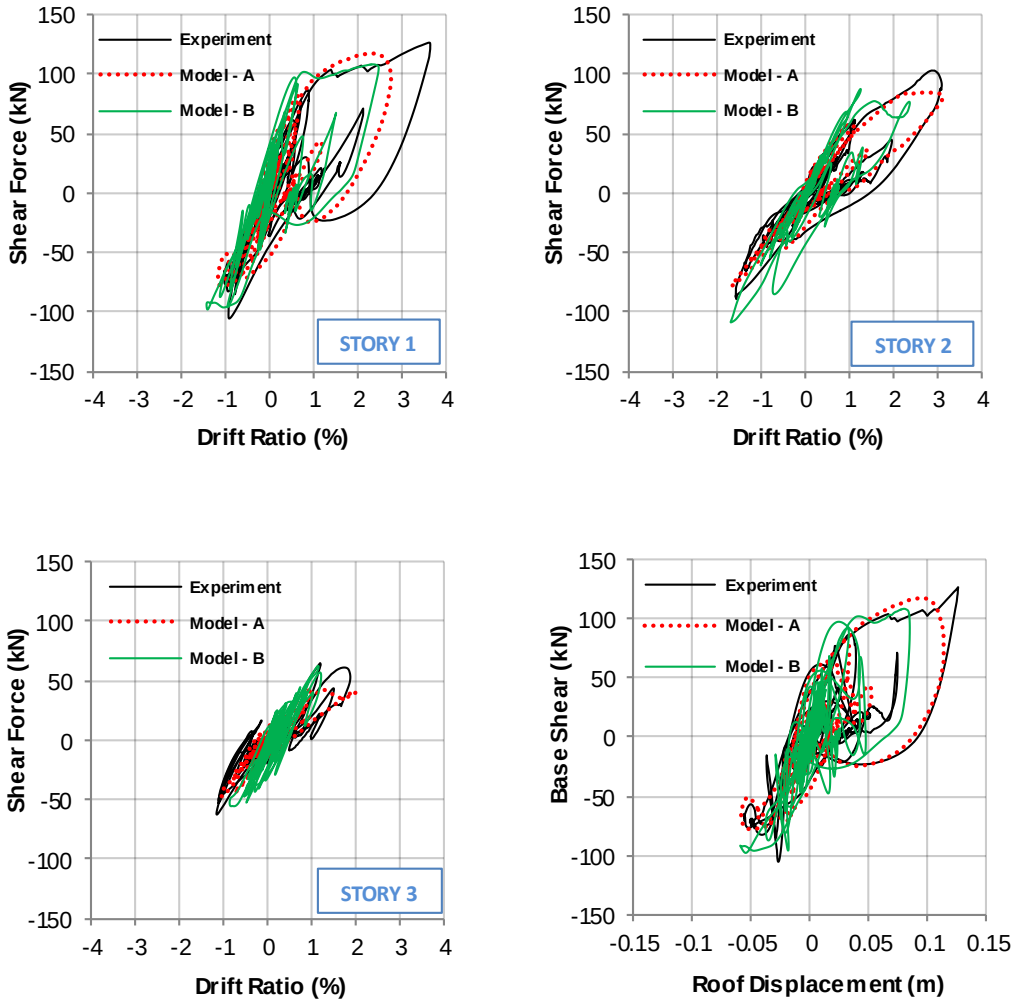

Figure 3. 6: Comparison of story shear force vs. drift response for SP1

Table 3. 1: Error estimations for peak roof displacement response (SP1)

Ground Motion	Maximum Roof Displacement(mm)			Error (%)	
	Experiment	Model - A	Model - B	Model - A	Model - B
D1	7.7	8.77	13.2	14.1	72.3
D2	55.4	58.1	58.8	4.8	6.1
D3	126.4	114	85.3	9.8	32.6

Table 3. 2: Error estimations for peak base shear response (SP1)

Ground Motion	Maximum Base Shear(kN)			Error (%)	
	Experiment	Model - A	Model - B	Model - A	Model - B
D1	32.3	36.8	57.9	13.9	79.3
D2	86.8	81.8	97.8	5.8	12.7
D3	126.8	117.6	108.5	7.2	14.4

Table 3. 3 Error estimations for peak inter-story drift response (SP1)

	Inter-story drift (%)			Error (%)	
Story	Exp.	Model - A	Model - B	Model - A	Model - B
1	3.64	2.75	2.47	24.44	32.11
2	3.10	3.13	2.37	1.02	23.41
3	1.88	2.00	1.22	6.44	35.24

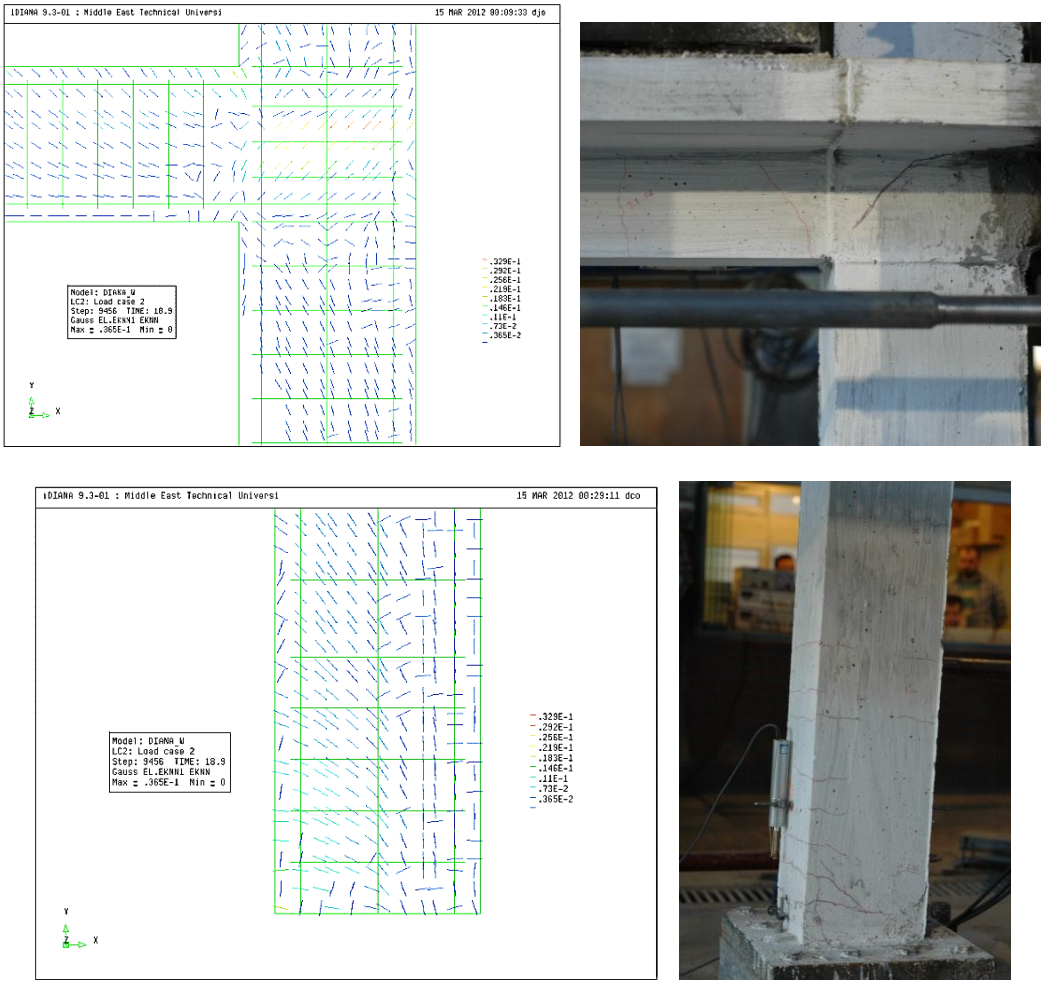

Figure 3. 7: Crack pattern comparison in critical damage regions for the first story exterior column 104 and the first story exterior joint (SP1)

Bottom end rotations in 1st story columns were calculated from the measurements of LVDT's placed on both sides of the plastic hinge regions as shown in Figure 2. 8. For a consistent comparison of the experimental findings and the analysis results, these rotation demands were calculated using Model A from the nodal displacement histories. Results are presented in Figure 3. 8. It can be stated that nonlinear

analysis results are in good agreement with column base rotations measured within the potential plastic hinge regions during the experiments.

With the confidence obtained by above comparisons, average curvature profiles at the bottom ends of 1st story columns were obtained and they are presented in Figure 3. 9. Curvature profiles obtained for peak roof displacements and at first yield point of each level are shown separately in these figures with the corresponding damage views at ultimate deformations. Using these curvature profiles, plastic hinge regions were identified and the amounts of plastic rotations were calculated by integration of curvatures for these columns at the time step where the peak roof displacement response was obtained. Calculated bottom end rotations and estimated plastic hinge lengths of columns are presented in Table 3. 4. Our results show that significant plastic rotation demands (between 1 to 2%) were observed at the column bases. The estimated plastic hinge lengths vary between 200 mm to 350 mm, indicating the difficulty of providing one single value for columns with similar dimensions.

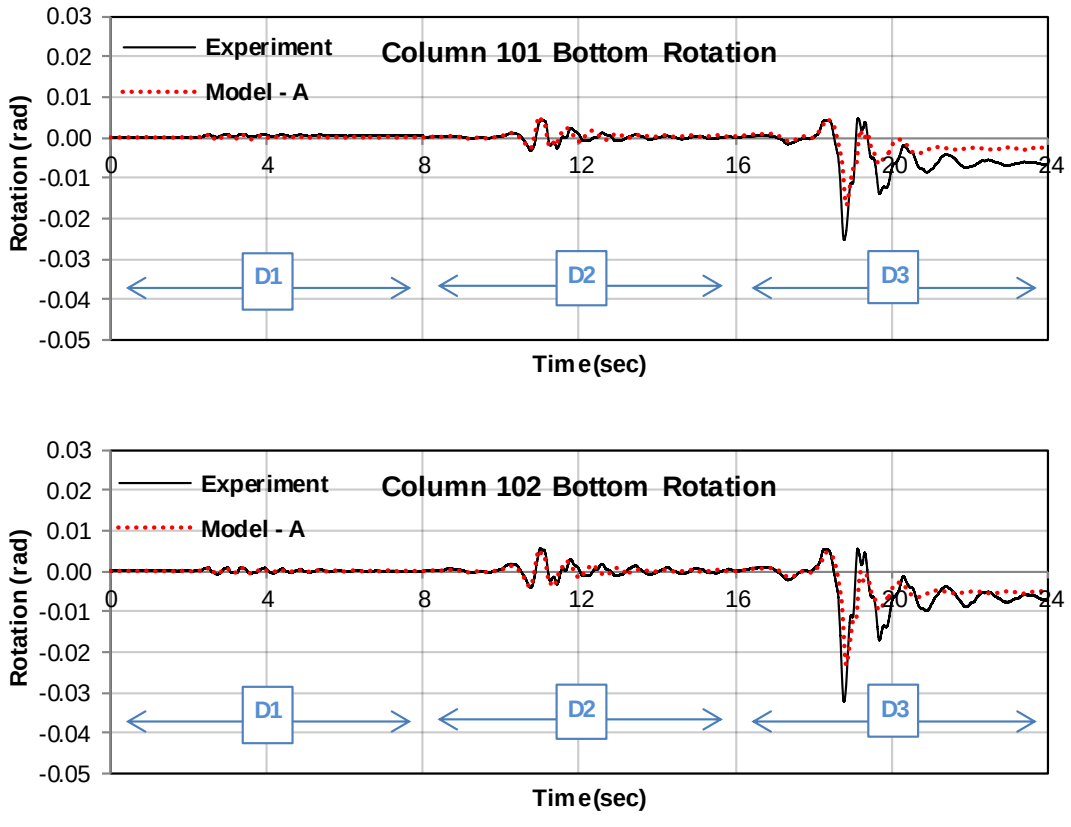

Figure 3. 8: Comparison of bottom end rotations of 1st story columns (SP1)

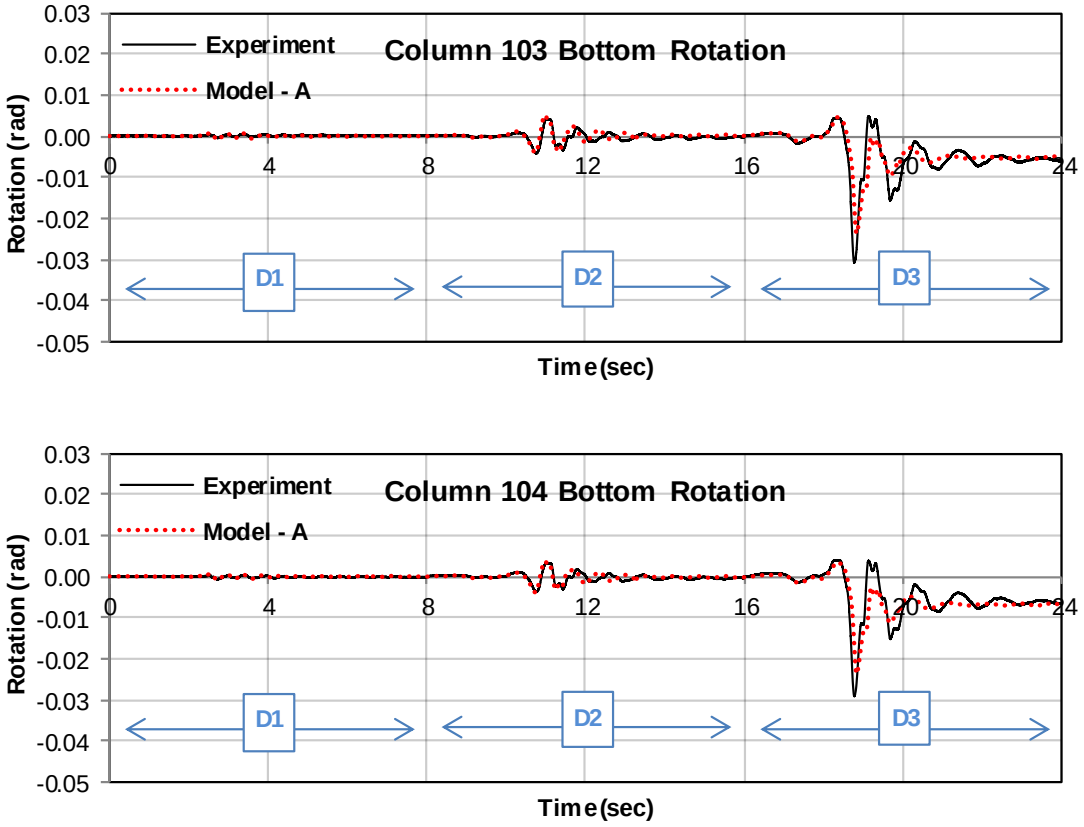

Figure 3. 8: Comparison of bottom end rotations of 1st story columns (cont'd)

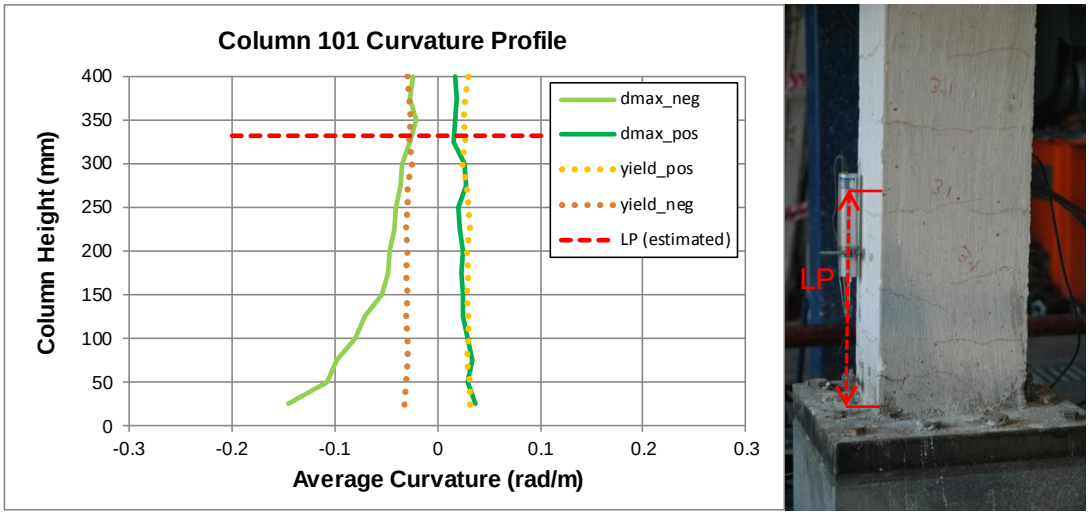

Figure 3. 9: Curvature profiles of 1st story column bases (SP1)

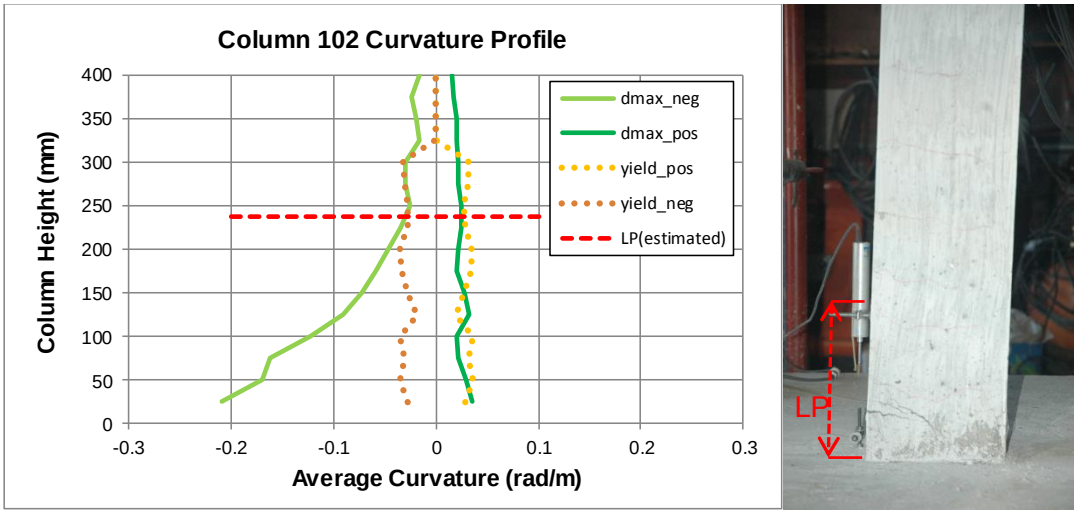

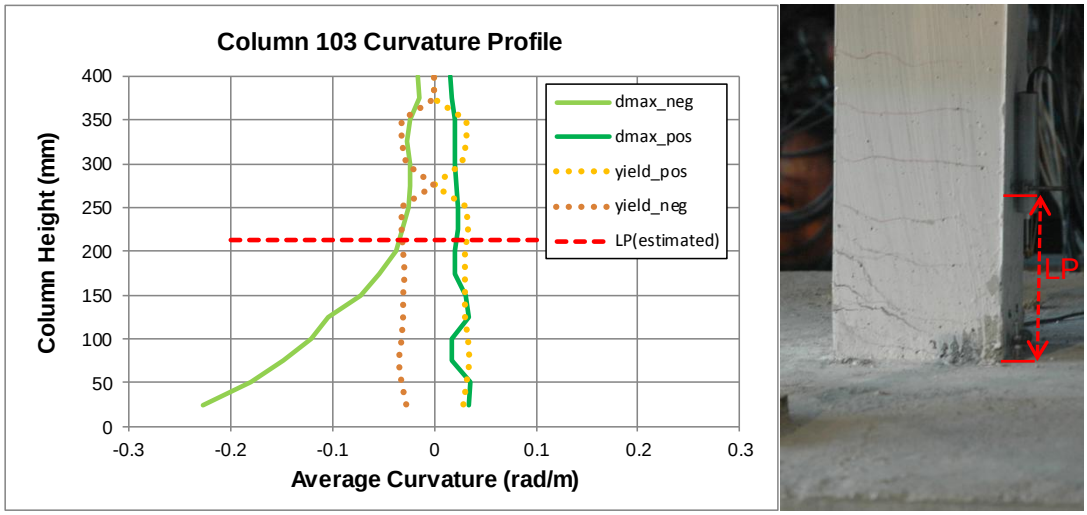

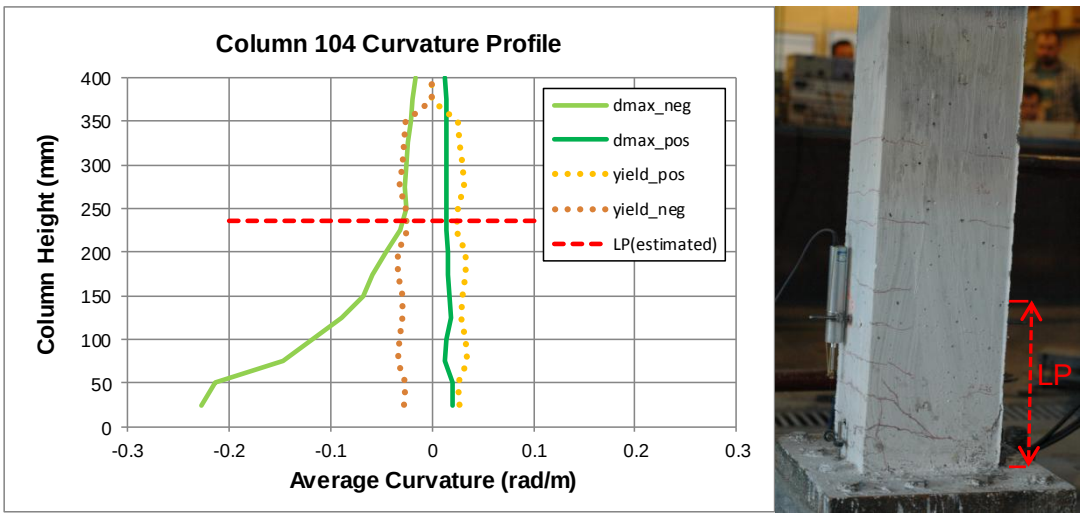

Figure 3. 9: Curvature profiles of 1st story column bases (cont'd)

Table 3. 4: Bottom End Rotations of 1st Story Columns (SP1)

	Column Bottom End Rotations			
Column ID	101	102	103	104
Lp (mm)	331	237	213	237
$\Theta_{plastic}$ (rad)	0.0106	0.0164	0.0165	0.0172
$\Theta_{elastic}$ (rad)	0.0090	0.0065	0.0059	0.0064

Shear deformation of the 1st story columns of Model A was calculated by dividing the column height into seven sub-grids with equal heights (h_s) as shown in Figure 3. 10. Shear distortion of each square shaped segment (Δ_{sh}) was calculated by using the average shear strain values (γ_{av}) as explained in Ozcebe (1987).

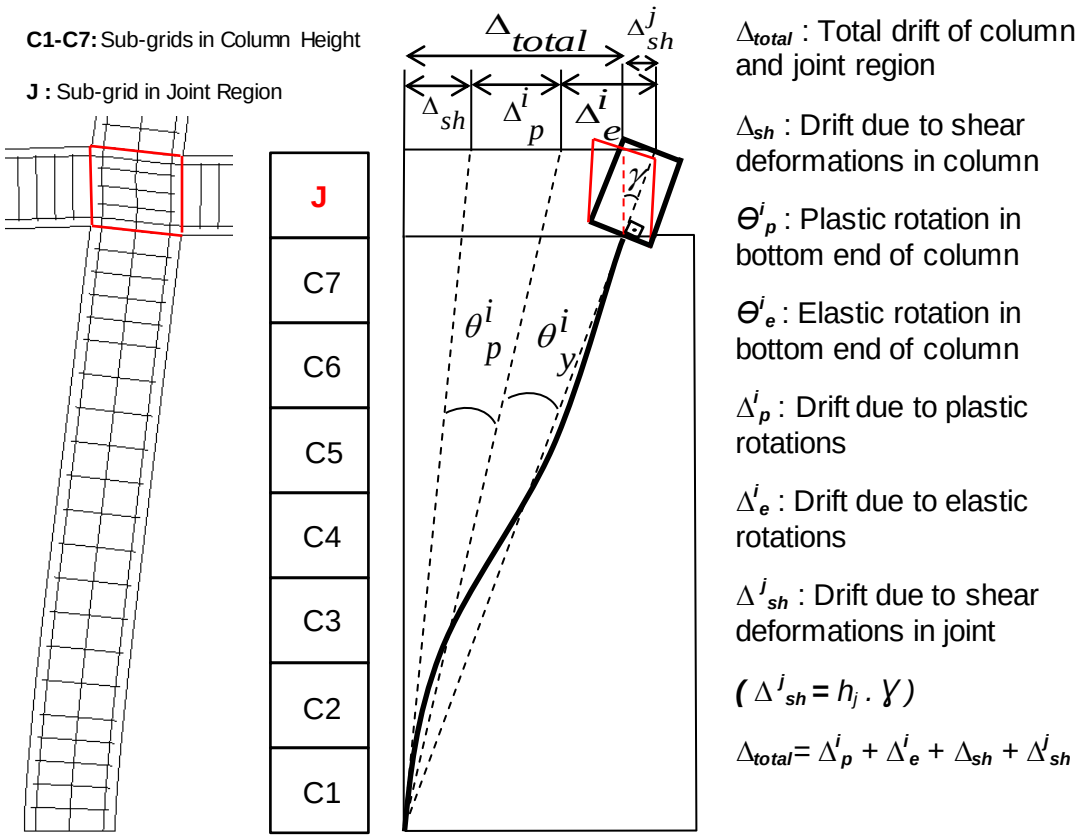

Figure 3. 10: Drift contributions of deformation components

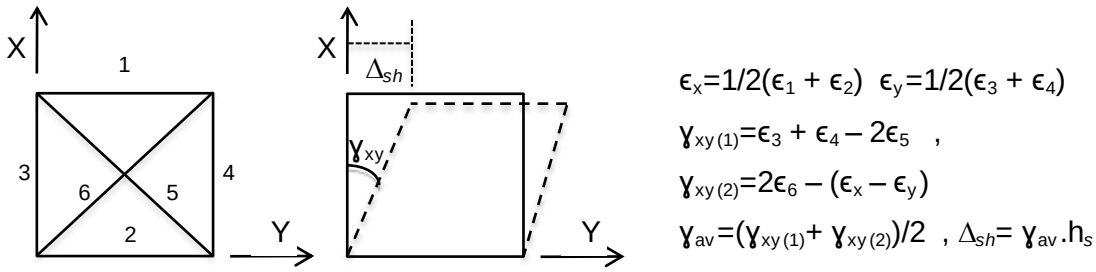

Figure 3. 11: Shear deformation formulation

Longitudinal strains in each of the edges and the diagonals are obtained from the nodal displacements recorded for the corner nodes of each segment. The formulation used in the shear deformation calculations are presented in Figure 3. 11. Average shear distortion profiles of 1st story columns are presented in Figure 3. 12 together with corresponding joint distortions for the time step of analysis that the maximum roof displacement was reached. It can be observed that shear distortions were large in the plastic hinge regions indicating strong coupling of the two deformation components.

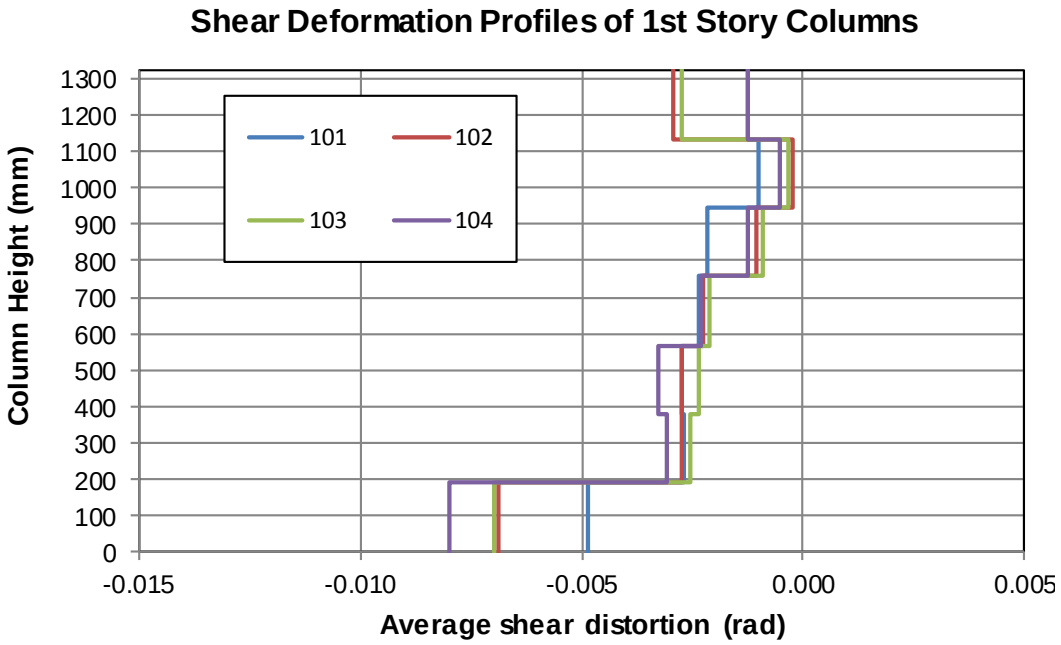

Figure 3. 12: Shear deformation profiles of 1st story columns (SP1)

After obtaining the amount of elastic and plastic rotations, shear deformations in the columns and contribution of each of these components to the total drift of each column at the time step of maximum roof displacement was calculated and

presented in Table 3. 5. The total drift of a column was measured from the bottom face of the column to the top face of the slab level in the 1st story (Figure 3. 10). The results presented in the Table 3. 5 demonstrate that shear deformations in columns and joint regions have some contribution to the total deformation demands and including these deformation components in analytical models may affect the story displacement estimations in the order of about 10%.

Table 3. 5: Percent contributions of each deformation component (SP1)

		Drift Contributions			
Column	Lp (mm)	Plastic Rotation(%)	Shear Deformation(%)	Joint Deformation(%)	Elastic Rotation(%)
101	331	32.1	8.3	-1.7	61.3
102	237	53.4	9.2	-12.3	49.7
103	213	54.8	8.9	-9.8	46.1
104	237	56.1	9.6	-8.3	42.6

Time histories of the shear distortions in the first story joints are presented in Figure 3. 13. It can be observed that joint shear angles reach up to 2% indicating the source of shear damage especially for the D3 motion. Drift contribution results also showed that shear distortions in joint regions were in opposite direction and significantly higher than the distortions along the clear heights of the columns. Especially in the internal joints, the shear distortion contributed to the total drift more than the shear deformations in column height. Although, these two deformation components contributed to story drift in opposite directions and resulted in a neutralizing effect on each other, it should be noted that the joint distortions have significant effect on the deformation demands and the behavior of the connecting beams and columns of the next story, which consequently affects the overall behavior of the structure.

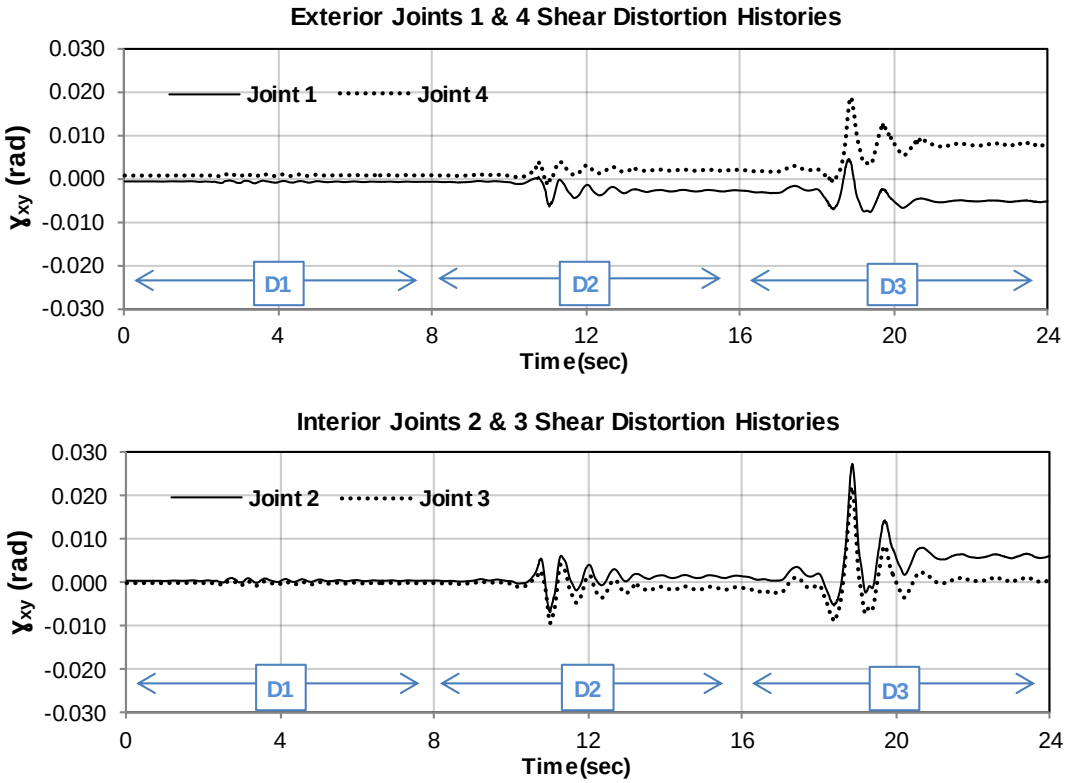

Figure 3. 13: Joint deformation time histories for Specimen-1

3.2.2. Specimen-2

In this section, results of consecutive time-history analyses for Specimen-2 are presented along with the comparisons with the pseudo dynamic test results of ground motions D1, D2 and D3. Initial 1st mode periods of Model-A and Model-B after gravity loading were calculated as 0.31 and 0.43 seconds respectively. Roof displacement time history estimations of the two models are compared with the experimental results in Figure 3. 14. Inter-story drift ratio time histories are presented in Figure 3. 15 for each story. Shear force versus deformation estimations of the numerical simulations are compared with the test results in Figure 3. 16. Accuracy of the two numerical models in estimating the experimental results by means of global response parameters, which are the peak roof displacement and peak base shear forces, was evaluated for each of continuously applied ground motions. Error estimations are presented in Table 3. 6, Table 3. 7 and Table 3. 8.

Results, presented in this part, show that ability of both models of Specimen-2 to capture the experimental results was not as successful as in the case of Specimen-1, although the same modeling strategy was followed. However, similar to Specimen-1, it can be observed that simulations on Model-A captured the experimental results more successfully compared to estimations of Model-B in terms of global response parameters. Therefore, further investigations on Model-A for local deformations were carried out for Specimen-2 following a similar strategy with the simulations of Specimen-1. In this way, it was aimed to compare the results of local demand parameters obtained from different models corresponding to different specimens.

Ability of Model-A of the Specimen-2 in capturing the damage locations and patterns was also examined using the same strategy that was followed for Specimen-1. Visible cracks that were marked during the experiments were compared with crack strains in the material points of the numerical model for the time step of maximum roof displacement. Figure 3. 17 presents the crack pattern comparison for the interior column 103 and the interior joint connected to that column. It can be observed that the model is quite successful in estimating the location and extent of inclined cracks in the test specimen.

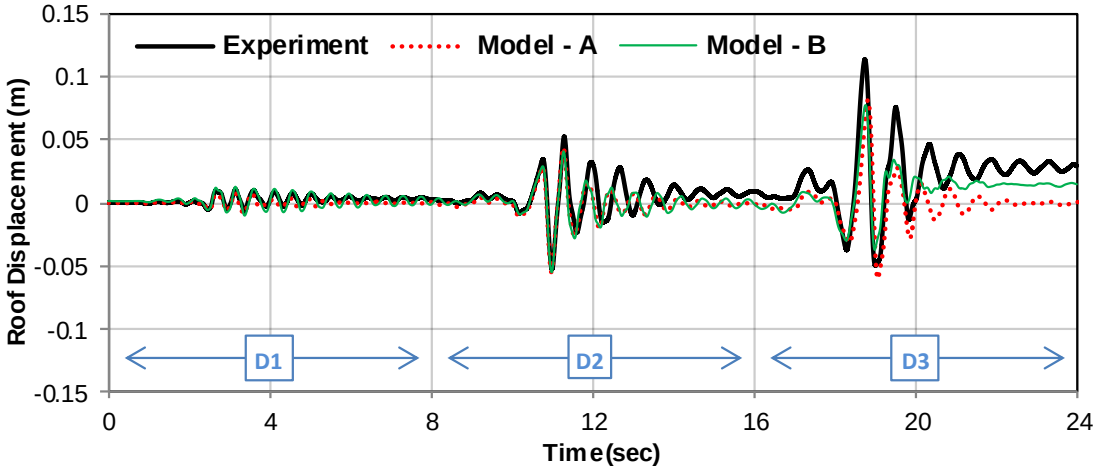

Figure 3. 14: Roof displacement history comparison for SP2

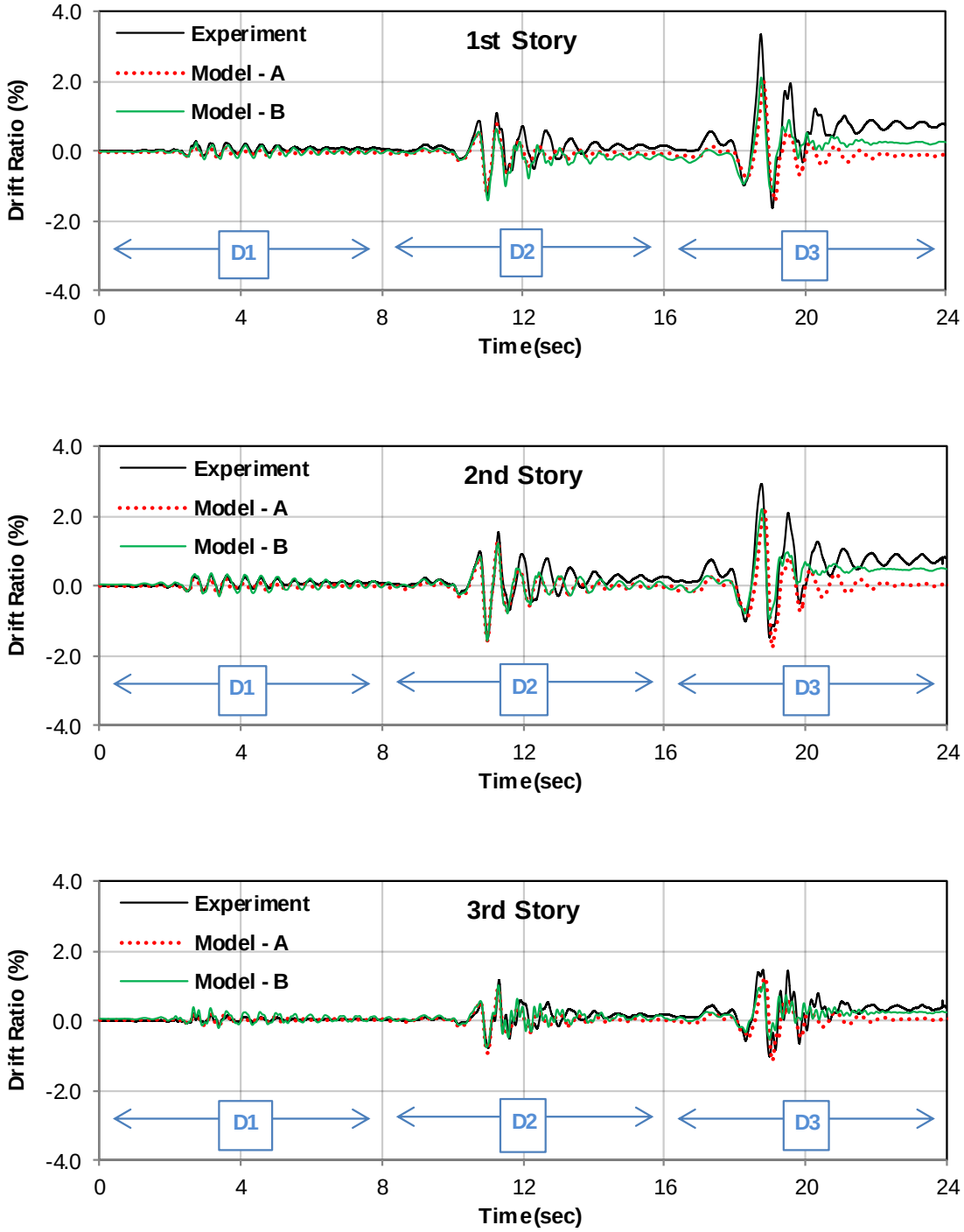

Figure 3. 15: Comparison of inter-story drift ratio histories for SP2

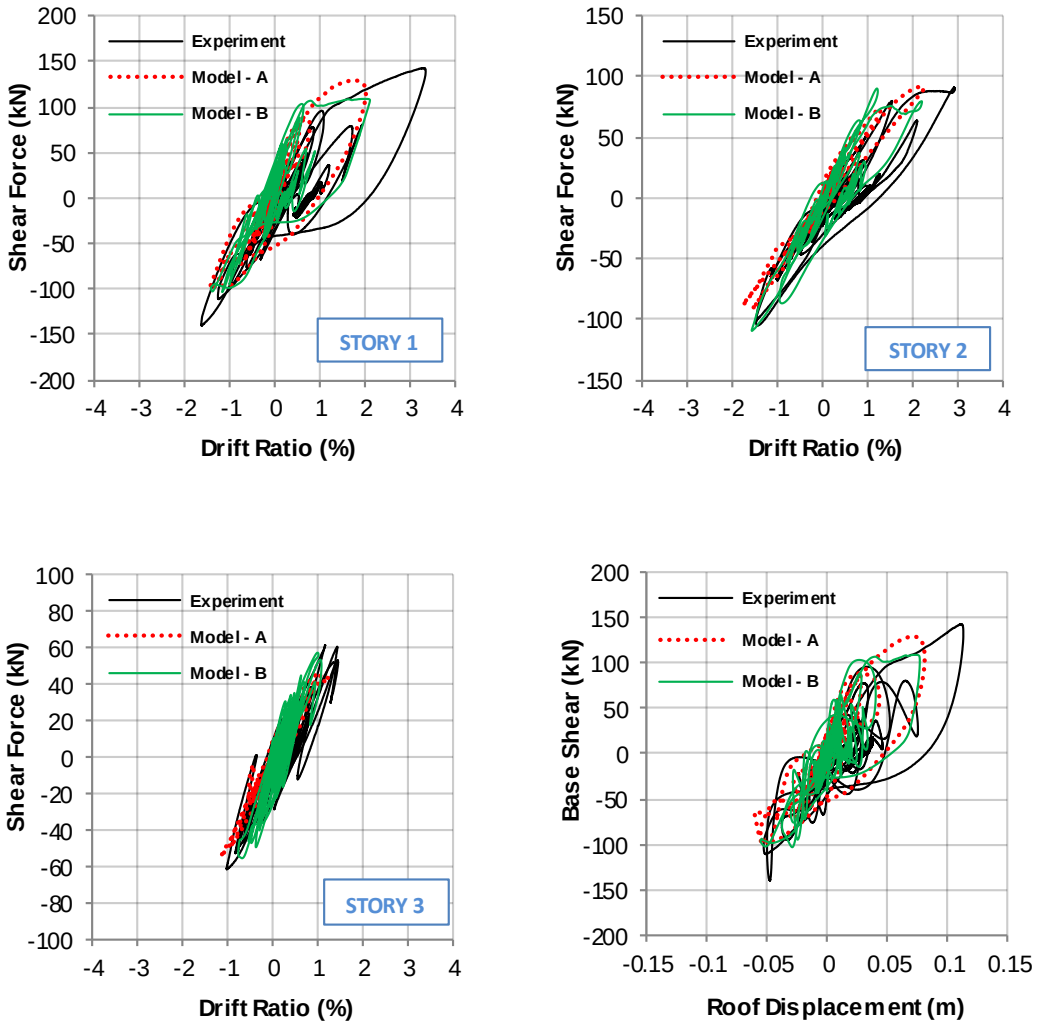

Figure 3. 16: Comparison of story shear force vs. drift response for SP2

Table 3. 6: Error estimation for peak roof displacement response (SP2)

Ground Motion	Maximum Roof Displacement(mm)			Error (%)	
	Experiment	Model - A	Model - B	Model - A	Model - B
D1	10.7	8.45	12.6	20.8	18.4
D2	52.4	55.0	55.0	4.9	4.9
D3	113.5	81.4	77.3	28.3	31.9

Table 3. 7: Error estimations for peak base shear response (SP2)

Ground Motion	Maximum Base Shear(kN)			Error (%)	
	Experiment	Model - A	Model - B	Model - A	Model - B
D1	36.2	33.1	57.0	8.8	57.3
D2	111.0	96.9	103.4	12.8	6.8
D3	142.9	129.3	109.0	9.5	23.7

Table 3. 8: Error estimations for peak inter-story drift response (SP2)

	Inter-story drift (%)			Error (%)	
Story	Exp.	Model - A	Model - B	Model - A	Model - B
1	3.35	2.02	2.11	39.65	36.92
2	2.93	2.25	2.21	23.25	24.65
3	1.45	1.24	1.09	14.72	25.37

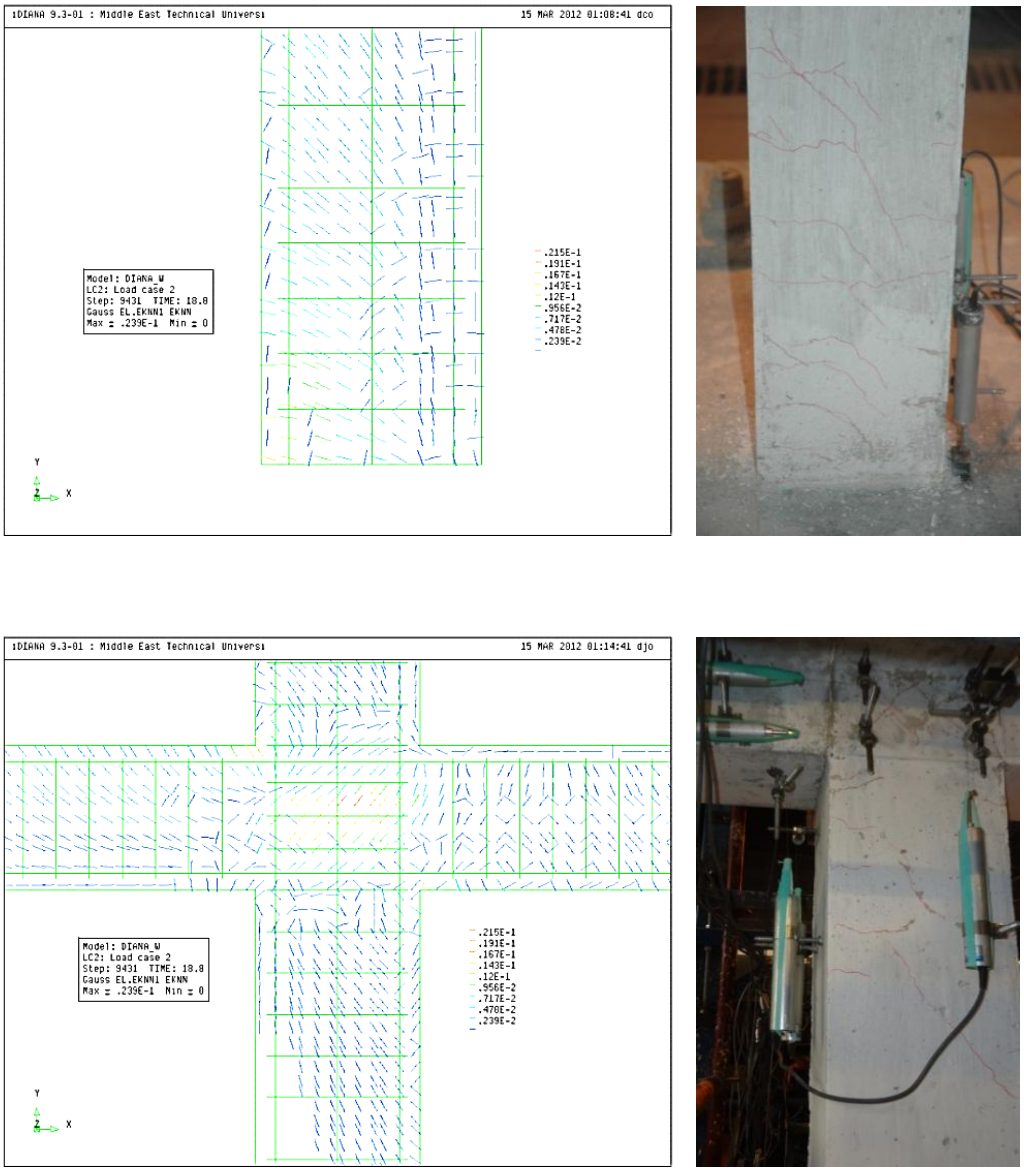

Figure 3. 17: Crack pattern comparison in critical damage regions interior column 103 and the first story interior joint (SP2)

Bottom end rotations of 1st story columns in the potential plastic hinge regions were calculated using the translational displacement histories of nodes of Model-A of Specimen-2 and presented in Figure 3. 18. It can be observed that there is a general agreement between numerical simulation results and the experimental results for column bottom rotations. However, the residual displacements are grossly underestimated by the numerical model as can be seen during the D3 ground motion. This can be attributed to the lack of modeling the cyclic damage characteristics of concrete in tension and compression in the rotating crack models.

Based on the comparisons given above, it was found sufficient to conduct further investigation on the local deformations. Average curvature profiles at the bottom ends of 1st story columns are presented in Figure 3. 19 for the time step of peak roof displacement with corresponding damage views. Curvature profiles for the first yield point of each level of column ends are shown separately in the plots. Following the same strategy with Specimen-1, obtained curvature profiles were used for estimation of plastic hinge lengths and the amounts of plastic rotations which were calculated by integration of these curvature profiles. Table 3. 9 shows the estimated bottom end rotations and plastic hinge lengths for each column. Plastic rotations values at the column bases were higher than 1%. The plastic hinge lengths varied between about 250 mm and 380 mm similar to those computed in Specimen 1.

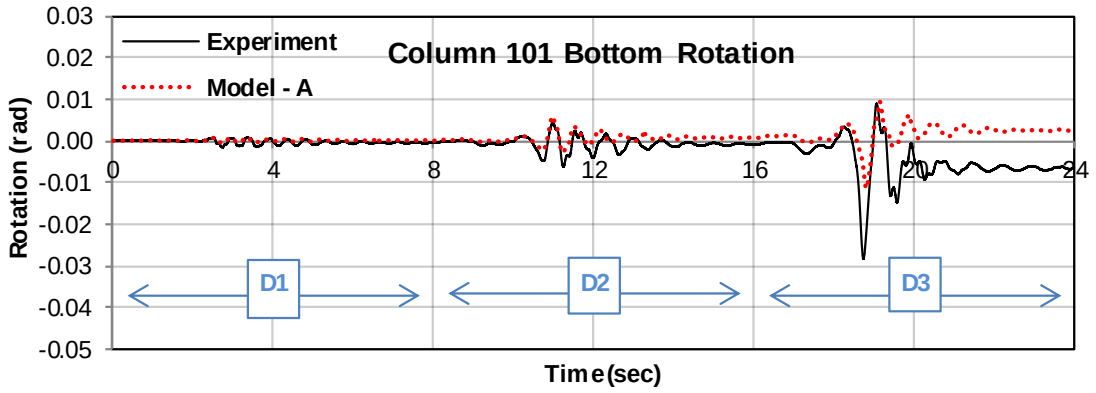

Figure 3. 18: Comparison of bottom end rotations of 1st story columns (SP2)

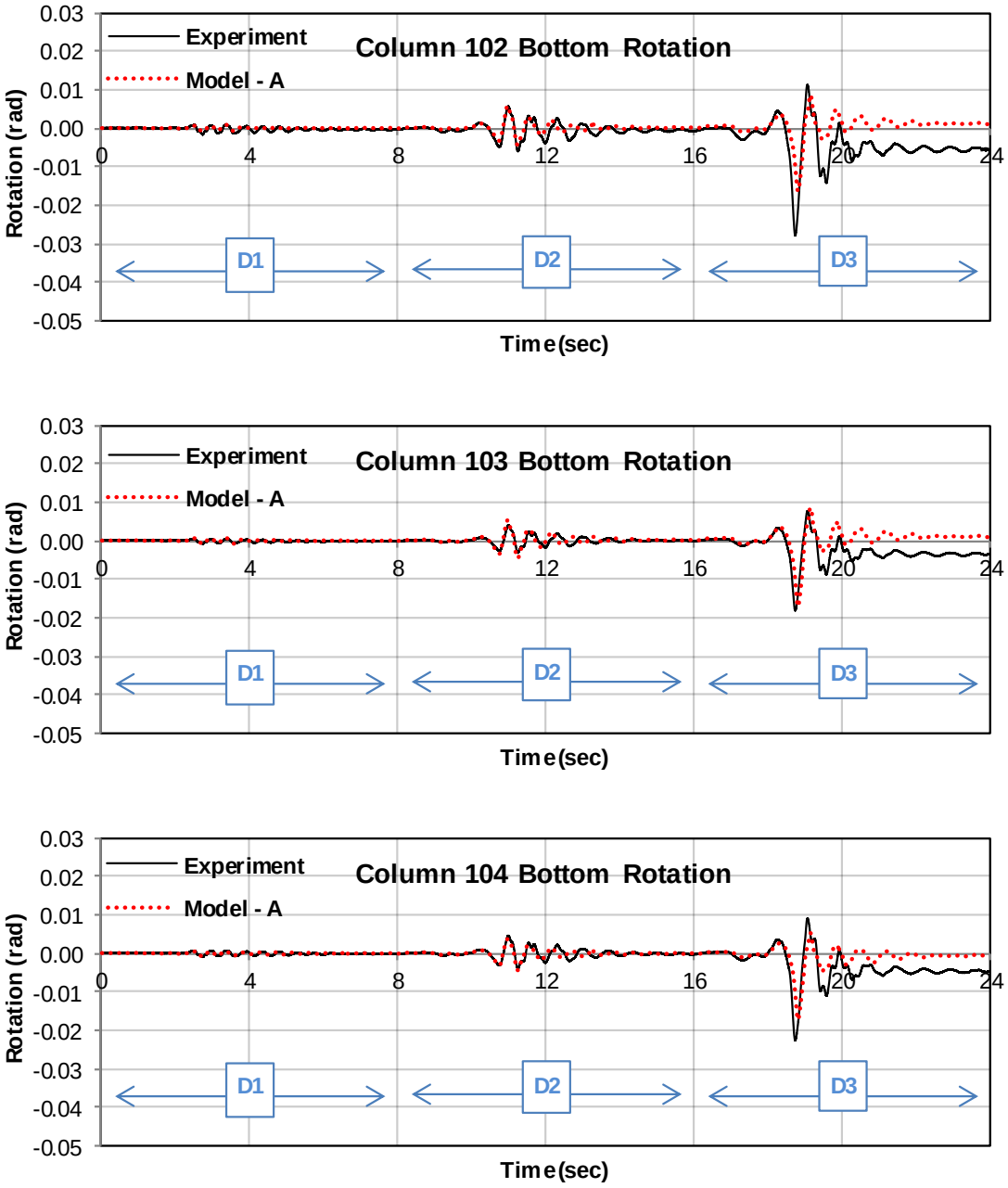

Figure 3. 18: Comparison of bottom end rotations of 1st story columns (SP2) (cont'd)

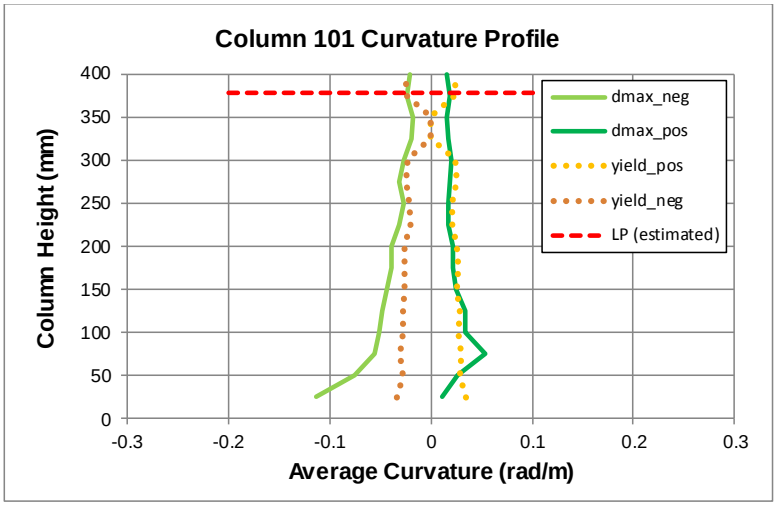

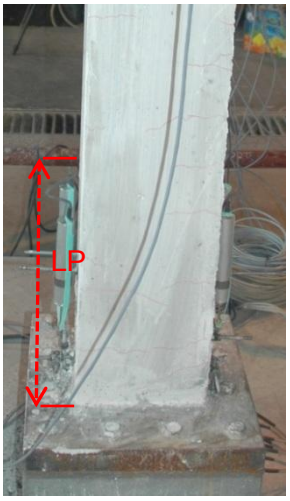

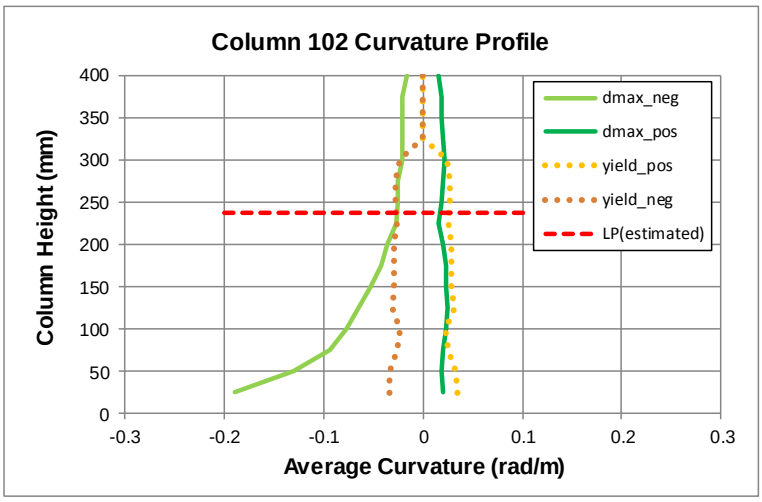

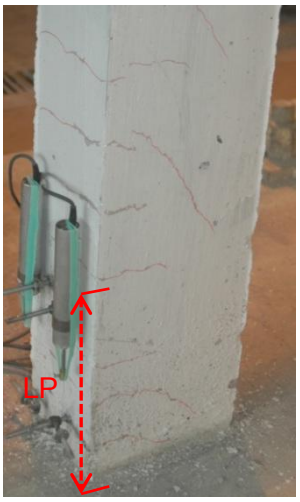

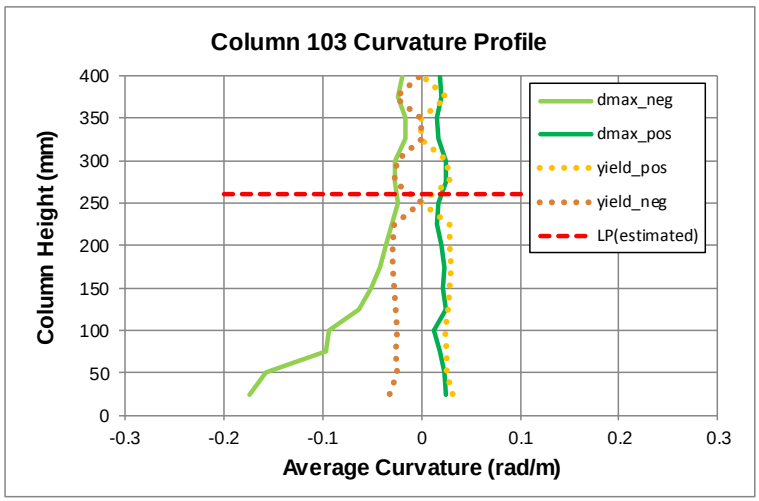

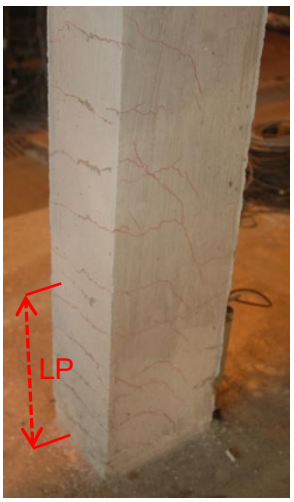

Figure 3. 19: Curvature profiles of 1st story column bases (SP2)

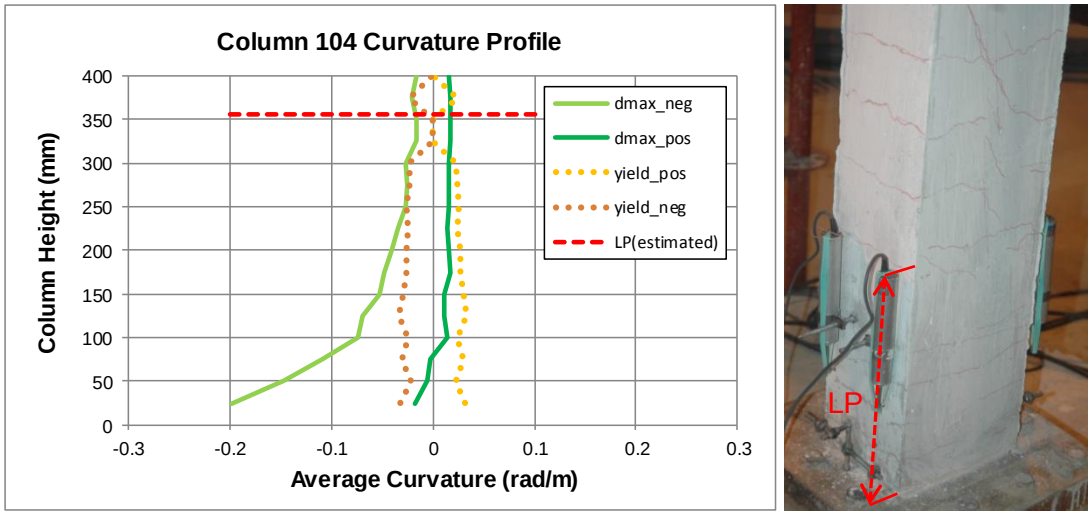

Figure 3. 19: Curvature profiles of 1st story column bases (cont'd)

Table 3. 9: Bottom End Rotations of 1st Story Columns (SP2)

	Column Bottom End Rotations			
Column ID	101	102	103	104
Lp (mm)	379	237	260	355
$\Theta_{plastic}$ (rad)	0.0072	0.0108	0.0123	0.0134
$\Theta_{elastic}$ (rad)	0.0080	0.0061	0.0059	0.0076

Considering the amounts of plastic rotations and height of the plastic hinge lengths, estimated and presented in Table 3. 9 it was observed that there are significant differences between the behavior of each column, although the total drift was the same for the columns of the 1st story. Therefore, it can be concluded that direction of loading and amplitude of loading cycles and variations in the axial loads may have significant effects on the plastic hinge length and amounts of local deformations in the column ends.

Following the same calculation strategy with Specimen-1, shear deformations were calculated using the strain values obtained from the recorded nodal displacement histories of the corner nodes of segments. Results presented in Figure 3. 20

correspond to average shear distortion profiles of 1st story columns and joints at the time step of analysis with the maximum roof displacement.

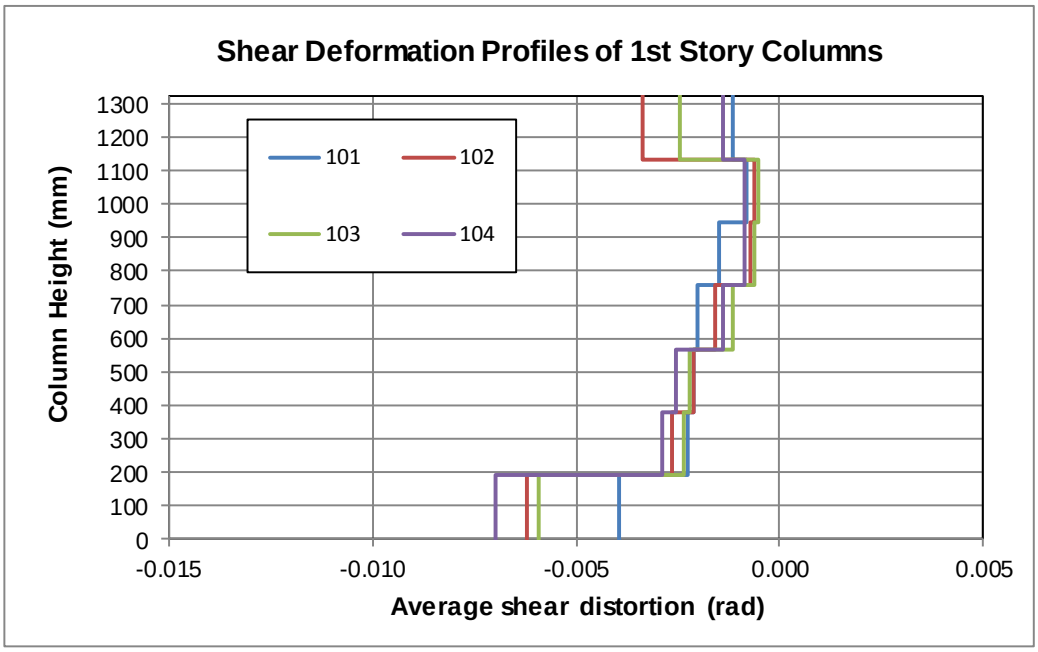

Figure 3. 20: Shear deformation profiles of 1st story columns (SP2)

Contribution of each of these deformation components to the total drift was determined from average curvature profiles and amounts of shear deformations in columns and joints obtained form average shear distortion profiles. Results are presented in Table 3. 10 for each column at the time step of maximum roof displacement.

Table 3. 10: Percent contributions of each deformation component (SP2)

		Drift Contributions			
Column	Lp (mm)	Plastic Rotation(%)	Shear Deformation(%)	Joint Deformation(%)	Elastic Rotation(%)
101	379	26.9	8.8	-1.0	65.3
102	237	45.5	10.9	-9.3	52.9
103	260	51.0	9.7	-7.1	46.5
104	355	51.4	10.7	-4.7	42.7

Contributions of deformation components presented in Table 3. 10 demonstrate the necessity of including shear behavior in modeling of frames, since the shear deformations in both columns and joint regions have some effect on the behavior of

the frame. Joint deformation histories of Specimen-2 are presented in Figure 3. 21. It can be observed that the joint deformations are larger in interior connections and the shear angle may reach the values as high as 1.5%. Joint deformation comparison of analyses on Model-A, and available experimental data is also presented in Figure 3. 21, for Joint-2.

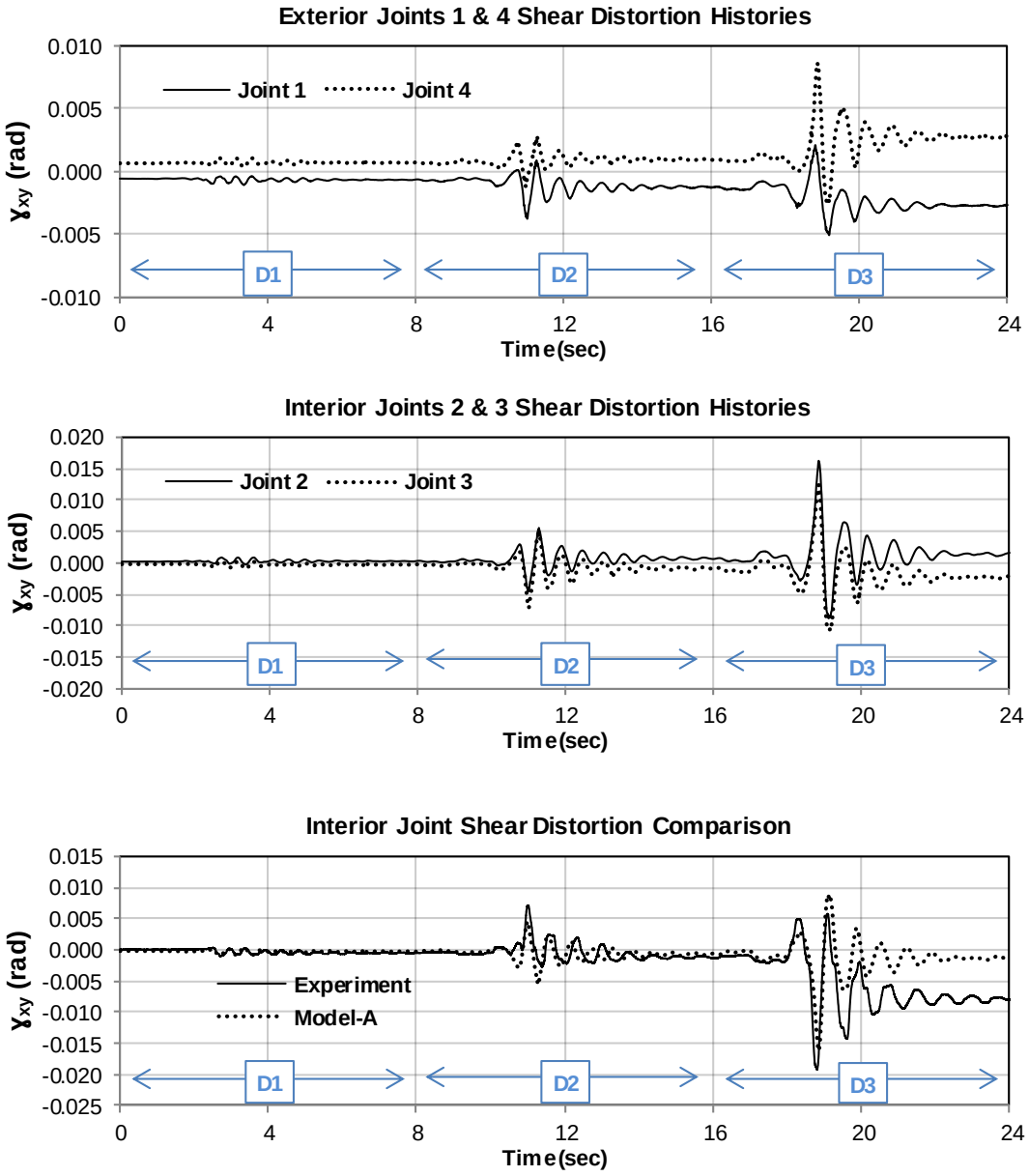

Figure 3. 21: Joint deformation time histories for Specimen-2

3.2.3. Specimen-3

Numerical simulations results of two numerical models were presented in this part and compared with the test results of consecutively applied ground motions D1, D2 and D3. Initial 1st mode periods of Model-A and Model-B after gravity loading were calculated as 0.37 and 0.52 seconds respectively. Comparison of roof displacement histories of simulations and experiments are presented in Figure 3. 22. Inter-story drift ratio response histories are compared for each story and presented in Figure 3. 23. In Figure 3. 24, story shear force versus story displacement estimations obtained from numerical simulations are compared to the test results. Global responses obtained from simulations were compared in terms of maximum roof displacement and base shear force for evaluation of performance of modeling techniques. Error estimations for each ground motion and response type are presented in Table 3. 11, Table 3. 12 and Table 3. 13.

Considering the roof displacement history, peak values and residual displacements, the Model-B seems to be matching better with experiments. However, performance of numerical simulations should be evaluated in terms of story forces and inter-story drift ratio responses rather than roof displacement response for a better understanding of model behavior and its reliability. Error estimation results, presented in the tables, indicate that simulations on Model-B were more accurate in terms of roof displacement, base shear, and residual displacement than the results from Model-A. However, when the performance of models were compared in terms of story drift and distribution of inter-story drift ratios to each story, it was observed that the Model-B was not accurate in simulating the general behavior of the test specimen, since the 1st story drift ratio reached a value of 8% while the test specimen reached the value of 4%. In fact, this overestimation of the 1st story response provided a better match of the roof displacement for Model-B.

As far as the displacement response of the 1st story is concerned, performance of Model-A was regarded as sufficient for comparison of bottom end rotation histories of 1st story columns and further investigations on the model for damages and contributions of displacement components following a similar strategy with the Specimens1 and 2. In this way, it was also aimed to compare the results of further study on unmeasured local deformations and plastic hinge length estimations of different specimens.

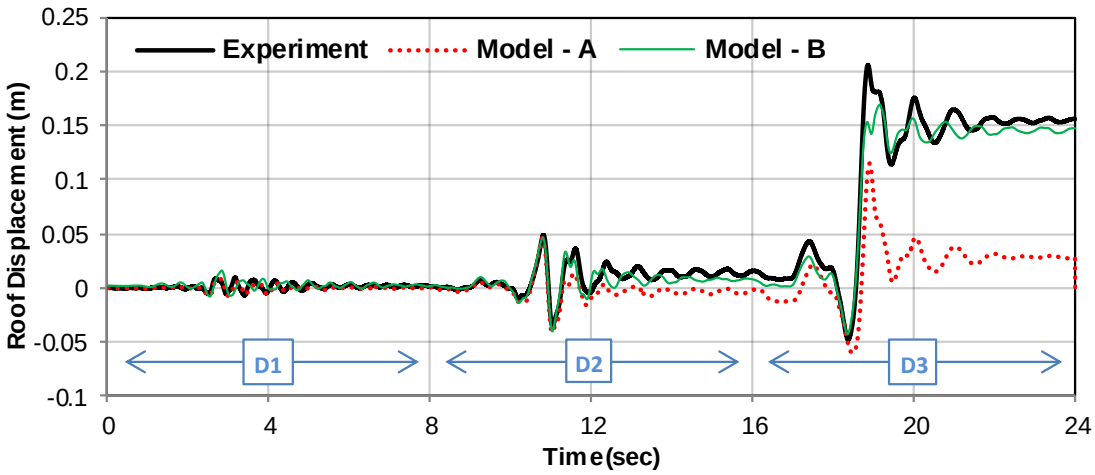

Figure 3. 22: Roof displacement history comparison for SP3

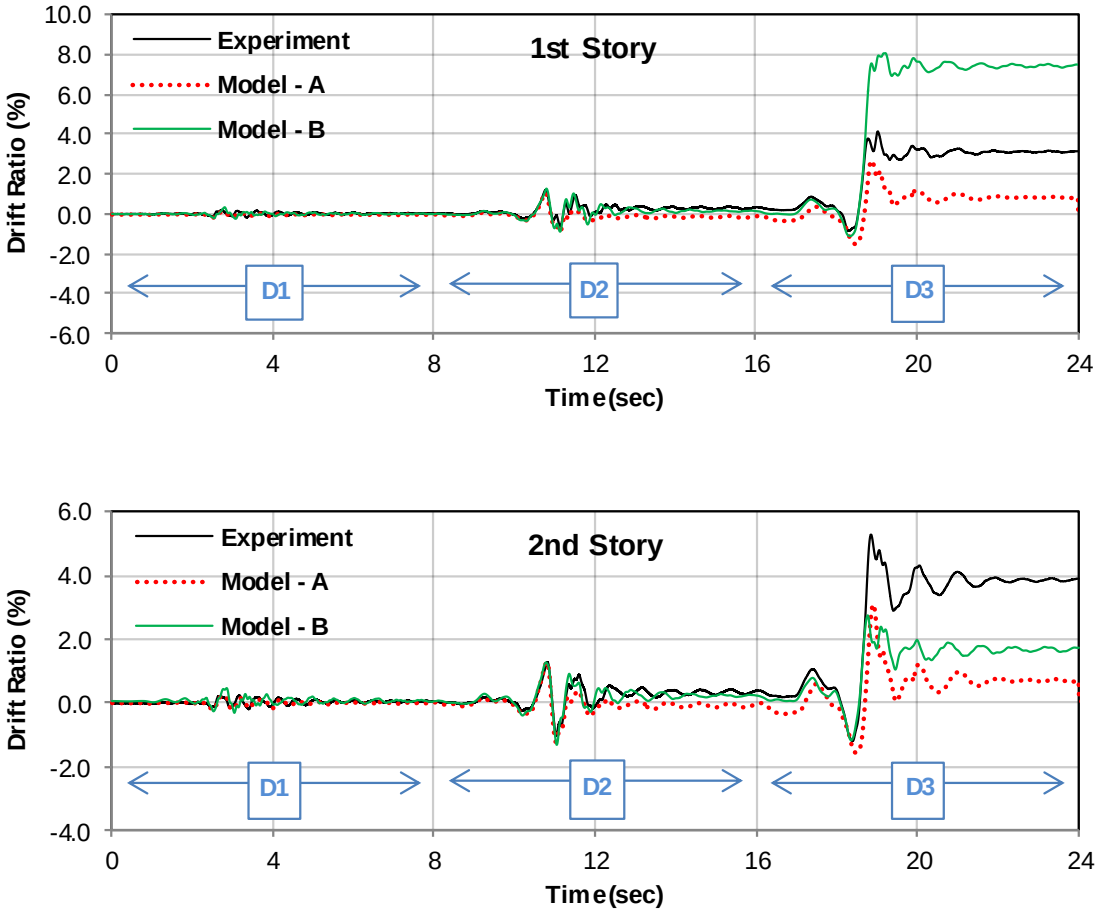

Figure 3. 23: Comparison of inter-story drift ratio histories for SP3

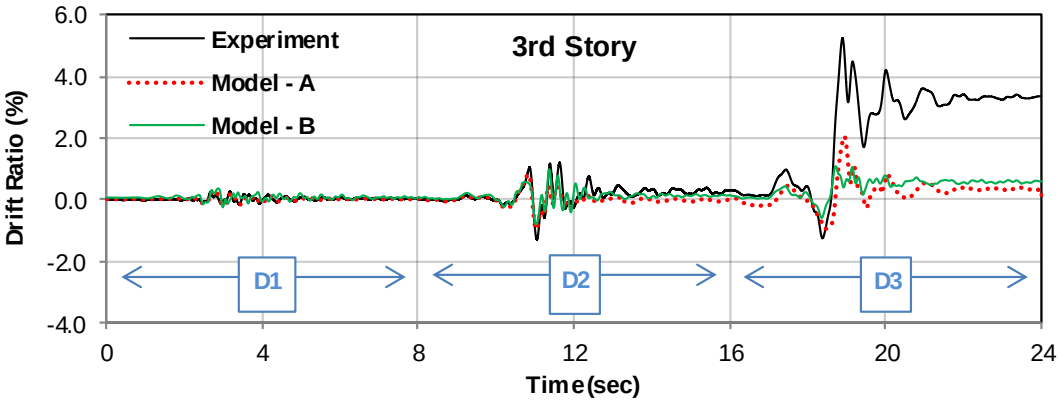

Figure 3. 23: Comparison of inter-story drift ratio histories (cont'd)

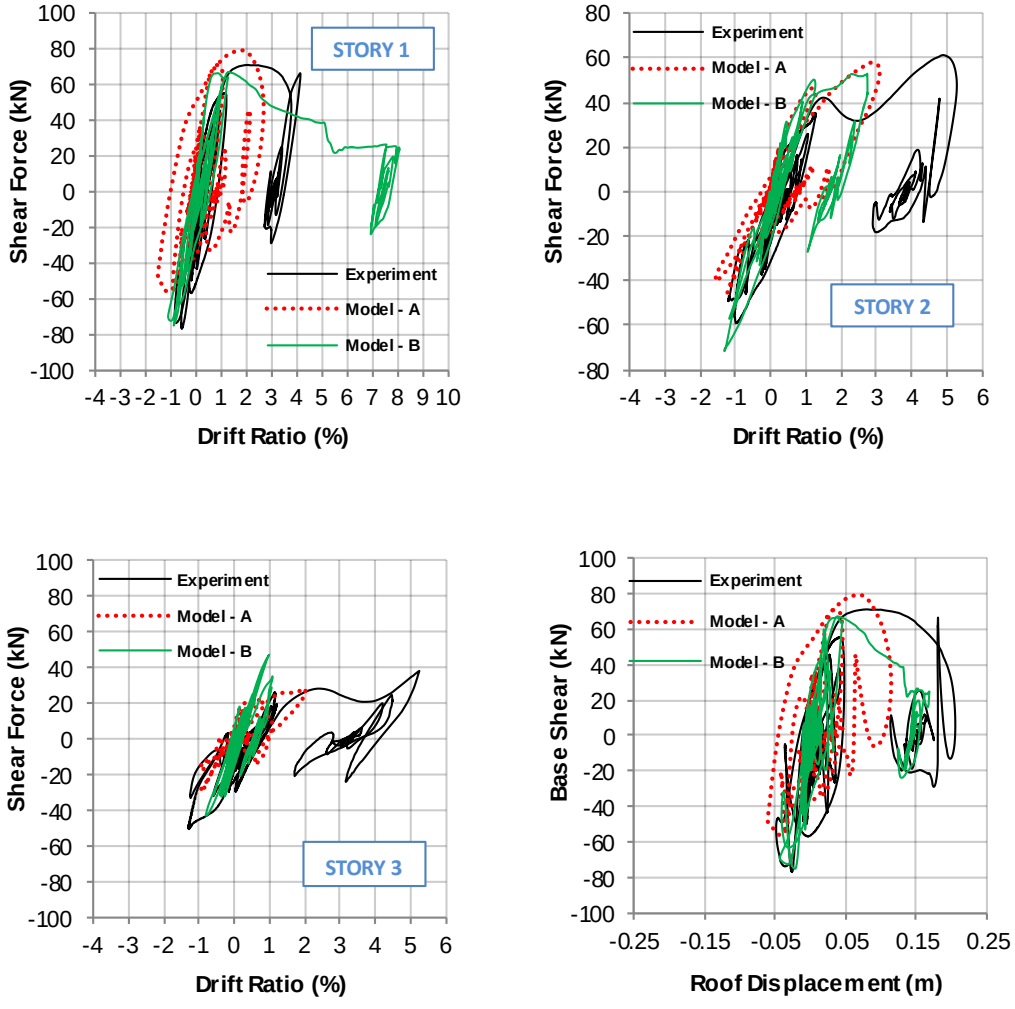

Figure 3. 24: Comparison of story shear force vs. drift response for SP3

Table 3. 11: Error estimation for peak roof displacement response (SP3)

Ground Motion	Maximum Roof Displacement(mm)			Error (%)	
	Experiment	Model - A	Model - B	Model - A	Model - B
D1	9.4	8	16.0	14.8	70.3
D2	48.7	46.3	46.4	4.9	4.8
D3	206.0	115	169.4	44.2	17.7

Table 3. 12: Error estimations for peak base shear response (SP3)

Ground Motion	Maximum Base Shear(kN)			Error (%)	
	Experiment	Model - A	Model - B	Model - A	Model - B
D1	49.7	35.8	45.7	27.9	8.1
D2	76.8	71.1	75.1	7.4	2.1
D3	73.8	79.4	72.5	7.6	1.8

Table 3. 13: Error estimations for peak inter-story drift response (SP3)

	Inter-story drift (%)			Error (%)	
Story	Exp.	Model - A	Model - B	Model - A	Model - B
1	4.14	2.69	8.07	35.17	94.82
2	5.28	3.10	2.75	41.32	47.96
3	5.25	2.05	1.09	60.99	79.27

Results presented in Figure 3. 25 are used for further evaluation of Model-A in terms of damage locations and crack patterns in comparison with the experimental observations. Good agreement between the damage locations and crack patterns is considered as an indicator for ability of numerical model in simulating the observed behavior of the test frame.

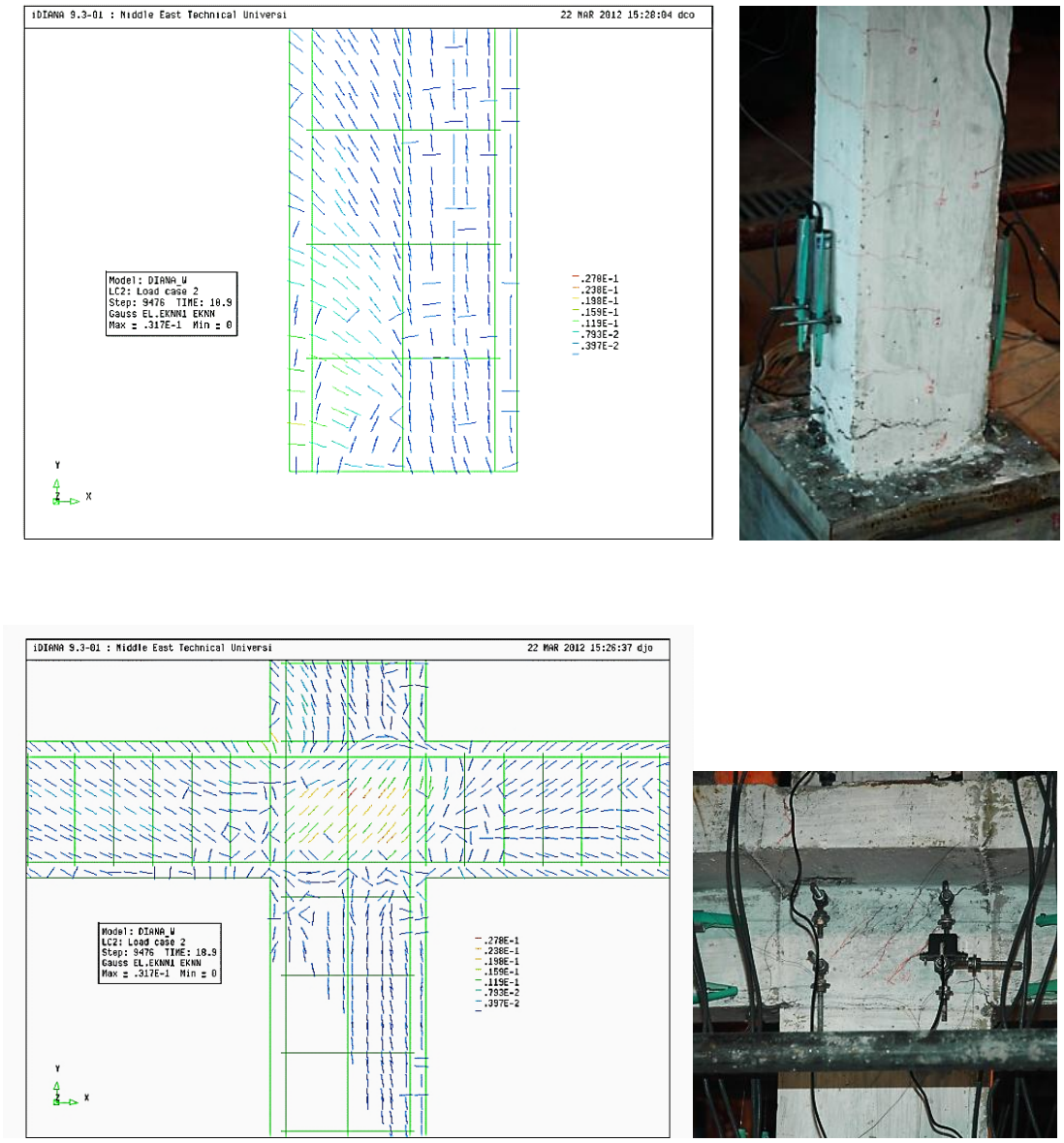

Figure 3. 25: Crack pattern comparison in critical damage regions (SP3)

Rotation histories of 1st story column bases are presented in Figure 3. 26 in comparison with the measured rotations in test. Rotation values were calculated using nodal displacement histories of nodes on the model corresponding to gage locations in potential plastic hinge regions of the specimen. It can be stated that the analysis results are in general agreement with the measured rotation demands.

Average curvature profiles at the bottom ends of 1st story columns are presented in the Figure 3. 27 for the time step of peak roof displacement with corresponding

damage views. Same strategy with Specimen-1 and Specimen-2 was followed for calculation of maximum and yield curvature values of each level in the column ends. Maximum and yield curvature profiles were used in determination of estimated plastic hinge lengths and the amounts of plastic rotations calculated by integration of the curvature profiles. Table 3. 14 shows the estimated bottom end rotations and plastic hinge lengths for each column of the 1st story. Results obtained in this part show that plastic rotation demands of significant amounts (higher than 2%) were reached in this specimen. Variation in the estimated plastic hinge lengths was smaller as compared to other two specimens with the values between 200 mm and 250 mm. This result shows the importance of detailing on the plastic hinge length.

Percent contributions of the estimated elastic and plastic rotations of columns to the total drift of the columns were presented in Table 3. 15 in comparison with the other deformation components.

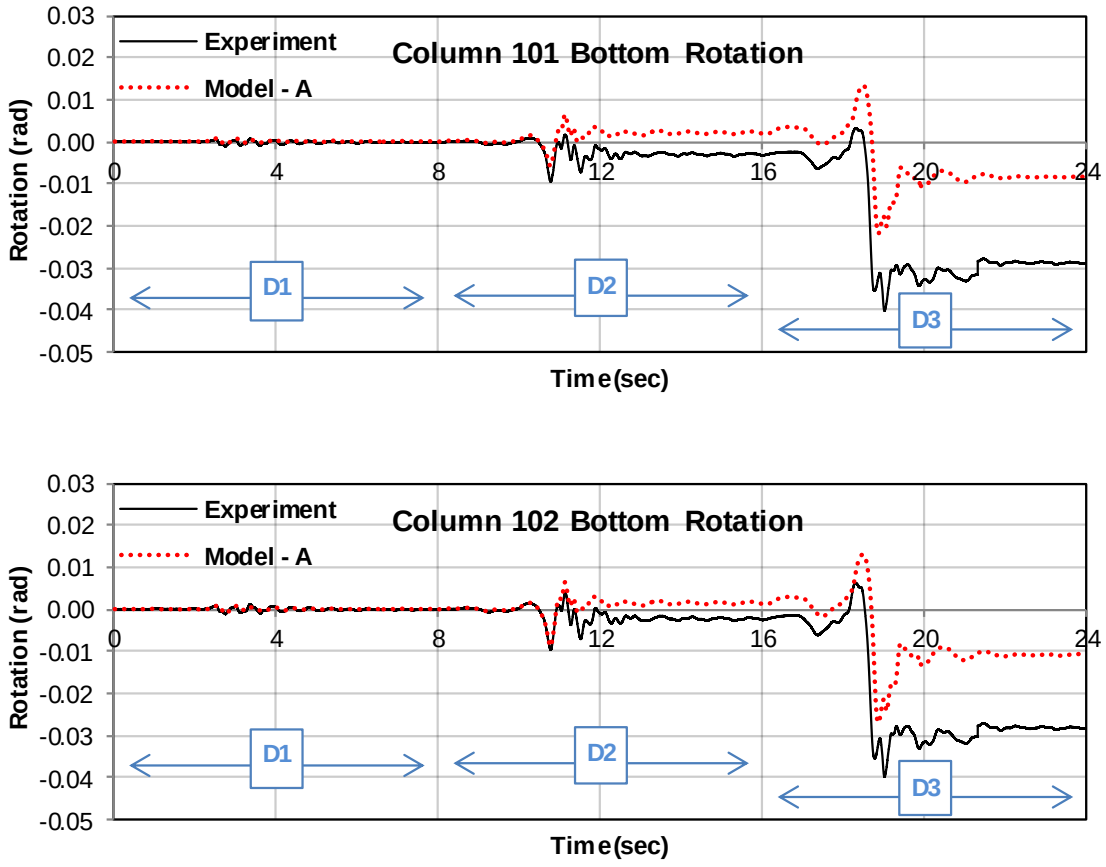

Figure 3. 26: Comparison of bottom end rotations of 1st story columns (SP3)

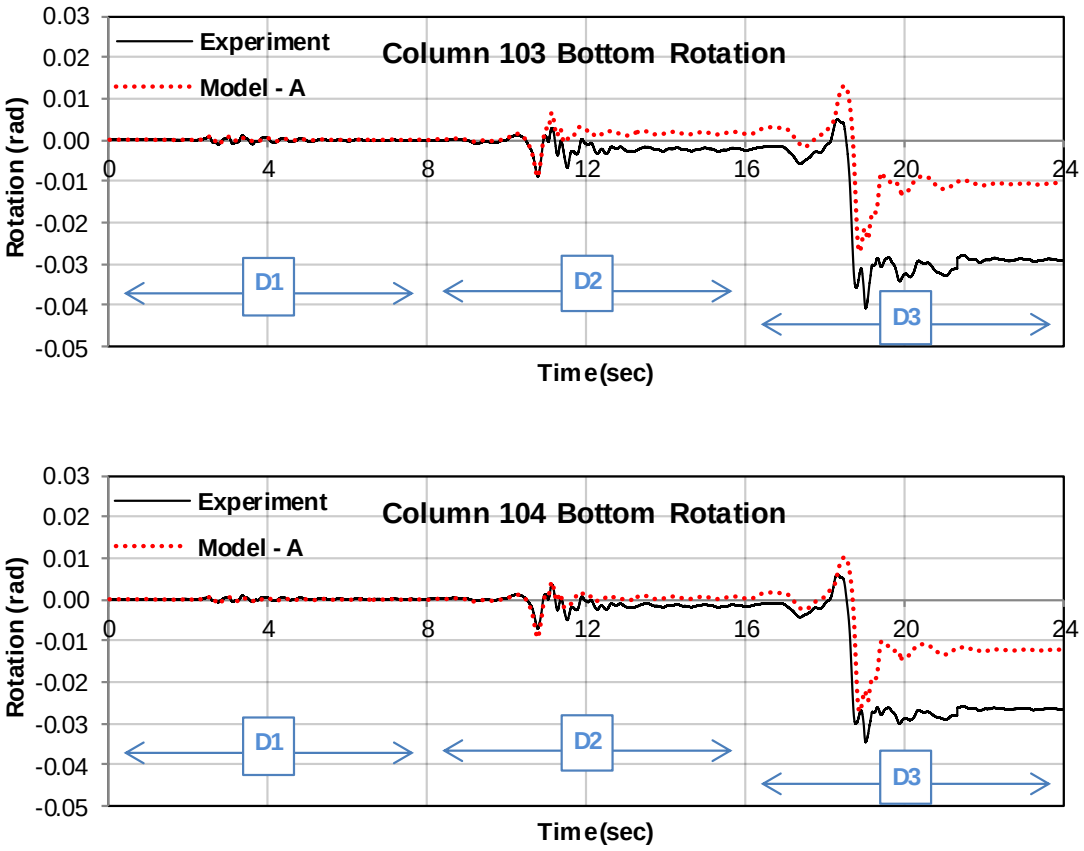

Figure 3. 26: Comparison of bottom end rotations of 1st story columns (SP3) (cont'd)

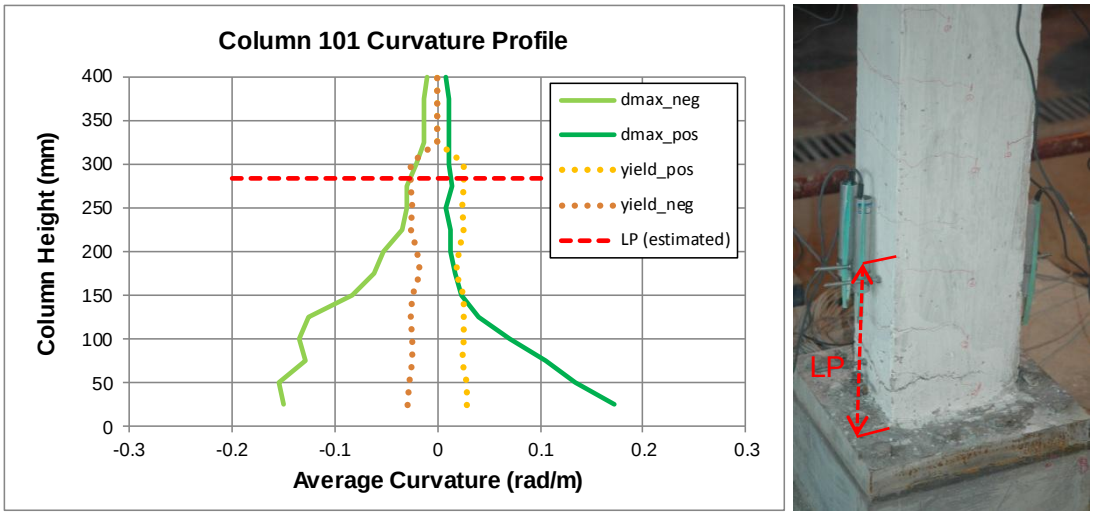

Figure 3. 27: Curvature profiles of 1st story column bases (SP3)

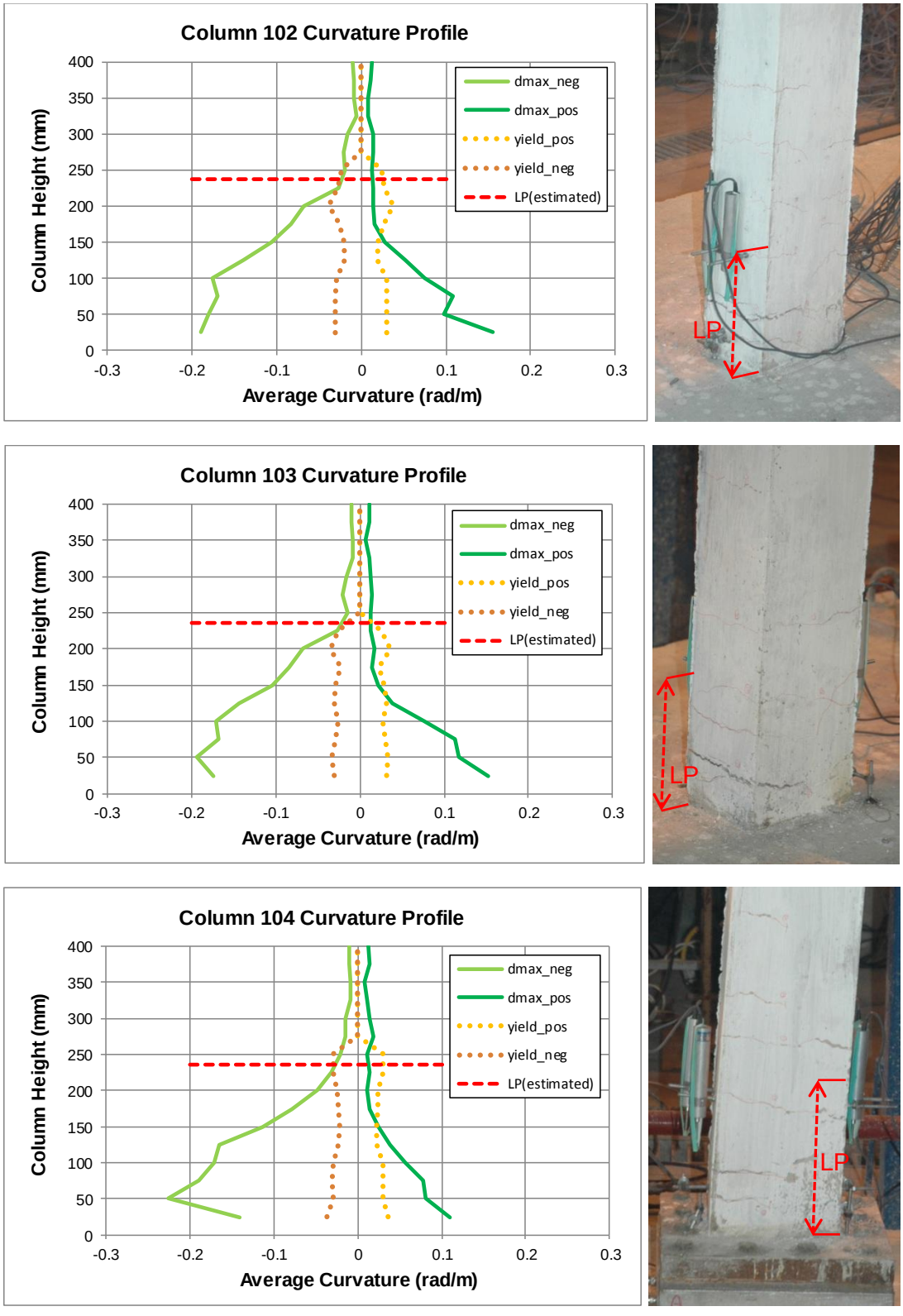

Figure 3. 27: Curvature profiles of 1st story column bases (cont'd)

Table 3. 14: Bottom End Rotations of 1st Story Columns (SP3)

	Column Bottom End Rotations			
Column ID	101	102	103	104
Lp (mm)	284	237	237	237
$\Theta_{plastic}$ (rad)	0.0168	0.0209	0.0206	0.0217
$\Theta_{elastic}$ (rad)	0.0064	0.0060	0.0062	0.0059

Shear distortions in clear heights of columns and joint regions were considered as the other deformation components contributing to the total drift. Following the same strategy with Specimen-1 and Specimen-2, average shear distortion profiles of 1st story columns of Specimen-3 was obtained and presented Figure 3. 28 for the time step of analysis with the maximum roof displacement.

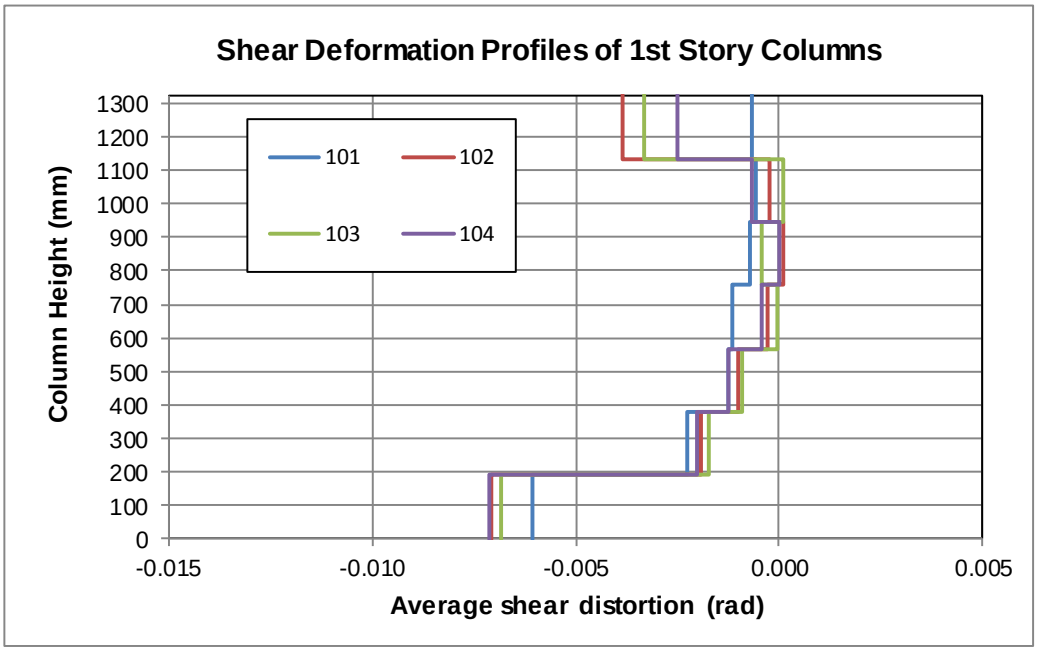

Figure 3. 28: Shear deformation profiles of 1st story columns (SP3)

Contribution of each of these deformation components to the total drift was presented in Table 3. 15 for each column of 1st story with estimated plastic hinge lengths. The results, showed that contribution of shear deformations in clear heights of columns were lower as compared to the other specimens while plastic rotations and joint deformations were higher. In consistence with the experimental findings and observations, deformations and damages at the element ends and joint regions governed the failure mode of the frame.

Table 3. 15: Percent contributions of each deformation component (SP3)

		Drift Contributions			
Column	Lp (mm)	Plastic Rotation(%)	Shear Deformation(%)	Joint Deformation(%)	Elastic Rotation(%)
101	284	52.8	6.2	-4.0	45.0
102	237	68.3	7.0	-12.4	37.1
103	237	67.1	6.4	-10.2	36.7
104	237	70.8	6.8	-10.2	32.5

Shear deformation time histories of the first story joints are presented separately for interior and exterior joints in Figure 3. 29. Joint deformation comparison of analyses on Model-A, and available experimental data is also presented in Figure 3. 29, for Joint-2.

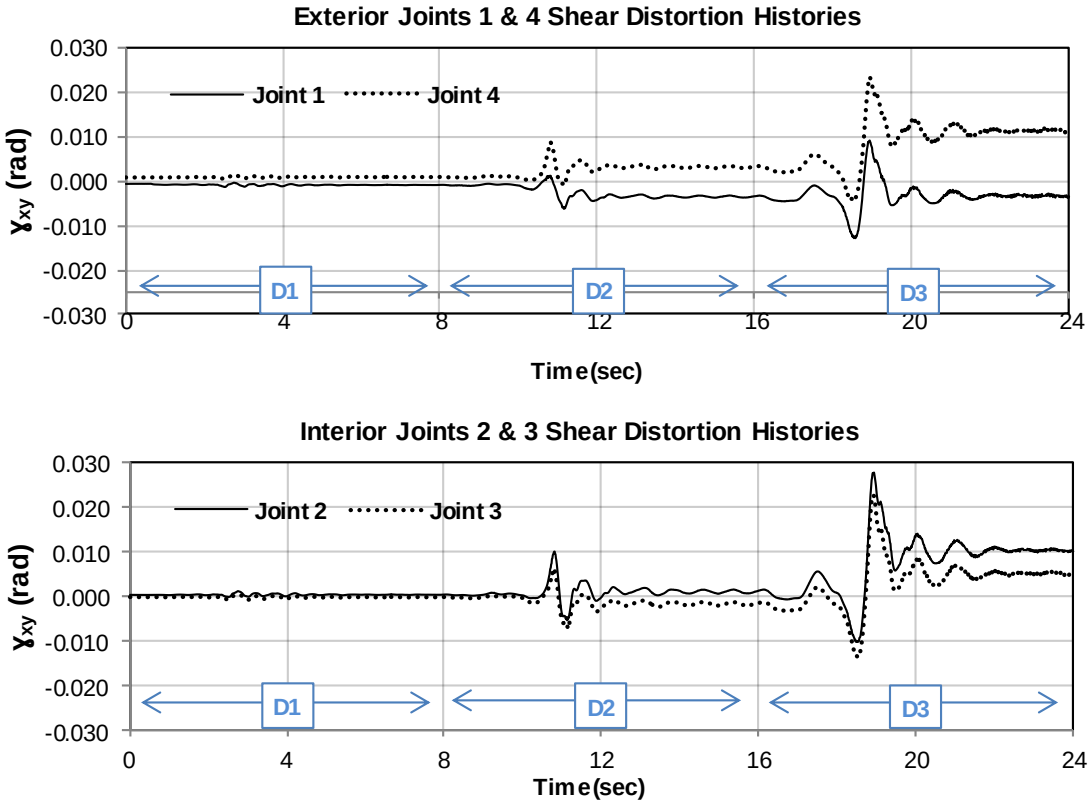

Figure 3. 29: Joint deformation time histories for Specimen-3

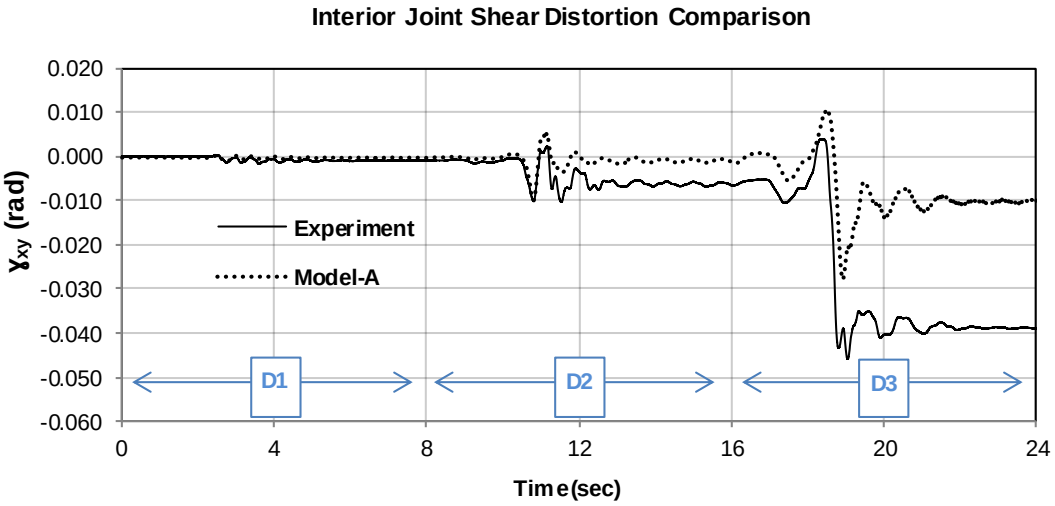

Figure 3. 29: Joint deformation time histories for Specimen-3 (cont'd)

As can be seen from these plots and results of drift contributions, deficiency of lack of shear deformations in Specimen-3 resulted in higher shear distortions and consequently higher contributions to story drift as compared to the other two specimens. The joint shear deformation demands reached the values of 3% in simulations while the measured shear distortion was higher than 4% with significant residual. Isolated connection test results (Walker (2001), Alire (2002)) show that, at such levels of joint shear distortions, shear degradation and significant joint damage are expected.

3.3. Performance Evaluation of Test Frames

Performance levels of beams and columns of each specimen were determined by the strain-based method suggested in Turkish Earthquake Code (2007). Performance evaluation was made using the results of time history analyses conducted on Model-A of each specimen throughout the ground motions used in experiments. The method is valid for evaluation of ductile reinforced concrete members. For this purpose, highest strain values for structural elements were determined under each ground motion for the plastic hinge regions at the element ends. Plastic hinge length definition of the Turkish Earthquake Code, which is given as h/2 for beams and columns, was considered for calculation of the strain values from the recorded nodal displacement histories on the model. Three performance

limits were defined for ductile members in section level. These limits are Immediate Occupancy (IO), Life Safety (LS) and Collapse Prevention (CP) as presented in Figure 3. 30. In the method of Turkish Earthquake Code (2007), strain limits for the longitudinal reinforcement are given for each performance level in the following form: ε_{IO}=0.010, ε_{LS}=0.40, ε_{CP}=0.60. Strain limits for concrete in compression at the stirrup level are: ε_{IO}=0.0035, ε_{LS}=0.0035+0.01(ρ_s/ρ_{sm}), ε_{CP}=0.004+0.01(ρ_s/ρ_{sm}) in terms of volume of existing confining steel (ρ_s) and volume of required confining steel (ρ_{sm}), where the ratio (ρ_s/ρ_{sm}) is defined with the upper limit of 1.0. These limits were calculated for each specimen and compared with the strain values in element ends according to the assumption of uniform strain distribution along plastic hinge length of h/2 as suggested in the code.

Performance evaluation of each specimen was conducted and obtained damage regions under each ground motion are compared with the observed damages in elements. It is important to note that, observed damage is a subjective statement and can be judged differently. Hence, our comparisons herein may suffer from our subjectivity is assessing the damage. The main aim of this section, however, is to compare the estimated damage levels computed by using the strain-based method with some physical damage under realistic ground motion demands.

It should be noted that above methodology of strain based assessment applies only to members classified as ductile. Although the columns of Specimen-1 did not satisfy the conditions of ductile behavior, performance evaluation was conducted assuming a ductile response owing to the observed deformability of the frame.

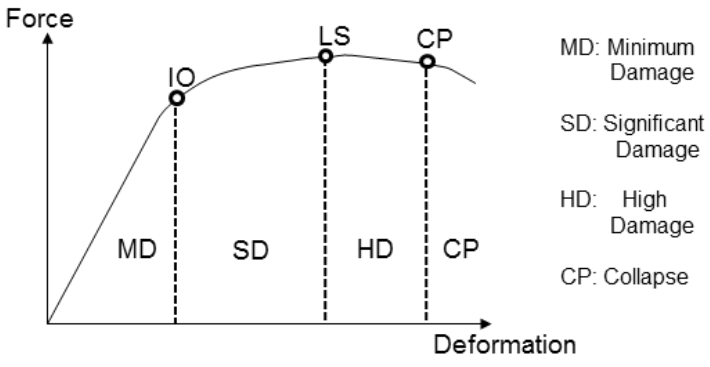

Figure 3. 30: Performance Limits and Damage Regions

3.3.1. Specimen-1

Continuous PsD test results of Specimen-1 under the ground motions D1, D2 and D3 were given in the Section 2.5.1 with the observations and classifications of damage regions. In this part, performance evaluation results are compared with the experimental observations. Damage regions corresponding to each element end are presented in Figure 3. 31.

Under the 1st ground motion D1 all of the members remained in minimum damage region (MD). Observations in the experiment are consistent with these results since no significant damage was observed.

The second ground motion, D2, resulted in significant damage in the first bay of 2nd story beams according to performance evaluation. Rest of the element ends remained in the limits of minimum damage region. In the experimental observations, initiation of flexural cracks in 1st story beams and columns was reported. However the crack widths were not large enough to indicate significant yielding at the element ends. Therefore, performance evaluation results were found to be consistent and perhaps slightly on the safe side in comparison to the damage levels in experimental observations.

Performance evaluation results under the design earthquake D3 estimated that some of the element ends in 2nd and 3rd stories passed the limits of minimum damage region. Bottom ends of first story columns were found to be exceeding the collapse prevention (CP) performance limit as shown in Figure 3. 31. Experimental observations showed that significant shear cracks in first story beams and flexural cracks at the bottom ends of 1st story columns were observed at inter-story drift ratio of about 3.5%. However, degree of damage was not considered to be in collapse region during the test and it can be said that the test frame satisfied the intended performance level of life safety. Therefore, it can be concluded that, performance evaluation of Specimen-1 yielded conservative estimations under the design ground motion.

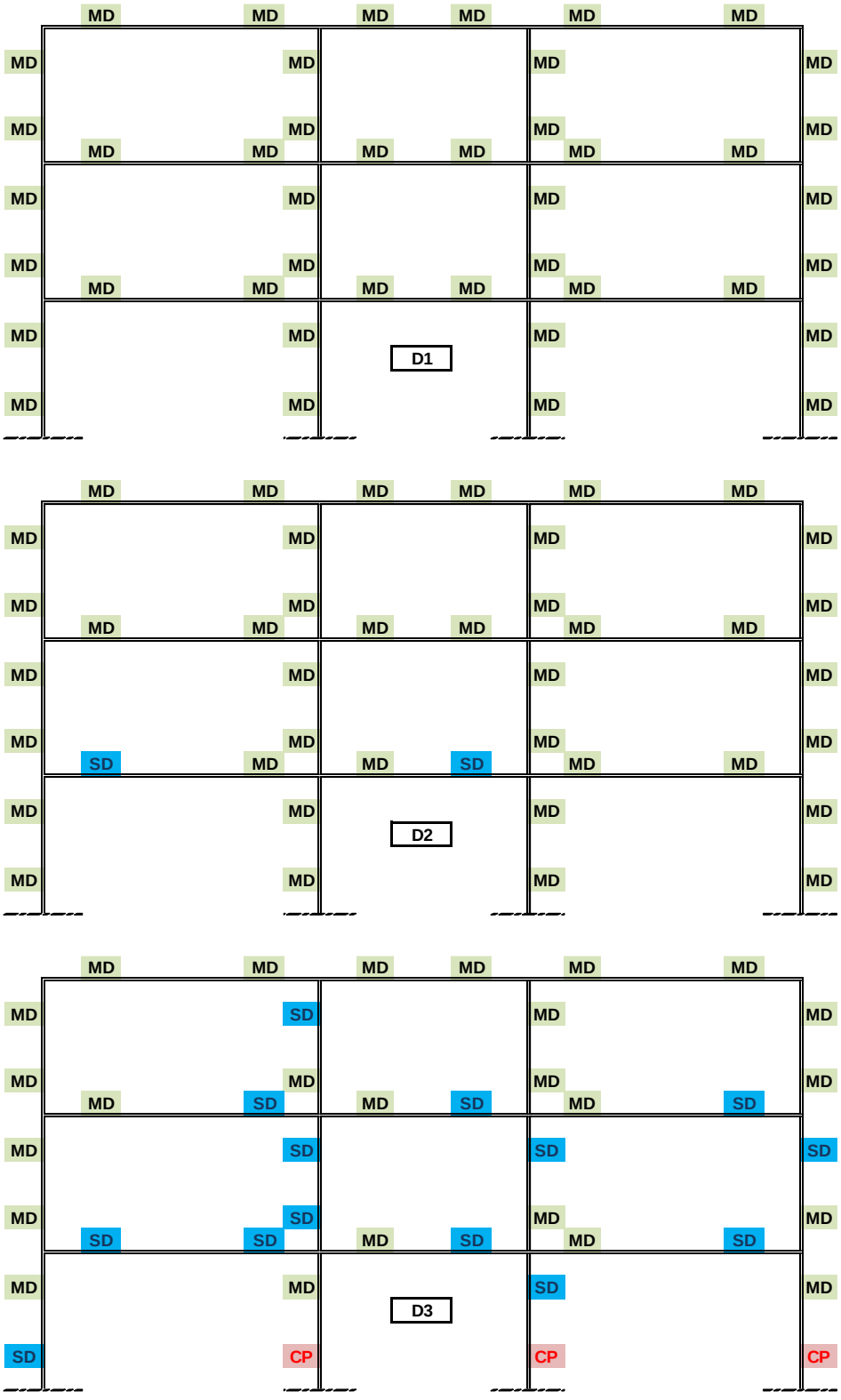

Figure 3. 31: Specimen-1 Damage Levels

3.3.2. Specimen-2

Performance evaluation results of Specimen-2 with code compliant design were presented in Figure 3. 32 for each ground motion to be compared with the experimental observations given in the Section 2.5.2. The first ground motion D1 applied to the specimen did not cause any significant damage and it was obvious that the frame remained in minimum damage region. Performance assessment results were found to be consistent with the observations.

Under the ground motion D2, initiation of flexural cracks in the bottom ends of 1st story columns was observed, whereas the rest of the structural elements were considered to remain in elastic limits. Although the performance evaluation resulted in minimum damage (MD) for almost all of the elements, initiation of the flexural cracks in the test specimen indicated that 1st story columns may have experienced some yielding and slightly passed the immediate occupancy (IO) performance limit. It should be noted that these damages pointed to early phases of plastic deformations. Hence, performance estimation of the method can be regarded as accurate in estimating the damage level for this ground motion.

The ground motion D3, corresponding to the design spectrum of the code compliant frame, was the most essential for evaluation of the suggested assessment method in the code. Performance evaluation results, presented in Figure 3. 32, shows that the frame satisfied the life safety performance level (LS) for all of the members. Significant damage was estimated for columns and beams in the 1st story, while rest of the members mostly remained in the minimum damage region (MD). These estimations were found to be consistent with the observations during the test. Although the opening and spread of flexural cracks in 1st story columns were observed, widths of cracks indicated that yielding in element ends was limited and can be considered as remained in significant damage region (SD). It can be concluded that, the specimen satisfied the design goal of life safety under the design earthquake and the performance evaluation results were found to be consistent with the observations and test performance of the frame.

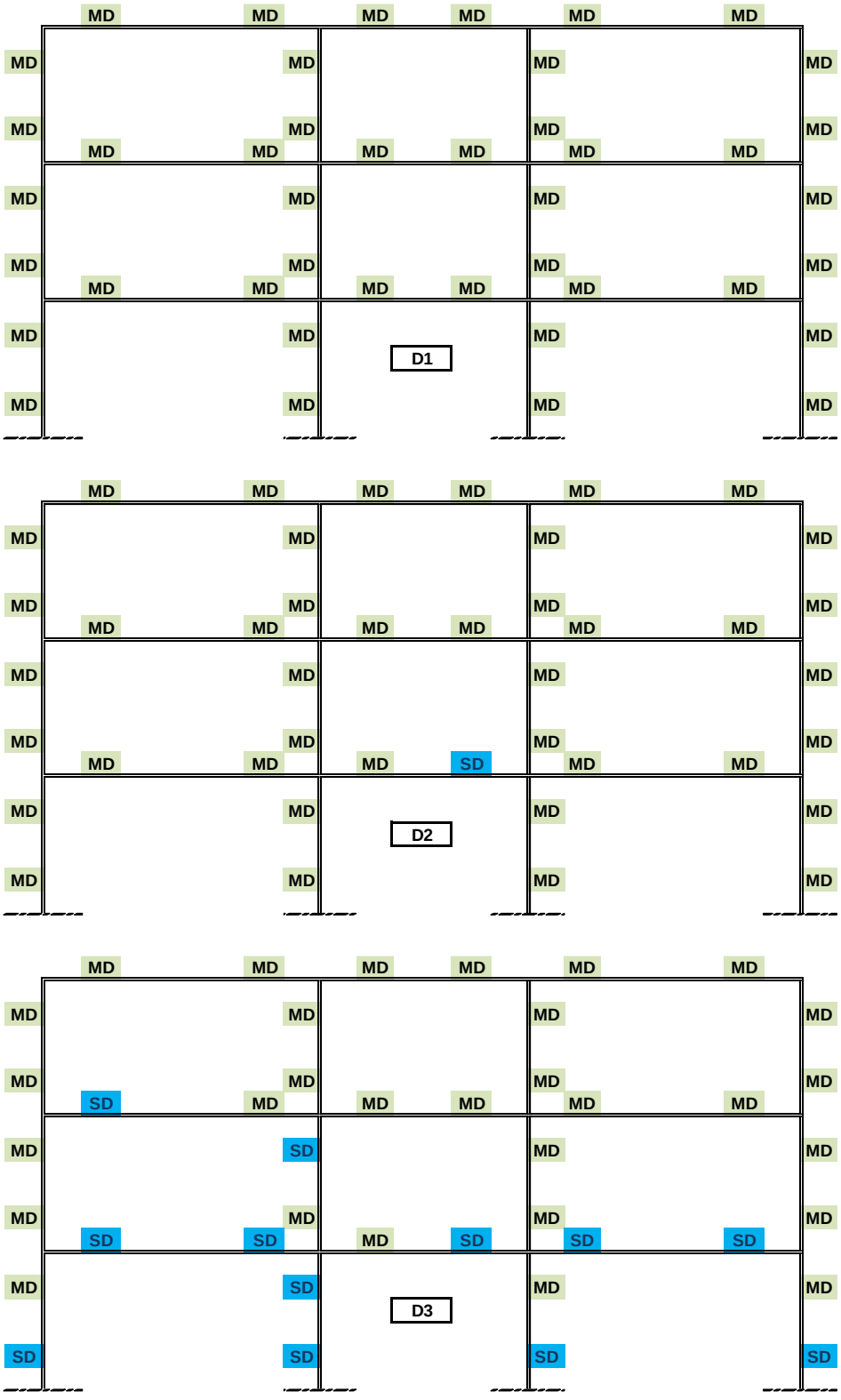

Figure 3. 32: Specimen-2 Damage Levels

3.3.3. Specimen-3

Performance evaluation of the specimen was conducted following the same method with the other specimens and the results are given in Figure 3. 33. Although the specimen was classified as a deficient frame, it should be noted that the columns of the specimen satisfies the ductile behavior condition required for the application of the performance evaluation method.

Under the ground motion D1, performance evaluation on Specimen-3 yielded minimum damage estimation for all members and the results were found to be consistent with the observations during the test.

All columns of the 1st story and some of the columns in 2nd story passed to significant damage region (SD) according to performance estimation results of the ground motion D2. Observation of visible flexural cracks on 1st story columns and measured story force vs. story drift response indicated that, inelastic deformations occurred in these elements. Hence, it can be concluded that performance evaluation results were consistent with the observed damages on the test frame for this ground motion.

Performance evaluation results under the ground motion D3, given in Figure 3. 33, showed that damage region for 1st and 2nd story columns were collapse region (CP) and significant damage (SD) for beams in these stories. Measured maximum inter-story drift ratios for 1st and 2nd stories exceeded the values of 4% and 5% respectively and significant amount of residual displacements were obtained in the level of 4% inter-story drift. Large flexural cracks in column ends and significant shear cracking on spans were followed by the spread of damage to the upper stories in terms of flexural cracks on beam ends and inclined cracks in joint regions. As stated in the Section 2.5.3, both measurements and observations during the test indicated that the specimen can be considered in collapse region under the ground motion D3. Therefore, it can be concluded that the performance evaluation method estimated the damage successfully for the deficient test frame.

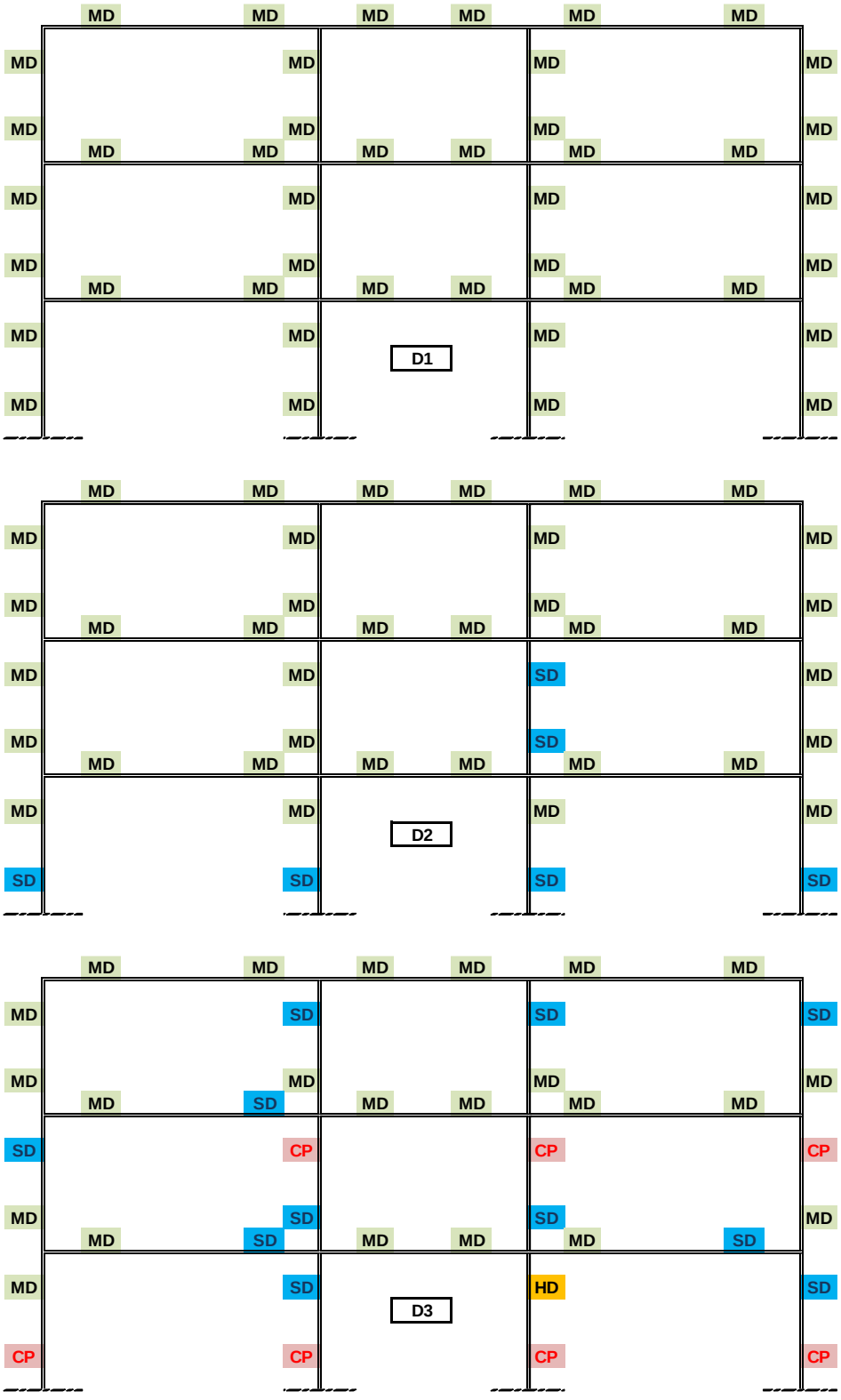

Figure 3. 33: Specimen-3 Damage Levels

3.4. Discussion of Results

Numerical simulations, conducted using two different modeling strategies, were compared with the results of pseudo-dynamic tests of three specimens in terms of global response parameters. Performance of two models showed some differences for each specimen. After comparing the model performance from different aspects, Model-A with continuum type finite elements was used for further analytical study on local deformations and performance evaluation of specimens. Contributions of different deformation sources were calculated and compared for each of the specimens representing distinctive cases. In addition, plastic hinge length estimations were calculated. Finally, results of performance assessment by employing the TEC (2007) were obtained. In this section, we further discuss the issues of plastic hinge length and shear deformations in columns in light of our numerical findings.

i) On the Plastic Hinge Length

Several researchers conducted experimental and analytical studies on the behavior of columns, plastic hinge lengths and contribution of shear deformations in the past. Experimental studies were mostly based on cyclic test results of RC columns with different geometrical and detailing properties.

As a result of these studies, several different plastic hinge length estimation approaches were developed for different column detailing, material strengths and levels of axial loads. Baker (1956) proposed an equation for plastic hinge length (*Lp*) based on the conducted experiments on beams and columns with test variable of concrete strength, yield strength, axial load and reinforcement detailing. It was reported that *Lp* ranged from 0.4*d* to 2.4*d*, where d is defined as the effective depth. Later on, Baker and Amarakone (1964) suggested a simplified version of that equation. Park et al. (1982) tested four columns under different axial loads ranging from 0.2*fc'Ag* to 0.6*fc'Ag*. The researcher concluded that experimentally observed *Lp* was insensitive to the level of axial load and proposed a simple *Lp* definition as 0.4*h*. Following a similar approach, Priestley and Park (1987) proposed another equation for *Lp* estimation of reinforced concrete columns. Suggested expression was revised by Paulay and Priestley (1992) to account for different grades of longitudinal reinforcement and it was reported that *Lp* was estimated as 0.5h for

typical columns. Sakai and Sheikh (1989) conducted a study based on review of literature and concluded that *Lp* was affected by transverse reinforcement ratio, axial load level and aspect ratio of columns. Bayrak and Sheikh (1998) conducted column tests with high axial loads and reported that measured *Lp* were approximately 1.0h in their tests. In the study of researchers Lu et. al.(2005), a survey of relevant experimental data from previous researchers was conducted and after a regression analysis, the nominal value of *Lp* was expressed with a modified Priestley and Park's formula as 0.077z + 8.16db.

Plastic hinge lengths (*Lp*) were calculated for the 1st story columns of each specimen using the expressions suggested by these different researchers.

Plastic rotation values, obtained for each the columns in Section 3.2, were used to calculate the plastic hinge lengths for the assumption of constant curvature through the height of the hinge region. Plastic hinge length calculated with this assumption were named as "average" plastic hinge length and calculated as $Lp_{(avg)}=\Theta_{plastic} / \emptyset_{ult}$. Figure 3. 34 represents the definition of $Lp_{(avg)}$ for the 1st story columns.

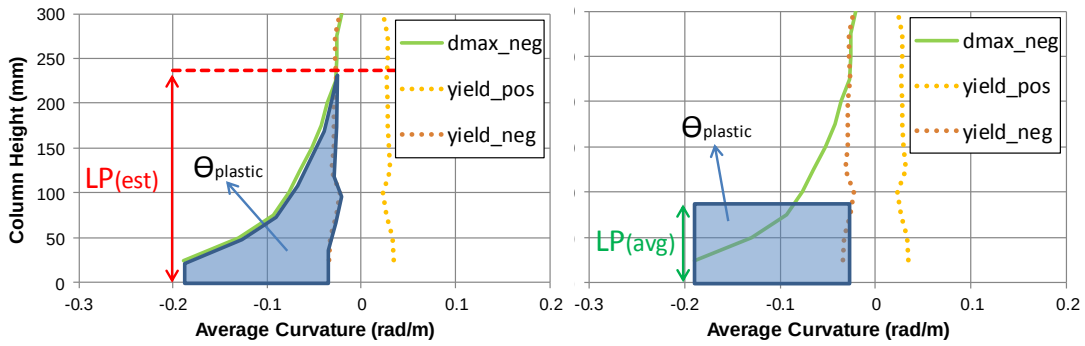

Figure 3. 34: Calculation of average Lp using constant curvature assumption

Calculated *Lp* values were presented in the following figures to be compared with the $Lp_{(est)}$ values estimated through the analytical study on Model-A (Section 3.2) and the $Lp_{(avg)}$ values calculated with the constant curvature assumption. Comparisons of the plastic hinge expressions with analytically estimated values are also presented in Table 3. 16 and Table 3. 17.

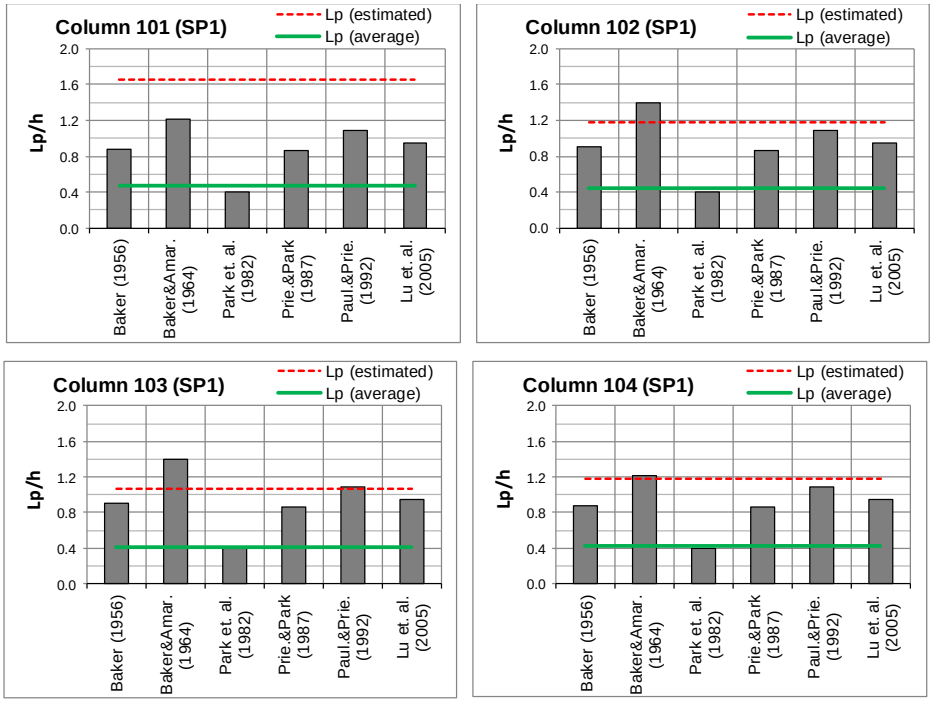

Figure 3. 35: Lp estimation comparison for Specimen-1

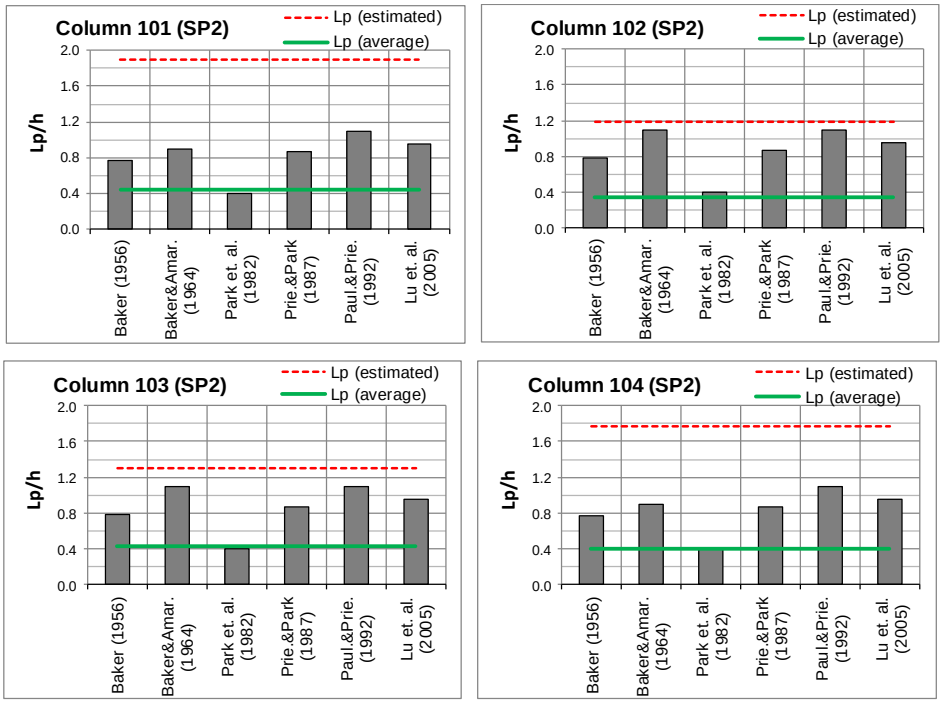

Figure 3. 36: Lp estimation comparison for Specimen-2

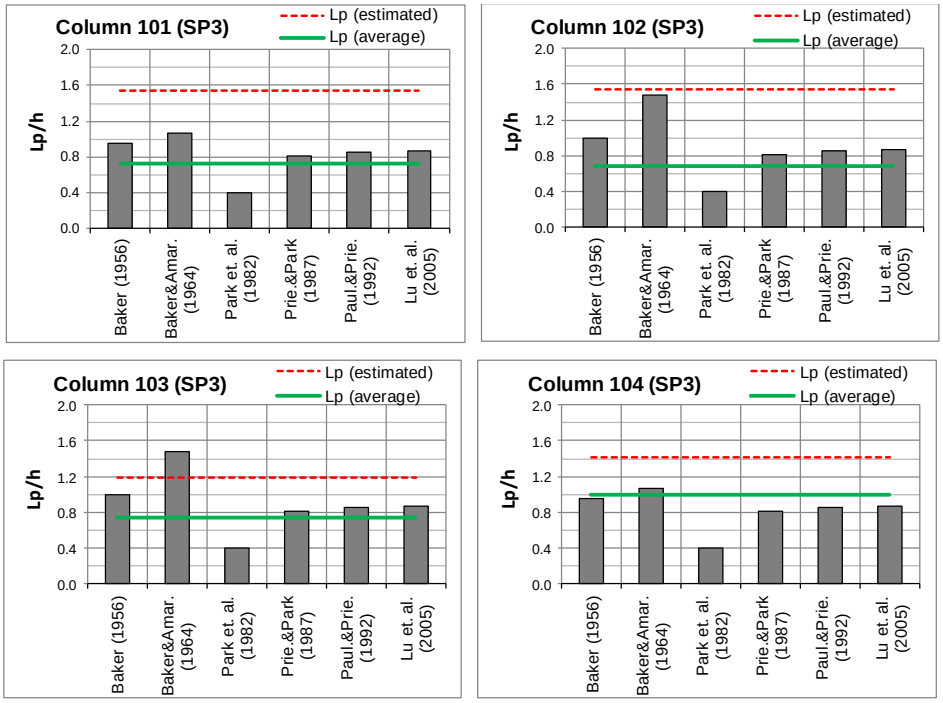

Figure 3. 37: Lp estimation comparison for Specimen-3

Table 3. 16: Comparison of plastic hinge expressions with estimated Lp

	Specimen1				Specimen2				Specimen3					
Lp(est)/Lp	101	102	103	104	101	102	103	104	101	102	103	104	Mean	St. Dev.
Baker (1956)	1.88	1.30	1.17	1.34	2.49	1.52	1.67	2.33	1.60	1.54	1.18	1.48	1.62	0.42
Baker&Amar. (1964)	1.37	0.85	0.76	0.98	2.10	1.08	1.19	1.97	1.45	1.04	0.80	1.34	1.24	0.43
Park et. al. (1982)	4.14	2.96	2.66	2.96	4.73	2.96	3.25	4.44	3.84	3.84	2.96	3.55	3.52	0.67
Prie.&Park (1987)	1.91	1.37	1.23	1.37	2.19	1.37	1.50	2.05	1.91	1.91	1.47	1.76	1.67	0.32
Paul.&Prie. (1992)	1.52	1.08	0.97	1.08	1.73	1.08	1.19	1.62	1.82	1.82	1.40	1.68	1.42	0.32
Lu et. al. (2005)	1.74	1.24	1.12	1.24	1.99	1.24	1.37	1.86	1.77	1.77	1.36	1.63	1.53	0.30

Table 3. 17: Comparison of plastic hinge expressions with average Lp

	Specimen1				Specimen2				Specimen3					
Lp(avg)/Lp	101	102	103	104	101	102	103	104	101	102	103	104	Mean	St. Dev.
Baker (1956)	0.54	0.50	0.46	0.49	0.59	0.45	0.55	0.53	0.76	0.68	0.73	1.05	0.61	0.17
Baker&Amar. (1964)	0.39	0.32	0.30	0.35	0.50	0.32	0.39	0.45	0.69	0.46	0.50	0.94	0.47	0.18
Park et. al. (1982)	1.18	1.13	1.04	1.07	1.12	0.87	1.08	1.01	1.83	1.70	1.83	2.51	1.36	0.49
Prie.&Park (1987)	0.55	0.52	0.48	0.50	0.52	0.40	0.50	0.47	0.91	0.85	0.91	1.24	0.65	0.26
Paul.&Prie. (1992)	0.43	0.41	0.38	0.39	0.41	0.32	0.39	0.37	0.87	0.80	0.87	1.18	0.57	0.28
Lu et. al. (2005)	0.50	0.47	0.44	0.45	0.47	0.37	0.45	0.42	0.84	0.78	0.84	1.15	0.60	0.24

It can be observed that estimated plastic hinge lengths are generally longer than the estimations of equations developed in the literature. This can be attributed to the level of conservatism in developing plastic hinge length expressions. In addition, the plastic hinge lengths are usually used with lumped plasticity approaches where the plastic curvature distribution is assumed to be constant within the plastic hinge length. Hence, the proposed plastic hinge length can be expected to be less than the zone of yielding. Among the plastic hinge length expressions, the equation proposed by Baker and Amarakone (1964) seems to provide the closest estimate for the columns under consideration (Table 3. 16). It is also important to note that definition of a single value for the plastic hinge length of columns with similar dimensions and longitudinal reinforcement ratio is not possible. Most of the previous experimental studies were based on flexural behavior of reinforced concrete columns with constant axial load condition. Gilbertsen and Moehle (1980) and Abrams (1987) are among few experimental studies where variations in axial force were considered. In addition to the constant axial loading condition, effects of proportionally and non-proportionally varying axial loads were also studied analytically. In the studies of Emori and Schnobrich (1978) and Keshavarzian and Schnobrich (1984), effects of fluctuating axial forces on the behavior of reinforced concrete structures where the axial force varied proportionally to lateral force and moment are investigated. Effects of non-proportionally varying axial force were considered through the experimental study of Kreger and Linbeck (1986) on a single column and analytical study of Saadeghvaziri and Foutch (1988). Both of these studies have shown that the post-elastic behavior of columns was significantly affected by the uncoupled variations of axial and lateral forces.

Considering the estimated plastic hinge lengths and observed damages of 1st story columns, it can be stated that deformation history and direction of peak response changed the inelastic behavior significantly among the columns of the same specimen. Under non-proportionally varying axial forces on columns due to earthquake loading and non-cyclic deformations, it was observed from each specimen that, higher axial forces did not necessarily cause higher plastic hinge lengths conversely to the case of cyclic deformations under constant axial force. Maximum and minimum axial force demands in the 1st story columns of test specimens are presented in Table 3. 18 in terms of axial load ratio. The results,

obtained from the simulations on Model-A, were given separately for each specimen and each of continuously applied ground motions.

Table 3. 18: Axial load variations under earthquake loads

SP1	Axial Load Ratio (%)							
	101		102		103		104	
Initial	10.1		17.1		17.1		10.1	
	max	min	max	min	max	min	max	min
D1	11.4	8.8	18.3	15.9	18.2	15.9	11.4	8.8
D2	15.3	6.2	19.5	15.0	19.2	14.7	13.9	4.9
D3	13.6	4.0	18.3	14.0	19.4	15.7	15.9	6.6

SP2	Axial Load Ratio (%)							
	101		102		103		104	
Initial	7.1		12.2		12.2		7.1	
	max	min	max	min	max	min	max	min
D1	8.1	6.0	13.0	11.1	12.9	11.1	8.2	6.1
D2	11.3	3.8	14.3	10.4	13.7	9.8	10.5	2.9
D3	11.2	2.9	13.4	10.3	13.8	10.6	11.5	3.1

SP3	Axial Load Ratio (%)							
	101		102		103		104	
Initial	13.3		22.8		22.8		13.3	
	max	min	max	min	max	min	max	min
D1	14.7	11.8	24.2	21.4	24.1	21.3	14.8	11.9
D2	17.6	8.8	24.5	20.8	24.8	21.1	17.5	8.5
D3	16.5	7.0	24.3	22.0	24.5	22.4	18.8	9.1

(Axial Load Ratio: N/N_0 where N:Axial Load and N_0: $A_c f_{ck}$)

Contributions of various deformation components to story displacement are compared for 1st story columns of each specimen at the instant that maximum drift demand. It was clearly observed that higher values of plastic rotations were calculated in the columns with higher axial force due to overturning effect whereas no direct correlation between the axial force and the height of plastic hinge region was observed.

ii) On the Shear Deformations of Columns

Özcebe (1987) has studied shear-flexure interaction on a series of column specimens both experimentally and analytically. In that study, design shear capacities of column specimens with heavy web reinforcement were 75% higher than the shear force corresponding to flexural yield capacities. But, shear yielding occurred in his sectional analysis at a value of 60% of design shear capacity in the hinging regions. Deflection profiles of column specimens were obtained separately for flexural, bar-slip and shear deformations and accumulation of shear deformations in hinging regions was observed. Using such observations, it was stated that there is a strong interaction between flexural and shear behaviors of the specimens and flexural yielding promoted the shear yielding significantly. Contributions of each of these deformation components to the total deflection were also determined in these specimens experimentally for different cycles of loading. Shear deformation contribution was about 10% for the highest drift values applied to the specimens in which transverse reinforcement amount was compliant with the design requirements.

Within the scope of this study, shear deformation profiles of 1st story columns of each specimen were also compared for the instant of maximum story displacement demand as presented in Figure 3. 12, Figure 3. 20 and Figure 3. 28 for Specimens 1,2 and 3 respectively. Each column height was divided into segments of equal height and shear distortion in each segment was calculated from the analytical model to obtain shear deformation profiles of columns for that instant. It was observed from the deformation pattern of each of 1st story columns that, amount of shear deformations in column end-regions were significantly high compared to the mid-regions due to shear-flexure interaction in plastic hinge formation in the end regions. Contribution of shear deformations in columns were also compared for each of 1st story columns using analytical results and it was observed that higher amount of shear deformations occurred as the amount of plastic rotations increased. These observations, which were consistent for each specimen of this study, were also found to be consistent with experimental and analytical findings of the previous research of Özcebe (1987).

iii) On the Performance Assessment of Test Frames

Performance evaluations of test specimens were carried out according to the strain-based method suggested in Turkish Earthquake Code (2007) for each of continuously applied ground motions. The 3rd and last ground motion applied to the specimens was the design earthquake D3 which was the most destructive one. Therefore, illustrative comparison of results for the efficiency of the suggested method is made by using this earthquake. Comparing the experimental damage observations in Section 2.4 and the damage levels estimated by using this method in the Section 3.3, it was observed that the method yielded consistent results for the Specimen-2 and the Specimen-3, whereas it was found to be overly conservative for the Specimen-1 which had flexural-shear critical columns. Specimen-3 was obtained by modifications in column detailing of the code compliant design to represent different deficiencies. The condition of strong column-weak beam was violated for this specimen as explained in Section 2.4.3. Columns of this specimen were classified as ductile as far as the shear capacity vs. shear demand ratio was concerned. It can be concluded that, performing the assessment assuming ductile response for columns is acceptable despite the presence of flexure-shear critical columns. As a result, assessment results of Specimen-1 calls for immediate necessity for definition of performance limits for the flexural-shear critical columns instead of classifying them as brittle members, considering the plastic deformation capacities of these columns.

On the other hand, considering the estimated plastic hinge lengths through analytical study on Model-A and curvature profiles obtained for the peak deformation response under design earthquake, it was observed that strain values are highly sensitive to the location of strain measurements. To demonstrate this sensitivity of the performance evaluation results to the location of strain readings was also examined for the Specimen-2 by repeating the calculations using a gauge length of h/4 for columns and h/3 for beams from the faces. Results of the comparison between these two cases are presented in Table 3. 19. When a shorter gauge length is selected for strain calculation, the assessment results tend to estimate higher damage than observed. This fact points the philosophical error in defining the performance through strains.

Table 3. 19: Comparison of performance level estimations (SP2)

	1st Story Columns								1st Story Beams					
Elem. ID	101		102		103		104		111		112		113	
End	Bot.	Top	Bot.	Top	Bot.	Top	Bot.	Top	i	j	i	j	i	j
D1	MD	MD	MD	MD	MD	MD	MD	MD	MD	MD	MD	MD	MD	MD
D2	MD	MD	MD	MD	MD	MD	MD	MD	MD	MD	MD	SD	MD	MD
D3	SD	MD	SD	SD	SD	MD	SD	MD	SD	SD	MD	SD	SD	SD

	2nd Story Columns								2nd Story Beams					
Elem. ID	201		202		203		204		212		212		213	
End	Bot.	Top	Bot.	Top	Bot.	Top	Bot.	Top	i	j	i	j	i	j
D1	MD	MD	MD	MD	MD	MD	MD	MD	MD	MD	MD	MD	MD	MD
D2	MD	MD	MD	MD	MD	MD	MD	MD	MD	MD	MD	MD	MD	MD
D3	MD	MD	MD	SD	MD	MD	MD	MD	SD	MD	MD	MD	MD	MD

(a) ***Gauge length of h/2 (both beams and columns) to estimate strains for assessment***

	1st Story Columns								1st Story Beams					
Elem. ID	101		102		103		104		111		112		113	
End	Bot.	Top	Bot.	Top	Bot.	Top	Bot.	Top	i	j	i	j	i	j
D1	MD	MD	MD	MD	MD	MD	MD	MD	MD	MD	MD	MD	MD	MD
D2	MD	MD	MD	MD	MD	MD	MD	MD	SD	SD	SD	SD	SD	SD
D3	SD	MD	CP	HD	CP	SD	CP	MD	SD	SD	SD	SD	SD	SD

	2nd Story Columns								2nd Story Beams					
Elem. ID	201		202		203		204		212		212		213	
End	Bot.	Top	Bot.	Top	Bot.	Top	Bot.	Top	i	j	i	j	i	j
D1	MD	MD	MD	MD	MD	MD	MD	MD	MD	MD	MD	MD	HD	MD
D2	MD	MD	SD	MD	SD	SD	MD	MD	MD	MD	MD	MD	CP	MD
D3	MD	MD	SD	HD	SD	SD	MD	SD	SD	SD	SD	SD	CP	SD

(b) ***Gauge lengths of h/4 in columns and h/3 in beams to estimate the strains for assessment***

It should be reminded that, *Lp* estimation results using different expressions suggested by previous researchers showed significant variations among themselves. Therefore, it was noticed that use of different gauge length values other than the suggested value of *Lp=h/2* may affect the calculated strain values used in the method of Turkish Earthquake Code (2007).

In short, it can be stated that, the performance evaluations on the continuum models (Model-A) of test specimens yielded consistent results with the experimental damage observations. However, conservative results, obtained for the Specimen-1, revealed the necessity of additional failure mode definitions for the suggested

method of Turkish Earthquake Code (2007). Comparison of the estimated performance levels, using the original and an alternative plastic hinge length definition, showed that the strain based evaluation method is highly sensitive to the location of strain readings and yielded more conservative results for the alternative definition of smaller plastic hinge lengths. Therefore, the strain based method may be more suitable for continuum modeling approach than the lumped plasticity approach which is used more extensively in practice. In the lumped plasticity approach, use of rotation based performance limits may be more reliable, considering the weaknesses of the strain based method, and more practical without conversion of the rotation output of numerical models to the strains through cross-section analysis.

iv) On the Joint Deformations

Depending on the deficiencies in reinforcement detailing in joint regions and damage response of the test specimen, significance of joint deformations in the behavior showed differences for each frame. It was observed from the numerical simulation results of continuum model that, the joint deformations had significant effect on the structural behavior in terms of direct contribution to the drift and deformation demands on columns and beams. In practice, modeling approach of line elements with lumped plasticity is used more widely as compared to continuum modeling. Although rigid joint assumption is acceptable in performance evaluation techniques proposed in the codes and regulations, it can be stated that flexible joint models must be used to obtain better estimate for member end deformations and to calculate shear deformations to judge the performance of connections.

CHAPTER 4

SUMMARY AND CONCLUSIONS

Results of pseudo-dynamic tests and numerical simulations of three ½ scaled three-story three-bay reinforced concrete frames were presented in this study. The main aim of this study was to investigate the behavior and performance of reinforced concrete frames, considering the effects of various deficiencies, through the results obtained from tests and numerical simulations of calibrated models. In this sense, accuracies of modeling techniques were evaluated in comparison with the test results. Using the calibrated continuum models of each specimen, local deformation components were investigated in terms of their interaction with each other and contributions of each deformation source to the overall seismic behavior of the specimens. Additionally, performance evaluation procedure of TEC (2007) was examined for each specimen in light of damage observations from pseudo-dynamic tests. Plastic hinge lengths, estimated through dynamic analyses on numerical models, were compared with experimental observations and proposed expressions in the literature. Following are the main concluding remarks of this study:

1- Continuum modeling approach yielded more accurate results in terms of global displacement estimations as compared to frame modeling approach. Further study on the dynamic analyses on continuum models estimated the locations and extent of damage with a sufficient accuracy. In this respect, it can be stated that continuum modeling approach may be used as a reliable tool for estimation of structural behavior.

2- Drift deformation sources of 1st story columns were investigated separately in terms of elastic, inelastic and shear deformations along the column height

and joint regions. It was found that modeling these deformation sources may significantly affect the accuracy of numerical models for simulating the behavior of reinforced concrete frames and estimating the displacement demands on structural members.

3- A strong interaction between flexural and shear deformation within the plastic hinge regions of columns were observed. Estimated plastic hinge length of columns varied significantly depending on the level of axial load and direction of loading. Non-proportionally varying axial loads, which may occur under seismic loading, were found to affect the length of plastic hinge regions. Therefore, the plastic hinge lengths given in codes should be carefully selected. Further study on the plastic hinge length of TEC (2007) is recommended.

4- Considering joint and column shear deformations is found to be important for accurate deformation and damage estimations. Simple models may need to be incorporated to TEC (2007) to account shear deformations.

5- Strain based procedure of TEC (2007) yielded successful estimations of seismic performance except Specimen-1 with flexure-shear critical failure mode. However, the results of assessment were found to be sensitive to the locations of strain readings (assumed plastic hinge length). Conservative estimations obtained for the Specimen-1 revealed the necessity of additional studies on the member acceptance criteria of TEC (2007) for shear-flexure critical columns.

REFERENCES

Abrams, D. P. (1987). "Influence of axial force variation on flexural behavior of reinforced concrete columns." *ACI Struct. J.,* May-June, 246-254.

ACI Committee 318, “Building Code Requirements for Structural Concrete (ACI 318-08) and Commentary,” American Concrete Institute, Farmington Hills, MI, 2008, 473 pp.

Alath, S., and Kunnath, S. K., 1995. Modeling Inelastic Shear Deformation in RC Beam-Column Joints, Proceedings of 10th Engineering Mechanics Conference, University of Colorado at Boulder, Boulder, Colorado, May 21-24, ASCE, New York, Vol.2, 822-825.

Alire, D., "Seismic evaluation of existing unconfined reinforced concrete beam-column joint", M.S.C.E, Department of Civil Engineering, University of Washington, 2002

Altoontash, A., 2004, "Simulation and damage models for performance assessment of reinforced concrete beam-column joints", PhD Dissertation, Stanford University, California, USA

ASCE/SEI 41-06, American Society of Civil Engineers, “Seismic Rehabilitation of Existing Buildings, Report”, Reston, Virginia, 428, 2007.

Baker, A. L. L., and Amarakone, A. M. N., “Inelastic Hyperstatic Frame Analysis,” *Flexural Mechanics of Reinforced Concrete*, SP-12, American Concrete Institute, Farmington Hills, MI, 1964, pp. 85-142.

Baker, A. L. L., *Ultimate Load Theory Applied to the Design of Reinforced and Prestressed Concrete Frames*, Concrete Publications Ltd., London, UK, 1956, 91 pp.

Bayrak, O., and Sheikh, S. A., “Confinement Reinforcement Design Considerations for Ductile HSC Columns,” *Journal of Structural Engineering*, ASCE, V. 124, No. 9, Sept. 1998, pp. 999-1010.

Birely, A. C., Lowes, L. N., and Lehman, D. E., “Linear Analysis of Concrete Frames Considering Joint Flexibility,” *ACI Structural Journal*, V. 109 No. 3, May-June 2012

EERI/PEER, 2006, New Information on the Seismic Performance of Existing Concrete Buildings,*Seminar Notes*, Earthquake Engineering Research Institute, Oakland, California.

Emori, K., and Schnobrich, W. C. (1978). "Analysis of reinforced concrete framewall structures for strong motion earthquakes." *Civ. Engrg. Studies,* SRS 457, Univ. of Illinois at Urban-Champaign, Urbana, 111., Dec.

FEMA 356, 2000, *Prestandard and Commentary for the Seismic Rehabilitation of Buildings*, prepared by the American Society of Civil Engineers for the Federal Emergency Management Agency, Washington, D.C. (FEMA Publication No. 356).

Gilbertsen, N. D., and Moehle, J. P. (1980). "Experimental study of small-scale R/C columns subjected to axial and shear force reversals." *Civ. Engrg. Studies,* SRS 481, Univ. of Illinois at Urbana-Champaign, Urbana, 111., Jul.

Karsan, I.D., and Jirsa, J.O., “Behavior of Concrete under Compressive Loading.” Journal of Structural Division, ASCE, ST12, 95, 2543-2563, 1969.

Kent, D. C., and Park R. (1971). "Flexural Members with Confined Concrete," Journal of the Structural Division, ASCE, Vol. 97, No. ST7, July, pp. 1969-1990.

Keshavarzian, M., and Schnobrich, W. C. (1984). "Computed nonlinear seismic response of R/C wall-frame structures." *Civ. Engrg. Studies,* SRS 515, Univ. Of Illinois at Urbana-Champaign, Urbana, 111., May.

Kreger, M. E., and Linbeck, L. (1986). "Behavior of reinforced concrete columns subjected to lateral and axial load reversal." *Proc, Third U.S. Nat. Conf. On Earthquake Engrg.,* Charleston, S.C., Aug. 24-28.

Lowes, L. N. (1999). Finite element modeling of reinforced concrete beam-column bridge connections. PhD thesis, Department of Civil Engineering, University of California, Berkeley, California

Lu, Y., Gu, X., and Guan, J. (2005). ”Probabilistic Drift Limits and Performance Evaluation of Reinforced Concrete Columns.” *J. Struct. Eng.*, 131(6), 966–978.

Mahin, S. A., and Shing, P. B. (1985). “Pseudodynamic method for seismic testing.” *Journal of Structural Engineering*, ASCE, Vol. 111,No. 7,pp 1482–1503.

Mazzoni, S., McKenna, H., Scott, M.H., and Fenves, G.L., “OpenSees Manual”, Pacific Earthquake Engineering Research Center, http://opensees.berkeley.edu, 01/09/2010.

Mitra, N. (2008). “Continuum model for RC interior beam-column connection regions”, *14 th World Conference in Earthquake Engineering*, Beijing, China, (Paper no. 14-0111).

Molina, F. J., Pegon, P., and Verzeletti, G. (1999). “Time-domain identification from seismic pseudodynamic test results on civil engineering specimens.” 2nd International Conference on Identification in Engineering Systems, Cromwell Press, Wiltshire, UK.

Mutlu, M. B., Ayatar, M. E., Binici, B., Kurc, O., Canbay, E., Sucuoglu, H., Ozcebe, G. (2011). “Üç Katlı Betonarme Bir Çerçevenin Dinamik Benzeri Deneyleri ve Sayısal Simülasyonları”. *1. Türkiye Deprem Mühendisliği ve Sismoloji Konferansı*, ODTÜ, Ankara.

Mutlu, M. B., Ayatar, M. E., Ezzatfar, P., Binici, B., Kurc, O., Canbay, E., Sucuoglu, H., Ozcebe, G. (2012). “Pseudo-Dynamic Testing and Numerical Simulations of Reinforced Concrete Frames”. *10th International Congress on Advances in Civil Engineering*, *Middle East Technical University, Ankara, Turkey*.

Nakashima, M. (1985a). “Part 1: Relationship between Integration Time Interval and Response Stability in Pseudo Dynamic Testing”, *Journal of Structural and Construction Engineering*, Transactions of AIJ, No. 353, pp. 29-34.

Ozcebe, G. (1987). "Inelastic Response of Reinforced Concrete Columns under Uni-directional and Bi-directional Load Reversals.," *Ph.D. Dissertation*, Univ. of Toronto, Toronto, Ontario, Canada

Park, R.; Priestley, M. J. N.; and Gill, W. D., “Ductility of Square- Confined Concrete Columns,” *Journal of Structural Division*, ASCE, V. 108, No. ST4, 1982, pp. 929-950.

Paulay, T., and Priestley, M. J. N., *Seismic Design of Reinforced Concrete and Masonry Buildings*, John Wiley and Sons, New York, 1992, 767 pp.

Priestley, M. J. N., and Park, R., “Strength and Ductility of Concrete Bridge Columns Under Seismic Loading,” *ACI Structural Journal*, V. 84, No. 1, Jan.-Feb. 1987, pp. 61-76.

Saadeghvaziri, M. A., and Foutch, D. A. (1988). "Inelastic behavior of R/C highway bridges under horizontal and vertical earthquake motions." *Civ. Engrg. Studies,* SRS 540, Univ. of Illinois at Urbana-Champaign, Urbana, 111., Jun.

Sakai, K., and Sheikh, S. A., “What Do We Know about Confinement in Reinforced Concrete Columns? (A Critical Review of Previous Work and Code Provisions),” *ACI Structural Journal*, V. 86, No. 2, Mar.-Apr. 1989, pp. 192-207.

Sezen, H. and Moehle, J.P., 2006 “Seismic Tests of Concrete Columns with Light Transverse Reinforcement” *ACI Structural Journal*, American Concrete Institute, V.103, No. 6, pp. 842-849.

Takanashi, K., Udagawa, K., Seki, M., Okada, T., and Tanaka H. (1975). “Nonlinear earthquake response analysis of structures by a computer-actuator on-line system,” Bulletin of Earthquake Resistant Structure Research Center 8, Institute of Industrial Science, University of Tokyo, Japan.

TEC-2007, Ministry of Public Works and Settlement, “Specifications for Buildings to be Built in Seismic Zones”, Ankara, Turkey, 159 (In Turkish), 2007.

TNO DIANA, (2008). Release 9.3. TNO DIANA Reference Manual

TS 500, (2000), *Requirements for Design and Construction of Reinforced Concrete Structures.* Turkish Standards Institute

Vecchio, F.J., Collins, M.P., 1986. The Modified Compression-Field Theory for Reinforced Concrete Elements Subjected to Shear. *ACI Structural Journal*, Vol. 83, No. 22, pp. 219-231.

Walker, S., "Seismic performance of existing reinforced concrete beam-column joints", M.S.C.E, Department of Civil Engineering, University of Washington, 2001.

APPENDIX A

TEST AND NUMERICAL SIMULATION RESULTS OF SPECIMEN-2 FOR GROUND MOTION D4

Consecutive pseudo-dynamic tests conducted on Specimen-2 included the 4th ground motion D4, differently from Specimen-1 and Specimen-3. Since this study mainly aimed at comparing the performance of the test frames under identical ground motions (D1, D2 and D3), test and numerical simulation results of the ground motion D4 were not investigated in detail for Specimen-2. In this part, comparisons of test results and numerical simulations are presented in terms of global response parameters including the ground motion D4.

Properties of ground motions used in the tests are presented in Table A.1. Acceleration time series with the sequence of application and corresponding spectra of the ground motions are given in Figure A.1.

Roof displacement time history estimations of the two models are compared with test results in Figure A.2. Inter-story drift ratio time histories are presented in Figure A.3. for each story. Shear force versus deformation estimations of the numerical simulations are compared to the test results in Figure A.4.

Table A.1: Ground motion properties

Earthquake	Probability of Exceedance in 50 years	Soil Class/Type	PGA (g)
D1	50 %	Z1 / Rock	0.254
D2	10 %	Z1 / Rock	0.545
D3	10 %	Z3 / Soft	0.604
D4	2%	Z1 / Rock	1.110

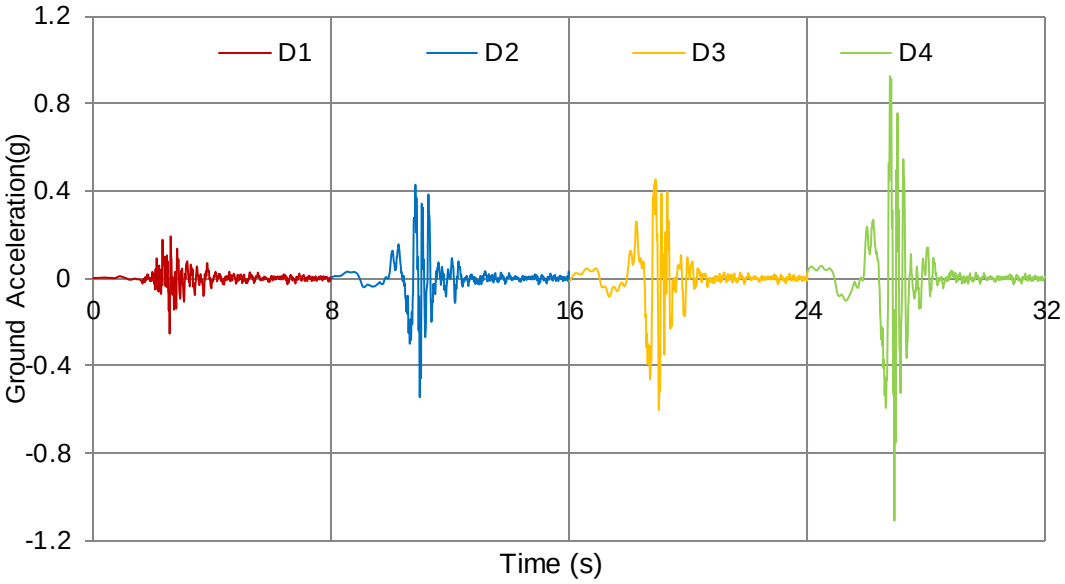

a) Acceleration-Time Series

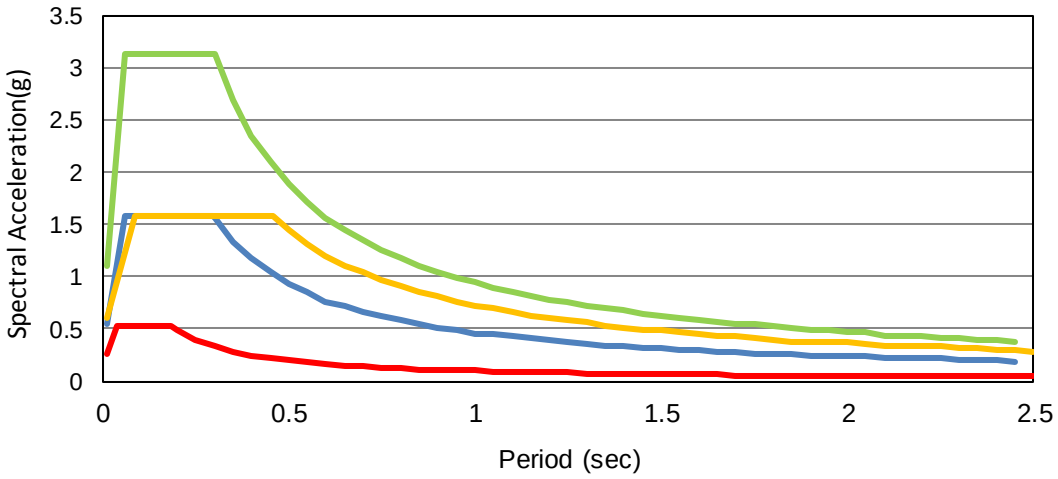

b) Acceleration Spectra

Figure A.1: Ground motions and acceleration spectra

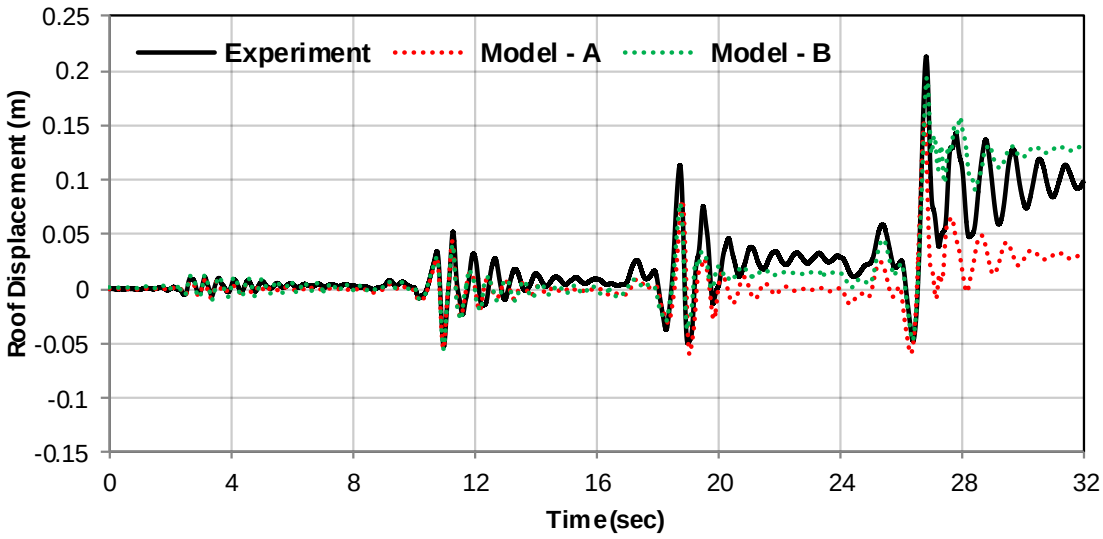

Figure A.2: Roof displacement history comparison for SP2

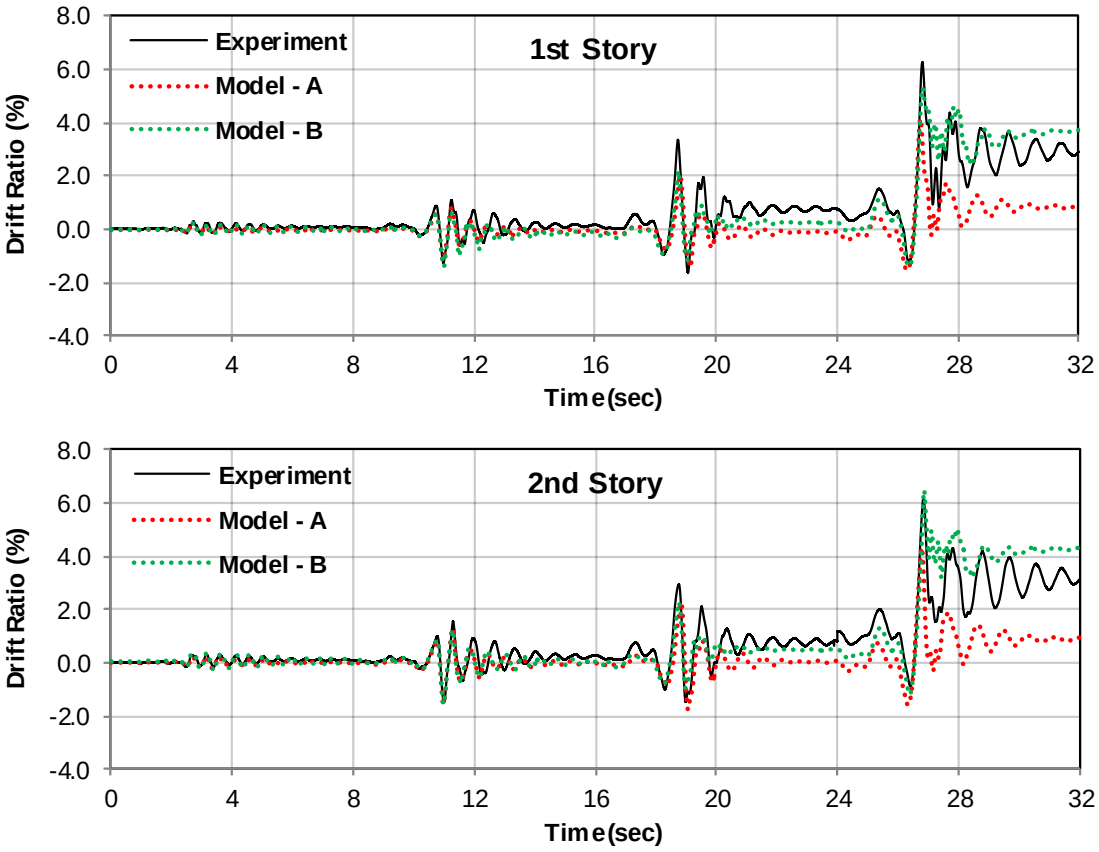

Figure A.3: Comparison of inter-story drift ratio histories for SP2

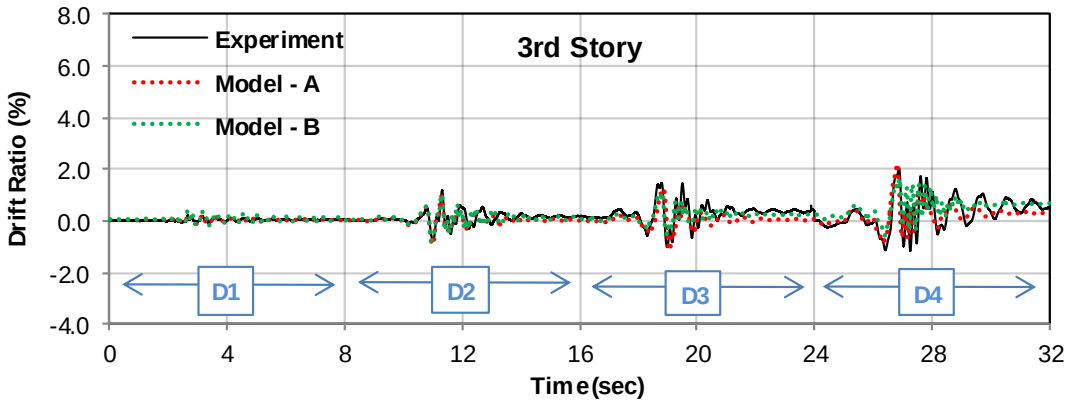

Figure A.3: Comparison of inter-story drift ratio histories for SP2 (cont'd)

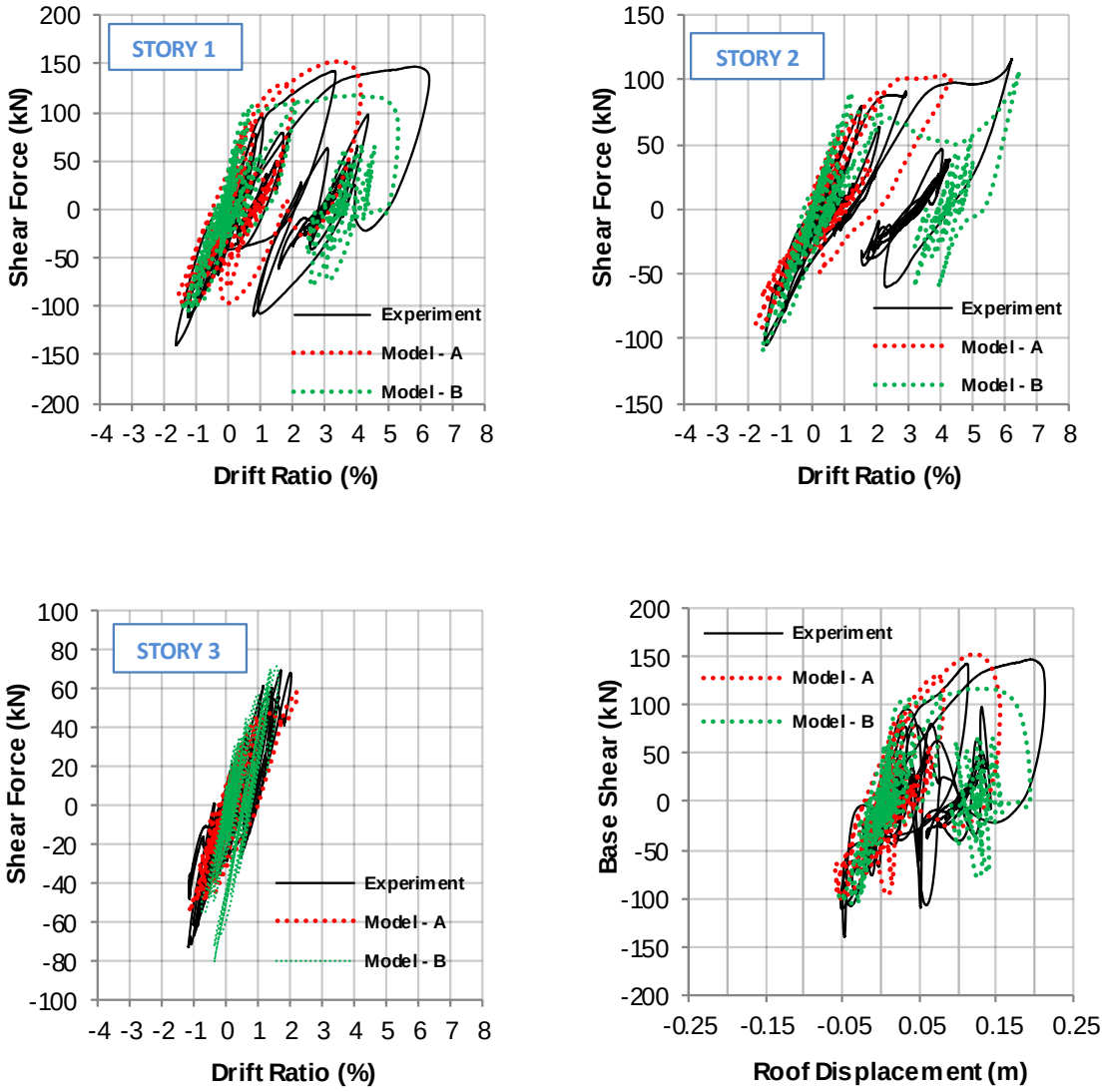

Figure A.4 : Comparison of story shear force vs. drift response for SP2